Dissertation zur Erlangung des akademischen Grades doctor rerum naturalium (Dr. rer. nat.) der Mathematisch-Naturwissenschaftlichen Fakultät der Universität Rostock

Titel der Dissertation:

Fundamental characterisation of the harbour seal (*Phoca vitulina*) brain

vorgelegt von:

Julia Susanne Schnermann

geb. am 23.10.1993 in Aachen

Rostock, 06.12.2024

https://doi.org/10.18453/rosdok_id00005145

Gutachter:
Prof. Dr. Frederike D. Hanke, Universität Rostock, Institut für Biowissenschaften

Prof. Dr. Markus Axer, Universität Wuppertal, Department für Physik
Forschungszentrum Jülich, Institut für Neurowissenschaften und Medizin (INM-1)

PD Dr. Stefan Huggenberger, Universität Witten/Herdecke, Department für Humanmedizin

Jahr der Einreichung: 2024

Jahr der Verteidigung: 2025

Angaben zur Person	**Schnermann, Julia**
Akademischer Werdegang	
2020-2025	Promotion Universität Rostock Fundamental characterization of the harbour seal (*Phoca vitulina*) brain
2017-2019	Universität Rostock Master integrative Zoologie Masterarbeit: Symmetrieerkennung beim Gemeinen Sonnenbarsch (*Lepomis gibbosus*)
2013-2017	Georg-August-Universität Göttingen Bachelor Biologie Bachelorarbeit: Riffkartierung entlang der Ostseite eines Transsektes in der Bucht von Bel Ombre, Mahé, Seychellen
Arbeitserfahrung	
Exkursion	Große marine Zoologische Exkursion Giglio/Italien (10 Tage) Zoologische Exkursion Seychellen (6 Wochen) Morphologische Exkursion Fiskebäckskil (Schweden) (10 Tage)
Konferenzteilnahmen	
2022	SMM: Macro- and microstructural analysis of the brain of a harbor seal (*Phoca vitulina*) (Poster)
2024	ECS: Neuroanatomy of the harbour seal (*Phoca vitulina*) brain (online oral presentation) ICN: Neuroanatomy of the visual pathway of the harbour seal (*Phoca vitulina*) brain (Poster)
Publikationen	Spratte C., Sandow L.-M., Schnermann J.S., Hanke F.D. (2021). Single target acuity in the common sunfish *(Lepomis gibbosus*). Journal of Experimental Biology 224(20):jeb243068

TABLE OF CONTENTS

LIST OF PUBLICATIONS

CONFERENCE CONTRIBUTIONS

Schnermann J.S., Axer M., Gräßel D., Stammsen V., Siebert U., Amunts K., Hanke F.D. Macro- and microstructural analysis of the brain of a harbor seal (*Phoca vitulina*). 24th Biennial Conference on the Biology of Marine Mammals, 2022, Palm Beach, Florida, United States of Amerika (poster)

Schnermann J.S., Axer M., Gräßel D., Siebert U., Amunts K., Hanke F.D. Neuroanatomy of the harbour seal (*Phoca vitulina*) brain. 35th European Cetacean Society conference workshop, 2024, Sicily, Italy (online oral presentation)

Schnermann J.S., Axer M., Gräßel D., Siebert U., Amunts K., Hanke F.D. Neuroanatomy of the visual pathway of the harbour seal (*Phoca vitulina*) brain. 15th International Congress of Neuroethology, 2024, Berlin, Germany (poster)

SUMMARY

This research provides a comprehensive analysis of the neuroanatomy of the harbour seal (*Phoca vitulina*) brain, a species well-adapted to a semi-aquatic lifestyle. Marine mammals exhibit unique neuroanatomical features due to their evolutionary adaptation to aquatic environments. While cetaceans have been extensively studied, pinnipeds, particularly harbour seals, remain underexplored. Advanced neuroimaging techniques for exploring both qualitative and quantitative aspects of the harbour seal's brain structure were needed to understand potential adaptations which are critical for sensory processing, spatial navigation and visual processing. To close this research gap, the study's primary objective was to establish a foundational anatomical 3D-atlas for future comparative and functional research. Therefore, a qualitative assessment, highlighting distinctive brain structures such as the caudate nucleus, *hippocampus*, and the *lateral geniculate nucleus* (LGN), was used.

Characterisation of neural structures with a focus on the visual and sensory processing systems that support the seal’s semi-aquatic lifestyle were done by using three-dimensional polarised light imaging (3D-PLI). Key methodologies include cryosectioning, blockface imaging, and high-resolution histological mapping of 1,668 50 µm thick coronal sections. Generated data within this study allow the precise measurement of cortical thickness (mean 2.35 mm), gyrification index (GI, 2.15), and the volume of critical brain regions such as the LGN (right: 0.17 cm³, left: 0.18 cm³), the caudate nucleus (right: 1.70 cm³, left: 1.70 cm³) and the *hippocampus* (right: 0.53 cm³, left: 0.56 cm³). Using histological techniques, the laminar organisation of the LGN and the primary visual cortex was analysed. The LGN exhibits a markedly distinct layering pattern compared to previously studied pinniped species. Furthermore, the primary visual cortex is characterised by the presence of only five discernible layers. The integration of 3D-PLI with histological techniques provides unprecedented insights into the neural architecture at axonal resolution, bridging the gap between macroscopic and microscopic analyses.

The research contributes valuable data to the field of marine mammal neuroscience, providing a comparative framework that can guide future investigations into sensory and cognitive functions in marine mammals. This study also highlights the potential of using advanced imaging techniques to bridge the gap between macroscopic anatomical analysis and microscopic details, offering new perspectives on the evolution of brain structures adapted to semi-aquatic environments. Future research should expand these findings to other pinniped species and include functional imaging and behavioural studies to explore the interplay between structure and function more comprehensively.

ZUSAMMENFASSUNG

Diese Dissertation bietet eine umfassende Analyse der Neuroanatomie des Gehirns des Seehundes (*Phoca vitulina*), einer Art, die hervorragend an einen semi-aquatischen Lebensstil angepasst ist. Meeressäugetiere zeigen aufgrund ihrer evolutionären Anpassung an aquatische Umgebungen einzigartige neuroanatomische Merkmale. Während Cetaceen intensiv untersucht wurden, sind Robben (Pinnipedia), insbesondere Seehunde, bisher vergleichsweise wenig erforscht. Es bestand Bedarf an fortschrittlichen Neuroimaging-Techniken, um qualitative und quantitative Aspekte der Gehirnstruktur des Seehundes zu untersuchen, um potenzielle Anpassungen zu verstehen, die für sensorische Verarbeitung, räumliche Navigation und visuelle Verarbeitung entscheidend sind.cUm diese Forschungslücke zu schließen, war das Hauptziel dieser Studie die Erstellung eines grundlegenden anatomischen 3D-Atlas, der zukünftige vergleichende und funktionelle Forschung unterstützt. Eine qualitative Bewertung, die charakteristische Gehirnstrukturen wie den *Nucleus caudatus*, den *Hippocampus* und den lateralen Kniehöcker (LGN) hervorhebt, wurde durchgeführt.

Die Charakterisierung neuronaler Strukturen mit einem Fokus auf die visuellen und sensorischen Verarbeitungssysteme, die den semi-aquatischen Lebensstil des Seehundes unterstützen, erfolgte mittels dreidimensionaler polarisiertem Licht-Bildgebung (3D-PLI). Zu den Schlüsselmethoden zählten Kryoschnitt-Techniken, Blockface-Bildgebung und hochauflösende histologische Kartierung von 1.668 koronalen Schnitten mit einer Dicke von 50 µm. Die im Rahmen dieser Studie generierten Daten ermöglichen präzise Messungen der Kortikaldicke (im Mittel 2,35 mm), des Gyrifikationsindex (GI, 2,15) und des Volumens kritischer Gehirnregionen wie des LGN (rechts: 0,17 cm³, links: 0,18 cm³), des *Nucleus caudatus* (rechts: 1,70 cm³, links: 1,70 cm³) und des *Hippocampus* (rechts: 0,53 cm³, links: 0,56 cm³). Mithilfe histologischer Techniken wurde die laminare Organisation des LGN und des primären visuellen Cortex analysiert. Das LGN zeigt ein deutlich anderes Schichtungsmuster im Vergleich zu bereits untersuchten Flossenfüßer-Arten. Der primäre visuelle Cortex weist zudem nur fünf erkennbare Schichten auf. Die Integration von 3D-PLI und histologischen Techniken liefert beispiellose Einblicke in die neuronale Architektur auf axonaler Auflösung und schlägt eine Brücke zwischen makroskopischer und mikroskopischer Analyse.

Diese Forschung liefert wertvolle Daten im Bereich der Neurowissenschaften von Meeressäugetieren und bietet einen vergleichenden Rahmen, der zukünftige Untersuchungen zu sensorischen und kognitiven Funktionen bei Meeressäugetieren leiten kann. Die Studie unterstreicht zudem das Potenzial fortschrittlicher Bildgebungstechniken, um die Kluft zwischen makroskopischen anatomischen Analysen und mikroskopischen Details zu überbrücken, und eröffnet neue Perspektiven auf die Evolution von Gehirnstrukturen, die an semi-aquatische Umgebungen angepasst sind. Zukünftige Forschungen sollten diese Erkenntnisse auf andere Flossenfüßer-Arten ausweiten und funktionelle Bildgebungs- sowie Verhaltensstudien einbeziehen, um das Zusammenspiel von Struktur und Funktion umfassender zu untersuchen.

LIST OF FIGURES

LIST OF TABLES

LIST OF ABBREVIATIONS

3D-FOM	3D fibre orientation map
3D-PLI	3D polarised light imaging
ANTs	advanced normalisation tools
AP	anterior-posterior
CA	*Cornu Ammonis,*
CCD	charge-coupled device
DNA	desoxyribonucleic acid
DTI	diffusion tensor imaging
fMRI	functional magnetic resonance imaging
fNIRS	functional near-infrared spectroscopy
GI	gyrification index
ICA	independent component analysis
ITAW	Institute for Terrestrial and Aquatic Wildlife Research
LED	light emitting diode
LGN	*lateral geniculate nucleus*
MGN	medial geniculate nucleus
MRI	magnetic resonance imaging
PBS	phosphate-buffered saline
RGB	red, green, blue
RNA	ribonucleic acid
TBV	total brain volume
V1	primary visual cortex
V2	secondary visual cortex

1. INTRODUCTION

The neuroanatomy of marine mammals, especially cetaceans, has long intrigued scientists due to the unique adaptations these species exhibit for life in water (e.g. Vreese et al. 2023; Marino et al. 2003; Wright et al. 2017; Reep & O'Shea 1990; Hof et al. 2005). The relative brain size in marine mammals, appears to be smaller in heavy species than in lighter species (Bininda-Emonds 2000; Marion 2009). Compared to their terrestrial counterparts, toothed whales typically show an enlarged cerebellum, which is thought to support their enhanced motor coordination required for swimming and diving (Ridgway et al. 2014; Ridgway et al. 2019). Additionally, sensory cortices such as the auditory and somatosensory regions are often expanded to accommodate specialised sensory modalities essential for underwater communication and tactile perception (Bauer et al. 2020). Cetaceans have intricately convoluted neocortices characterised by extensive surfaces (Eriksen & Pakkenberg 2014). The diversity in cortical thickness and folding in marine mammals is particularly striking. Indeed, cetaceans have the thinnest cortex and the strongest folding within the group of marine mammals (Marino et al. 2007; Hof et al. 2005). A striking comparison exists between dolphins, characterised by pronounced cortical folding, and manatees (*Trichechus manatus*), which exhibit a markedly lissencephalic brain structure with a thick cortex (Reep & O'Shea 1990).

To the contrary, pinniped neuroanatomy has not attracted much attention (but see eg. Dohmen et al. 2015; Cook & Berns 2022; Hoeksema et al. 2020). However, their neuroanatomy seems equally interesting to study as pinnipeds are secondarily adapted to an aquatic environment while retaining a terrestrial lifestyle. This semi-aquatic lifestyle challenges pinniped anatomy and physiology, given the different physical properties of water and air (Bauer et al. 2020; Pihlström 2008). Previous research has shed light on how pinnipeds cope with the continuous changes in, for example, buoyancy, light refraction, and sound propagation of the surrounding media, which sometimes even raise opposing demands (Beck et al. 2000; Mass & Supin 2003; Hanke et al. 2009a; Reichmuth et al. 2013). The transition to a semi-aquatic lifestyle likely necessitated distinct alterations not only to general anatomy and physiology but also to brain structure for example to facilitate the sensory adaptations for orientation and navigation in the predominantly featureless ocean environment or in the three-dimensional underwater realm (Hanke & Dehnhardt 2018; Maaß et al. 2022).

The current research focuses on the neuroanatomy of pinnipeds, with a particular emphasis on the neuroanatomy of harbour seals (*Phoca vitulina*). In the following, an overview of pinniped neuroanatomy (1.1) will be provided, before highlighting the specific features of the harbour seal brain in chapter 1.2 which remains the central subject of the current research. Chapter 1.3 emphasizes the current research gaps, systematically identifying and analysing areas where further investigation is needed.

1.1. PINNIPED NEUROANATOMY

The general outer morphology of pinnipeds has been described decades ago in great detail by several working groups (Flatau & Jacobsohn 1899; Fish 1898; Turner 1888; Krueg 1880; Owen 1868). Early investigations provide detailed descriptions of the external morphology and cortical folding of pinniped brains. Krueg (1880) conducted an analysis of harbour seal (*Phoca vitulina*), a species within the Phocidae family, and also described Steller sea lion (*Eumetopias jubata)*, belonging to the Otariidae family. Tiedeman (Tiedemann 1824) contributed additional macroscopic anatomical observations on a *Phoca sp.* brain. For completeness, it is important to acknowledge the studies by Flatau and Jacobsohn (1898) and Jelgersma (1934), which focus specifically on the harbour seal and are discussed in greater detail in Chapter 1.2. These foundational studies primarily examined the external gross anatomy of pinniped brains, consistently highlighting the pronounced cortical folding.

This characteristic folding, which was prominently noted in earlier studies, is quantitatively assessed using the gyrification index (GI) as defined by (Zilles et al. 1988). Up to now, only few studies determined gyrification, also known as cortical folding (Manger et al. 2012; Zilles et al. 2013) or cortical thickness (Hoeksema et al. 2020; Reep & O'Shea 1990) in the pinniped brain, and certainly not both values in combination. Particularly the interplay between these two parameters might offer interesting insights. A common and well researched hypothesis is that as brain size increases, folding also increases (Elias & Schwartz 1969; Marino et al. 2007; Brodmann 1913). On the other hand, the limited space in the skull might play a role in the folding, such that the limited spatial conditions allow the surface area to be increased by the folding (Welker 1990; Mota & Herculano-Houzel 2012; Essen 1997). For instance, previous studies have suggested that an increase in cortical thickness correlates with increased cellular accommodation, while greater cortical folding, measured via the GI, can enhance neural connectivity within a confined cranial space (Herculano-Houzel 2009; Herculano-Houzel et al. 2014; Shepherd 2015). Yet, the paradox is that excessive cortical thickness may reduce the brain's ability to fold optimally. Thus, understanding the balance between these two factors in the harbour seal brain may shed light on how the brain's structural organisation.

Welker (1990) and Zilles et al. (1989) were the first observing that mammals with larger brains tend to exhibit a higher degree of cortical gyrification compared to their counterparts with smaller brains. Although the study by Zilles et al. (1989) focussed exclusively on primates, subsequent Manger et al. (2012) as well as Pillay and Manger (2007) extended these findings to a broader range of mammals, including carnivores. The cerebral cortex, constituting the outer layer of the brain, plays a crucial role in higher-order cognitive functions, such as cognition, perception, and decision-making. In addition, the cerebral cortex serves as a critical hub for information processing within the brain. Each taxonomic order and family exhibit distinct gyrification patterns, as noted by Zilles et al. (2013) and Pillay and Manger (2007).

Few studies have focused on the detailed anatomy of the pinniped brain, especially concerning how different brain regions are specialised for their unique sensory and motor requirements (Oztas 2003; Sawyer et al. 2016; Turner et al. 2017). Both Fish (1898) and Levine et al. (2008) described that seals possess relatively small olfactory bulbs compared to their terrestrial counterparts, as the nose is functional only on land and remains closed underwater (Levine et al. 2008; Fish 1898). The limited functionality of the olfactory system in pinnipeds has resulted in a reduced olfactory bulb compared to terrestrial mammals (Pitcher et al. 2011). Additionally, Langworthy et al. (1938) and Rioch et al. (1937) conducted studies focused on the localisation of the motorcortex. The cerebral cortex of the harbour seal shows specialised areas for processing sensory information from the body and the environment, which are essential for navigating and hunting underwater (Langworthy et al. 1938; Rioch 1937).

To ensure a comprehensive understanding, it is critical to reference studies that have conducted in-depth analyses of specific brain regions. Hoeksema et al. (2020) and Montie et al. (2009) notably pioneered the development of the first neuroanatomical atlases for pinniped brains. Cook and Berns (2022) performed detailed examinations of the caudate nucleus, while Cook et al. (2018) further investigated the hippocampal structure and function in California sea lions. These foundational studies will be elaborated upon in Chapter 1.3.1. Concerning the visual system, which will be analysed in detail in Chapter 1.3.3, significant contributions include the work of Wohlert et al. (2016) and Dohmen et al. (2015).

1.2. HARBOUR SEAL NEUROANATOMY

With respect to harbour seals, the focal animal of this study, previous research described the outer gross morphology of the brain including the general brain size as well as sulcal and gyral pattern (Flatau & Jacobsohn 1899; Jelgersma 1934). According to Flatau and Jacobsohn (1898), a conspicuous feature of the harbour seal brain is the very deep Sylvian fissure and a long, broad and also frontally flattened cortex. A few decades later, a work by Jelgersma (1934) describes that the brains of seals are very individual and also differ in the hemispheres of the individuals. Furthermore, he observed that the brain exhibits only very weakly developed arcuate folds and is also structurally distinct from that of land-dwelling carnivores, as the folds are not as pronounced as those observed in other carnivorous mammals, such as felids or canids (Jelgersma 1934).

A review of the literature reveals a notable lack of studies on the neuroanatomy of harbour seals. This research aims to address these gaps, which are comprehensively delineated in Chapter 1.3.

1.3. RESEARCH GAPS REGARDING HARBOUR SEAL NEUROANATOMY

1.3.1. QUALITATIVE ANATOMICAL DESCRIPTION OF THE HARBOUR SEAL BRAIN

As outlined in Chapter 1.2, a detailed anatomical description of the harbour seal brain is presently lacking, representing a significant research gap in the understanding of its neurobiological organisation. Central to this endeavour is the generation of detailed atlas information to serve as a foundational resource for future comparative and functional studies. A first step to creating an atlas was made by Jelgersma (1934) by describing histologically stained slices of the harbour seal brain. Another method to create an atlas is using Magnetic Resonance Imaging (MRI) technology as Montie et al. (2009). They obtained high-resolution images of a live California sea lion's brain. As result, the study reports specific volume measurements for various brain regions. The studied California sea lion's brain showed notable adaptations, including an enlarged cerebellum, which is associated with motor coordination, potentially reflecting the demands of swimming and agile aquatic movement. The hippocampus, associated with spatial memory and navigation, was also prominently developed, which may be essential for migration and environmental navigation in the ocean (Montie et al. 2009; Hoeksema et al. 2020). Another study about grey seal published by Hoeksema et al. (2020) also used MRI to provide a foundational neuroanatomical map of the grey seal brain, emphasising structures that support vocal learning.

This study aims to address this gap by presenting a detailed external morphological description alongside an analysis of key anatomical regions. These regions have been selected for their significance in ongoing research projects and for their relevance in comparative studies across other pinniped species. The harbour seal's brain was reconstructed on the basis of blockface images of brain sections obtained during cryosectioning to enable general anatomical analysis, i.e. to set the foundation of a novel 3D atlas of the harbour seal brain. Therefore, selected anatomical structures such as the caudate nucleus or the hippocampus were identified and characterised in terms of their location, shape, and further structural features. To enhance the understanding of the morphological and structural characteristics of these areas, the advancing neuroimaging microscopy technique referred to as 3D Polarised Light Imaging (3D-PLI) was employed (Axer et al. 2011a; Axer & Amunts 2022) and combined with human homology considerations. While Cook (2018, 2022) and Hoeksema (2020) utilised MRI data for their 3D atlases, 3D-PLI was selected as the method of choice. This approach opened up a new way to provide a detailed anatomical characterisation at axonal resolution, while also offering preliminary insights into connectivity. A comprehensive evaluation of the methodologies employed, including their respective advantages and limitations, is presented in the appendix 3 (further discussion on methodological considerations and limitations).

1.3.2. QUANTITATIVE ANATOMICAL DESCRIPTION OF THE HARBOUR SEAL BRAIN

In addition to the descriptive analysis, volumetric measurements were conducted for the selected key regions.

On the quantitative side, specific attention should be directed towards structures such as the caudate nucleus and hippocampus. Determining their size and position would be particularly valuable, especially in the context of comparative analyses with other studies like Cook et al. who focused primarily on the brain of the California sea lion (*Zalophus californianus*) (Cook & Berns 2022; Cook et al. 2018). One study concluded that there are notable differences in the volumetric size and connectivity of the caudate nucleus between the California sea lion and the coyote, which reflect their respective ecological niches and behavioural adaptations (Cook & Berns 2022). Further Cook et al. (2018) found that chronic exposure to algal toxins, particularly domoic acid, leads to significant changes in the hippocampal connectivity of wild sea lions. These two structures are also integral to this thesis, and a comparative analysis between the harbour seal and the sea lion could provide valuable insights. Further, two fundamental microanatomical parameters of the harbour seal brain were determined: cortical thickness and the GI. Cortical thickness refers to the thickness of the outermost layer of the brain. The GI is a measure used in neuroanatomy and neuroscience to quantify the degree of cortical folding or gyrification in the brain (Zilles et al. 1988). It provides information about the complexity of the outermost layer of the brain, particularly the cerebral cortex.

The GI of the harbour seal has been reported as 2.38 (Manger et al. 2012). To the best of current knowledge, there is no data available regarding cortical thickness in the harbour seal. However, there may be a relationship between cortical thickness and folding (Gautam et al. 2015). While a thicker cortex may theoretically accommodate a greater number of neurons, efficient folding of the cortical surface becomes a limiting factor (Hofman 1985). Gyrification, which enhances the brain's surface area within the confines of the skull, allows for greater neuronal density and synaptic connectivity, even when cortical layers are thinner (Zilles et al. 1988). Moreover, the investigating cortical thickness is crucial for understanding the structural and functional organisation of the harbour seal’s brain. All these indications suggest, that this lack of information highlights the necessity and importance of studies aimed at addressing this research gap. Studies, such as those by Mota and Herculano-Houzel (2015), have shown that cortical folding scales with surface area and thickness, emphasising the importance of joint analysis to unravel the biophysical principles governing brain architecture. The analyses have been a good starting point to close the mentioned research gap, meaningful data on the brain of harbour seals are currently still completely lacking in the literature.

The fundamental goal of this work is to achieve a comprehensive characterisation of the harbour seal brain, encompassing both quantitative and qualitative aspects.

1.3.3. DETAILED ANATOMICAL DESCRIPTION OF THE VISUAL PATHWAY OF THE HARBOUR SEAL BRAIN

The visual system of seals is of particular scientific interest, as it remains controversial to what extent and for what purposes seals actually use their visual system because they often hunt in turbid or dark water conditions (Renouf 1989). Research has shown that seals could navigate using stars as reference points for spatial orientation (Mauck et al. 2008; Mauck et al. 2005). Additionally, seals perceive optic flow (Gläser et al. 2014). This indicates that the visual system of seals exhibits specific adaptations regarding sensitivity and resolution, with particular emphasis on motion perception. The latter aspect, optical flow perception, is particularly intriguing, as it suggests that suspended particles in the water, traditionally viewed as obstacles that limit visibility and reduce visual acuity, may instead play a crucial role. As the seal moves through these particles, they generate optical flow, which can be exploited for various functional purposes. Thus, even and particularly in turbid water, seals can access valuable optical information (Gläser et al. 2014).

Past research on the vision of pinnipeds has focused on the adaptations of their eyes and neural visual system (e.g. Jamieson & Fisher 1971; Hanke et al. 2008). As semi-aquatic mammals, pinnipeds experience vastly different optical challenges in air and water. Understanding how their visual systems have evolved to function optimally in both media has been the focus of numerous studies (Hanke et al. 2009a; Hanke et al. 2008; Hanke et al. 2006b). Additional studies have investigated the gross anatomy of the eye, with focus on for example the structural anatomy of the cornea (Hanke et al. 2006a), lens (Hanke et al. 2008) or retina (Jamieson & Fisher 1971; Hanke et al. 2009b). The neuronal processing of visual information in pinnipeds has been less researched (Dohmen et al. 2015; Wohlert et al. 2016). A morphometric comparison of the cranial nerves between two closely related seal species, the hooded seal (*Cystophora cristata*) and the harbour seal, was conducted to better understand their neural adaptations. The optic nerve was significantly larger in the hooded seal compared to the harbour seal (Wohlert et al. 2016).

In cetaceans, the visual cortex is relatively less developed (Kesarev et al. 1977) compared to their auditory and somatosensory cortices, reflecting their reliance on echolocation. In contrast, a pinniped study with California sea lions and northern elephant seals (*Mirounga angustirostris*) showed a well-developed visual cortex, underscoring their need for effective visual processing both in water and on land (Turner et al. 2017). The primary visual cortex (V1), a brain region which is responsible for processing visual input from the retina, is relatively well-developed in pinnipeds, particularly when compared to other sensory cortices (Turner et al. 2017). Further the visual system in the northern elephant seal displayed adaptations for deep-sea vision, including structures that support vision in low-light conditions, such as

enhanced sensitivity in the optic nerve and the LGN. In contrast, the California sea lion's visual system may be structured for dual environments, supporting both land-based and shallow-water vision with high contrast sensitivity (Turner et al. 2017). The cerebral cortex of certain dolphins, such as the bottlenose dolphin (*Tursiops truncatus*), exhibits deviations from the classical six-layered neocortex observed in most mammals. Notably, layer IV, which is typically associated with thalamic input and is a defining feature of the neocortex, is poorly defined or absent. This structural characteristic is consistent with observations in other odontocetes, reflecting a unique adaptation within this group (Furutani et al.).

Despite this, the neural basis of visual processing remains insufficiently understood, underlying the importance of investigating the key regions such as the LGN and the visual cortex. Through a rigorous examination of the structural and comparative characteristics of critical brain regions, such as the LGN, and visual cortex, this research aims to elucidate the potential evolutionary modifications in neural architecture. Additionally, cresyl violet staining was employed to visualise the distributions of neuronal cell bodies (i.e., the brain's cytoarchitecture), in analogy to current approaches used in human brain mapping (Amunts et al. 2020). By combining blockface Imaging, 3D-PLI, and cellular staining this work also aims to elucidate the complex architecture of the visual system and its associated neural circuits, contributing to a deeper comprehension of sensory processing in the brain.

2. MATERIAL AND METHODS

To address the above-mentioned research objectives comprehensively, 3D-PLI was selected as the methodological approach. This technique is preceded by a preparatory cryosectioning and blockface imaging step, which ensures optimal sample integrity and structural preservation for subsequent imaging. A detailed discussion, including a comparative analysis of alternative methodologies, can be found in the appendix 3. This comparison outlines the advantages and limitations of various approaches, providing a rationale for the selection of 3D-PLI in the context of the specific research goals.

Given the complexity and length of the workflow in this study, a comprehensive overview of all methodologies has been consolidated into a single, summarising figure (Figure 1). This schematic provides a visual outline to enhance both clarity and accessibility, allowing for an easier grasp of the interconnections and sequence of methods employed. Additionally, each methodological component is thoroughly elaborated upon in the subsequent chapters.

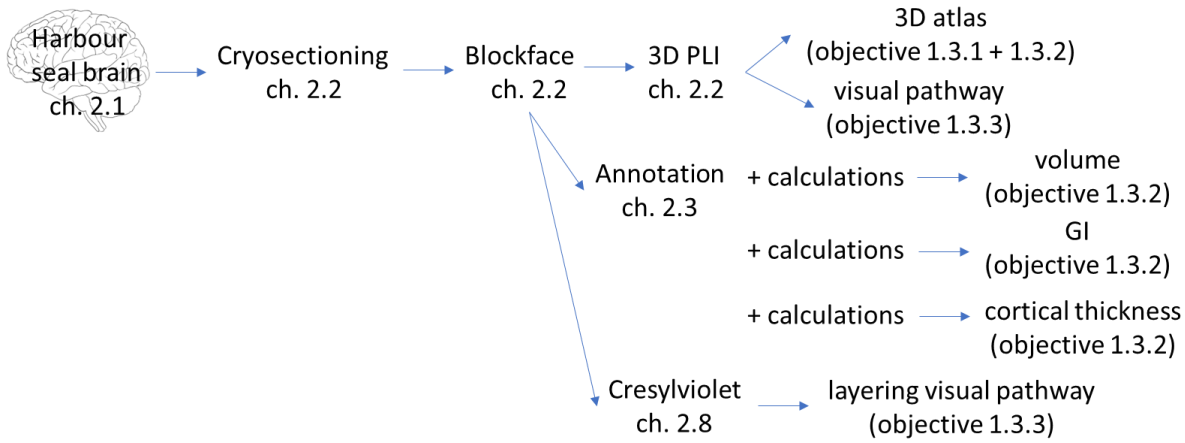

Figure 1: Overview of the workflow of the current study with all methods included.

2.1. BRAIN TISSUE

The brain (

Figure **2**) with a weight of 230 g was dissected from a juvenile female harbour seal with a body length of 106 cm and a body weight of 10 kg at the ITAW (Institute for Terrestrial and Aquatic Wildlife Research) Büsum. The animal had died of endoparasitosis in several organs and cachexia. The brain was fixed in 4% formaldehyde. It remained in the fixative for nine years before the preparation for this study started.

As part of the dead body monitoring program, a 2 cm sagittal part of the right cortex was removed for further analyses at the ITAW.

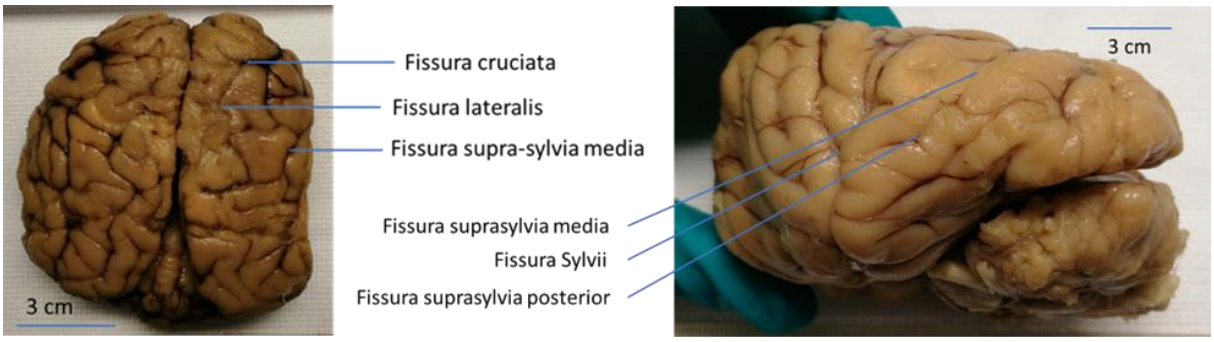

Figure 2: Harbour seal brain. (a) Dorsal view of the seal brain with the labelling of some prominent fissures. 2 cm of the right cortex were removed according to the dead body monitoring program, and therefore were not available for the current thesis. (b) Lateral view of the seal brain (left side). (a) and (b) with labels of some prominent fissures (Flatau & Jacobsohn 1899; Jelgersma 1934).

2.2. Cryosectioning and Blockface imaging

Blockface imaging enables the generation of high-resolution, 3D reconstructions of the brain. Unlike traditional histological methods that involve staining of individual brain sections, blockface imaging retains spatial information across tissue sections. To prepare for all upcoming techniques the formalin-fixed brain was embedded in a solution of Tissue Freezing Medium (Leica, Wetzlar, Germany) and 15% glycerol (Merck, Darmstadt, Germany). In addition, blue wax strips as markers were embedded, which were needed for the later three-dimensional reconstruction. It was cut coronally in a cryostat microtome (Poly-cut CM 3500, Leica, Wetzlar, Germany) with a section thickness of 50 µm. The brain sections (N = 1668) were mounted on object glass slides and frozen at - 80°C (until further imaging). During cryosectioning, the surface of the frozen brain tissue was photographed with a charge-coupled device (CCD) camera (acA5472-17uc, Basler, Ahrensburg, Germany), equipped with a Linos MeVis-C 35 mm objective lens (Qioptiq, Göttingen, Germany) to obtain blockface images at 30 microns pixel size for each generated brain section. The blockface images were analysed to gain information about the general anatomy and also served as reference data for registration of the brain sections (Schober et al. 2015).

2.2.1. Blockface data modality

The blockface images (Figure 3) serve as a key tool for the identification and delineation of distinct anatomical structures. Due to the high-resolution (pixel size 30 microns) nature of these images, many of the structures can be visually tracked and analysed without the need for additional magnification or specialised equipment. As indicated in Figure 3, blockface images enable delineations of grey and white matter, as well as massive blood vessel structures down

to the level of the achieved blockface image resolution. Consequently, these images provide a fundamental first layer of data, offering critical insights into the spatial organisation and morphological characteristics of many fundamental anatomical structures. This initial dataset is invaluable for subsequent analyses, laying the groundwork for more detailed investigations using complementary imaging like 3D-PLI or staining-based histology.

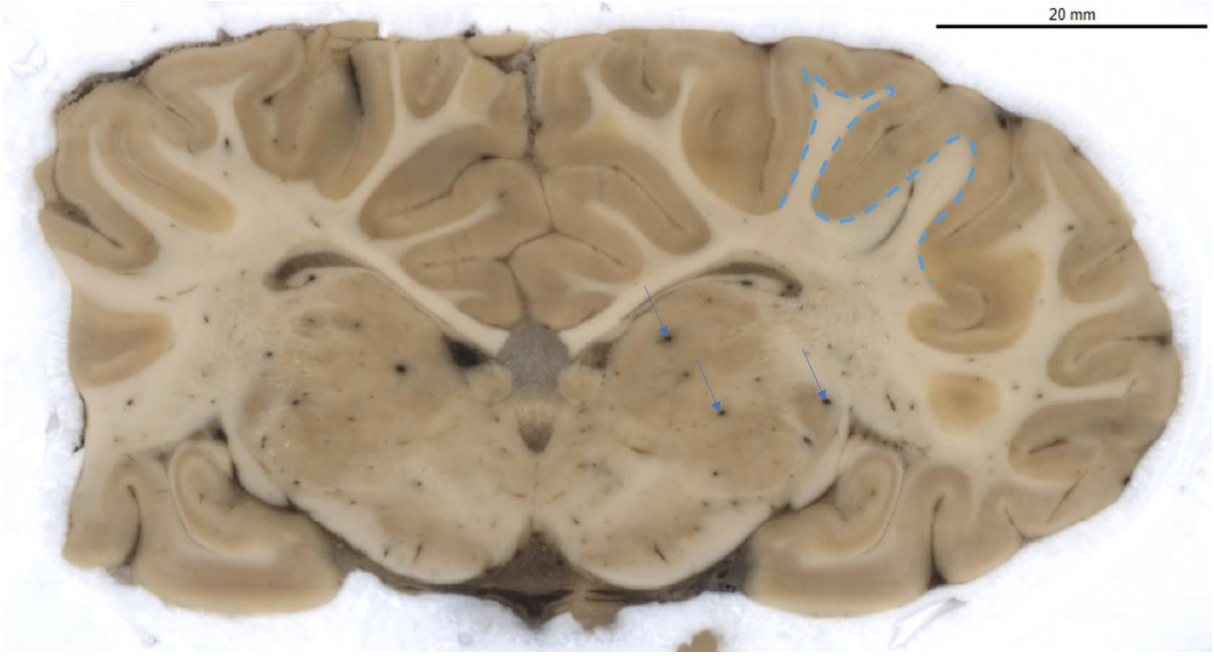

Figure 3: Example section of a blockface image of a harbour seal brain (section no. 825). Blockface images offer a valuable source of anatomical information, allowing for the visualisation and assessment of cortical gyrification and the spatial localisation of specific brain structures even before further histological or imaging analysis. Dashed blue line: exemplary border of grey and white matter. Blue arrow: exemplary blood vessel. Scale 20 mm.

2.2.2. BLOCKFACE RECONSTRUCTION

The reconstruction of blockface images comprises two major parts: marker-based alignment and refinement of the volume stack using tissue information.

Marker-based alignment: Part I(a)

First, a segmentation image of blue markers was created for each section of the volume using the Multi-Otsu algorithm (Liao et al. 2001). Following this, the Connected Components algorithm was applied to label the markers within each segmentation image (Wu et al. 2005). For each section, two values were recorded: the number of markers and the number of pixels per marker. These values were utilised to identify outliers, ensuring consistency in the number

of markers per section and uniformity in marker size, within a given tolerance. Subsequently, the centre of mass of each marker was calculated to estimate a translation transformation for each section.

Marker-based alignment: Part I(b)

Each section was then aligned to its neighbouring section using intensity-based registration with the Advanced Normalisation Tools (ANTs). This alignment employed a rigid transform model, a gradient descent optimiser, and the mutual information metric (Avants et al. 2014). The translation transformation estimated in Part I(a) was used as the initial transformation for this process. During each optimisation step, only marker information was used to calculate the metric value.

Refinement of the volume stack: Part II

Outliers were identified through a visual inspection of the reconstructed volume. For each detected outlier, the registration process described in Part I(b) was repeated. In this iteration, the metric was evaluated over the entire images, incorporating tissue information in addition to the markers, to ensure a more comprehensive alignment.

2.3. ANNOTATIONS OF BLOCKFACE IMAGES

The annotations of blockface images, manually drawn by hand, have been meticulously added to the blockface images to provide detailed reference points. These annotations were developed based on homologies with human anatomical structures, allowing for accurate cross-species comparisons and a reliable framework for further analysis. The annotations were strategically applied to establish precise spatial references for individual anatomical structures, serving as foundational markers for subsequent quantitative analyses. These annotations were not only critical for the spatial mapping but also formed the basis for determining all following computations, such as the GI, cortical thickness, and volumetric measurements. To achieve a balance between accuracy and efficiency in these calculations, annotations were systematically applied to every 10^{th} section. Further the data derived from the 3D-PLI measurements (chapter 2.7) were further employed to more precisely delineate structural boundaries through the examination of nerve fibre organisation and orientation.

2.4. DETERMINATION OF THE GYRIFICATION INDEX

The determination of the GI, was based on a protocol by Zilles et al. (1988). In every 10^{th} brain slice, the complete contour of the brain surface (Figure 4), defined as pial surface including the sulci, and the outer contour, defined as pial surface excluding the sulci, were traced with the

polygon tool of MicroDraw (https://microdraw.pasteur.fr; modified by INM-1 at FZ Jülich, Germany). The GI was calculated as the quotient of the complete pial contour and the outer pial contour for each brain slice (Figure 4). The calculations were made for the preserved left hemisphere of the harbour seal brain. The GI is computed exclusively in 2D from individual brain sections, instead of using a 3D model, as is the case with measurements of cortical thickness.

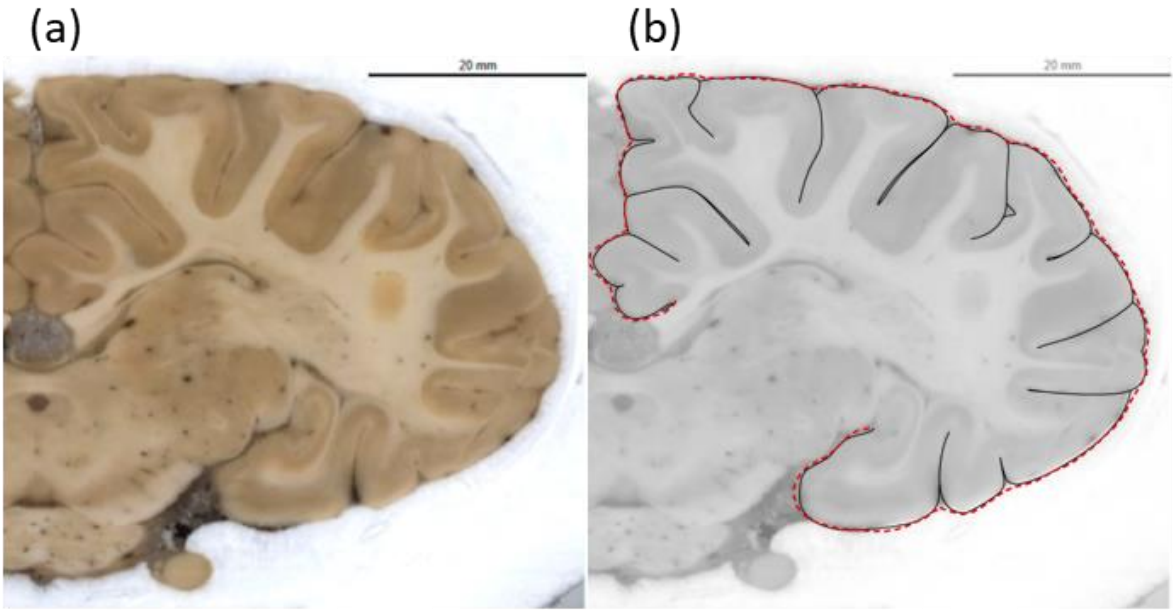

Figure 4: Determination of the gyrification index. Contours of (a) a coronal blockface image of the harbour seal brain (left hemisphere of coronal section no.860) was used to determine the gyrification index. (b) The blockface image with complete pial contour (black) and outer pial contour (red dashed) of the brain on the particular slice overlaid. Scale 20 mm.

2.5. DETERMINATION OF THE CORTICAL THICKNESS

Cortical thickness was calculated using the complete outer contour and the boundary between grey and white matter (Figure 5). Both were obtained by tracing the contour and the boundary with the polygon tool in MicroDraw. The annotated polygons were used to create segmentation masks of background, cortical grey-matter and white-matter for each annotated brain section. The segmentation masks were stacked to a voxel volume in the NIfTI-1 data format of size 769 × 463 × 165 and voxel spacing 0.12 × 0.12 × 0.5 mm. For the voxel volume, a three-dimensional Laplacian field was computed between the grey-white matter interface and pial surface using brain-visa high-res cortex toolbox (Leprince et al. 2014; Leprince et al. 2015). The length of field lines along the gradient of the Laplacian field was computed to obtain the cortical thickness (Jones et al. 2000), using Eulerian advection. Cortical thickness was again determined for the intact left hemisphere of the harbour seal brain. The Laplacian field was

further used to compute an equi-volumetric cortical depth (Leprince et al. 2015) for each cortical voxel with values between 1 (near white-matter) and 0 (near pial surface). A mesh was extracted at the equivolumetric depth level of 0.5 between the surfaces of pial and grey-matter/white-matter boundary using the marching-cubes algorithm (Lorensen & & Cline 1987). The mesh was postprocessed in the software Meshlab (Cignoni et al. 2008) using Screened Poisson reconstruction (Kazhdan & & Hoppe 2013), Isotropic Explicit Remeshing (Hoppe et al. 1993) with a target length of the remeshed edges of 222 µm and Laplacian smoothing (Vollmer et al. 1999). Unwanted surface representations of, for example, subcortical structures or *hippocampus* were manually cut out from the mesh thereafter. To each vertex of this surface the value of the local cortical thickness was assigned.

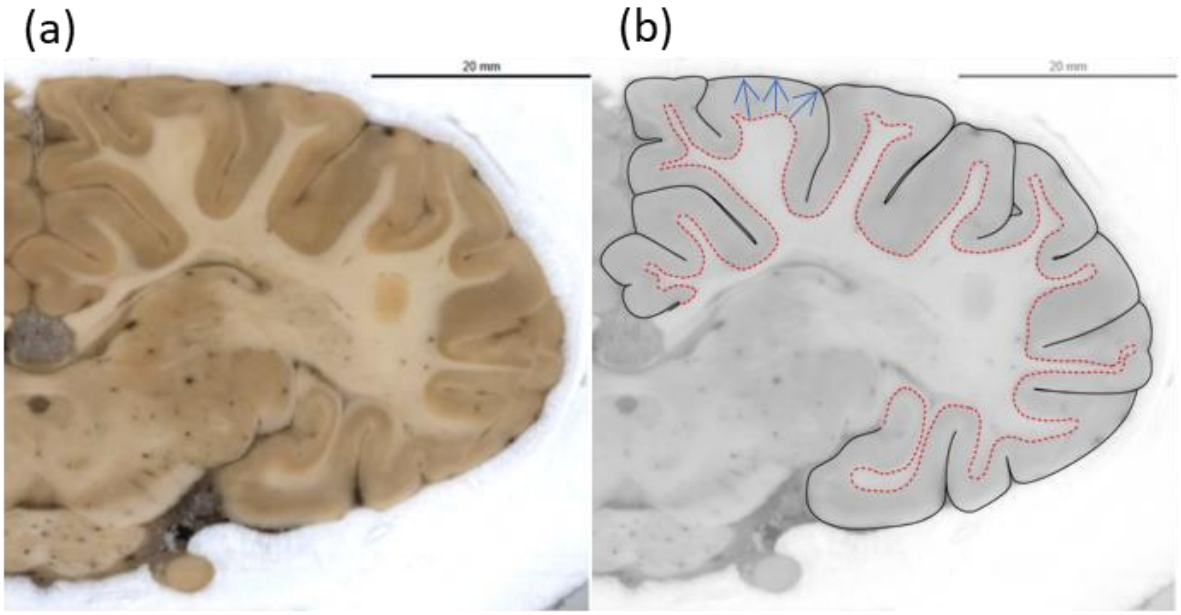

Figure 5: Determination of the cortical thickness. Contours of (a) a coronal blockface image of the harbour seal brain (left hemisphere of coronal section no.860) was used to determine the cortical thickness. (b) The blockface image with complete pial contour (black) and contour between white and grey substance (orange) of the brain on the particular slice overlaid. The arrows indicate the length of the field lines along the gradient of the Laplacian field. Scale 20 mm.

2.6. Determination of the Volumes of brain structures

Blockface Brain Background Segmentation

Annotations were derived from the gyrification index to effectively segment pixels representing both brain tissue and non-brain regions. The segmentation process involved selecting 10,000 randomly chosen pixels from each manually annotated section, which served as training data for a random forest classifier. This classifier was trained on a comprehensive dataset

comprising all manually annotated sections to enhance its predictive accuracy. After training, the classifier was applied to all sections to generate an initial mask representing the brain and its surrounding background. However, due to the inherent noise produced by the classifier, post-processing was necessary. To mitigate this noise, a two-dimensional Gaussian filter with a sigma of 3.0 pixels was employes, followed by thresholding at a value of 0.5. This smoothing step improved the mask's quality, ensuring a more accurate representation of brain tissue for subsequent analysis.

Mesh Generation

Following the creation of individual masked sections, these were combined into a 3D representation. This 3D data was analysed using the marching cubes algorithm implemented in ParaView (Ahrens et al. 2005; Ayachit 2015), enabling the generation of a detailed mesh of the brain structures. To refine the mesh further, a series of filters were applied using the software MeshLab (Cignoni et al. 2008). Initially, the mesh underwent Laplacian smoothing to enhance surface continuity and reduce irregularities. Subsequently, decimation was performed to decrease the number of vertices by 0.5%. This reduction in vertex count facilitated more efficient processing without significantly compromising the mesh's fidelity. Finally, the mesh was smoothed three additional times using the Laplacian smoothing algorithm to achieve an optimal surface quality.

Annotation

Each distinct brain structure was meticulously, manually annotated in two dimensions across at least every 10^{th} section, ensuring thorough representation of the anatomical features. For sections that were not directly annotated, interpolation was conducted using a Laplacian field approach, which allowed for seamless integration of the missing data. Subsequently, the 2D annotations were transformed into three-dimensional representations, generating a cohesive mesh as previously described.

Volume Measurement

The volume of the brain and its constituent structures was calculated using the generated three-dimensional section masks. These masks, representing the segmented brain regions, were analysed by quantifying the number of voxels contained within them. Each voxel, the three-dimensional equivalent of a pixel, is defined by a specific volume determined by its dimensions, in this case, 30 x 30 x 50 μm^3. By multiplying the total number of voxels identified in the mask by the volume of a single voxel, it is possible to obtain an initial estimation of the overall volume for the brain and individual structures. To assess the variability and reliability of the volume measurements, morphological operations were applied to the 3D-masks.

Specifically, dilation and erosion were performed, each by one voxel, to create a range of volume estimates. Dilation involves expanding the boundaries of the segmented regions, effectively increasing the number of voxels counted within the mask, while erosion contracts the boundaries, leading to a decrease in the voxel count. This dual approach allowed the capturing a more comprehensive range of potential volume measurements, accounting for the variability introduced by the segmentation process and the inherent uncertainties in anatomical delineation. The dilation operation provided an upper estimate of the volume, reflecting a more inclusive representation of the brain structures, while the erosion provided a lower estimate, reflecting a more conservative interpretation. Subsequently, the volumes were obtained from both the dilated and eroded masks to establish a variance range, providing insights into the potential variability and accuracy of the volume measurements. This methodical approach not only enhances the robustness of the volume estimations but also aids in understanding the structural complexities and anatomical variations present within the brain and its various regions.

2.7. 3D-POLARISED LIGHT IMAGING SETUP AND PROCEDURE

For the 3D-PLI process, brain sections were scanned using a polarising microscope (LMP-1, Taorad, Germany), as described in detail in previous research (Axer et al. 2011a; Axer et al. 2011b; Axer & Amunts 2022). This technique enables the detailed visualisation of nerve fibre architecture at a fine resolution of 1.3 µm. The setup involves placing the brain section between a rotating linear polariser and a stationary circular analyser, which consists of a quarter-wave retarder and an additional linear polariser. Illumination is provided by an incoherent white light emitting diode (LED), equipped with a band-pass filter centred at 550 nm with a ± 5 nm half-width.

As the linear polariser rotates across nine evenly spaced angles over 180°, a CCD camera captures the resulting intensity variations in the transmitted light. These intensity fluctuations at each pixel follow sinusoidal patterns, reflecting the orientation of myelinated nerve fibres. The light intensity at a given polariser angle ρ\rhoρ can be described using Jones calculus as:

$$I_{\rho} = \frac{I_T}{2} \times (1 + \sin(2\rho - 2\varphi) \times sin\ \delta) \quad (1)$$

I_T is called *transmittance* and reflects the light extinction behaviour of the brain tissue and represents the average of the sinusoidal intensity profile. φ describes the in-plane direction angle of a fibre axis and is referred to as *direction*. The *retardation* Δ includes some setup and tissue properties (section thickness, illumination wavelength, birefringence strength), in particular, the out-of-plane direction angle referred to as *inclination* α.

Consequently, the analysis of each pixel's intensity profile across rotation angles provides detailed information on local 3D fibre orientations described by φ and α, allowing for the spatial characterisation of fibre tracts in brain tissue sections.

2.7.1. PREPARATION, IMAGING AND COMPUTATIONAL ANALYSIS OF HARBOUR SEAL BRAIN TISSUE

3D-PLI was performed on *postmortem* harbour seal brain tissue. The preparation process included the following steps:

Fixation, embedding, and sectioning were performed following the previously outlined protocols. These sections were then mounted onto glass slides using Aquatex© (Merck, Germany) and covered with coverslips. Proper fixation and freezing were confirmed to preserve the integrity of myelin sheaths, provided that the *postmortem* interval did not exceed within 24 hours.

Imaging Protocol and Image Processing

This tissue preparation ensures high-resolution imaging of brain sections with accurate polarisation information, supporting detailed analysis of fibre orientation and tissue structure. Each brain section was imaged using 3D-PLI at 18 equidistant rotation angles of the polarimeter, ranging from 0° to 170°.

The accuracy of fibre orientation determination using 3D-PLI depends significantly on the quality of intensity profiles obtained. However, several external factors such as noise, light scatter, and absorption can interfere with the original sinusoidal intensity profiles. To mitigate these issues and refine the raw data, a two-step pre-processing approach was employed:

1. Pixel-wise Calibration: A standardised calibration technique was applied to correct inhomogeneities of the light source, the diffusor plate, the polar and retarder filters across the field of view, using flat-field images to account for variations introduced by the optical system.
2. Noise Reduction: Independent Component Analysis (ICA) was used to reduce noise and artifacts in the 3D-PLI images, improving the signal-to-noise ratio and enhancing the accuracy of subsequent analyses.

3D Fibre Orientation Map: Image Registration and Correction

To accurately reconstruct and analyse 3D fibre orientations from 3D-PLI data, it is essential to address distortions and misalignments between serial brain sections. Histological distortions and variations in section positioning were corrected using advanced image registration techniques. Initially, blockface images, which served as undistorted reference images, were 3D reconstructed through a 2D affine transformation without shearing, using a normalised

correlation similarity metric. Non-linear registration was chosen for its ability to handle complex distortions, and normalised mutual information was used as the similarity metric for multi-modality registrations. Once parameter maps were correctly aligned and corrected, they were used to create the 3D Fibre Orientation Map (3D-FOM). This map visualises fibre orientations as a vector field, where each vector represents the local fibre orientation in 3D space, calculated from direction and inclination angles (Axer et al. 2011a). The 3D-FOM effectively captures the overall brain anatomy, in particular structural details of fibres and their tracts. The accurate alignment, correction, and processing of 3D-PLI data enabled the generation of high-resolution 3D-FOMs, providing indispensable insights into the fibre architecture of the brain.

2.7.2. 3D POLARISED LIGHT IMAGING DATA MODALITIES

Due to the large number of key data modalities in this work, all data modalities are summarised in the following table for a better overview and clarity (Table 1). In addition, all data modalities were described in detail with help of their respective images.

Table 1: Overview of the data modalities used for the 3D-PLI of the harbour seal brain and the information they provide.

Data modality	Information
Retardation	Information on the phase shift of polarised light
Transmittance	Information on the amount of light that passes through the sample
3D-FOM	Comprehensive representation of the local orientation of nerve fibres

Retardation

Retardation (Figure 6) is a measure of the phase shift that occurs when polarised light passes through an anisotropic material, such as birefringent tissue. It refers to the difference in the phase between the ordinary and extraordinary rays of light as they travel through a sample. When polarised light enters a birefringent material, it splits into two components that travel at different speeds. This difference in speed causes one wave to lag behind the other, creating a phase difference, known as retardation. The amount of retardation depends on the thickness of the material, the wavelength of the light, and the optical properties of the sample, specifically its birefringence birefringence, i.e. the difference between the maximum and the minimum refractive index. In 3D-PLI, measuring retardation provides critical information about the orientation and density of fibre structures, such as nerve fibres in brain tissue. Areas with higher retardation typically indicate fibres that run within the sectioning plane (i.e., they have a low inclination angle and might share a common direction), while low retardation suggests a

more inclined and/or more complex organisation of fibres (e.g., fibre crossings). This information is crucial for reconstructing the three-dimensional microarchitecture of the tissue.

Figure 6: Example section of a retardation image of the harbour seal brain (section no. 825). Retardation in 3D-Polarised Light Imaging (3D-PLI) measures the phase shift of polarised light as it passes through birefringent tissue, revealing information about the orientation and density of fibre structures. It shows great contrasts between different fibre tracts. Scale 20 mm.

Transmittance

Transmittance (Figure 7) is the measure of the intensity of light that passes through a material relative to the intensity of incident light. In other words, it quantifies how much light is transmitted through a sample without being absorbed, reflected or scattered. It is often expressed as a percentage, with higher transmittance values indicating that a greater proportion of light passes through the material. In the context of 3D-PLI, transmittance provides information about the optical properties of the tissue, such as its transparency and density. Analysing transmittance helps identify gross-anatomical regions (grey and white matter, subcortical nuclei), but also regions of variations in tissue structure (e.g., in fibre orientation), composition, and section thickness. While grey matter and nuclei are typically bright, white matter tracts appear dark in transmittance maps. Within the deep white matter, the darkest structures are the most inclined ones in the section. This kind of information is of utmost importance and additionally supports delineation of anatomical (micro-)structures and brain regions.

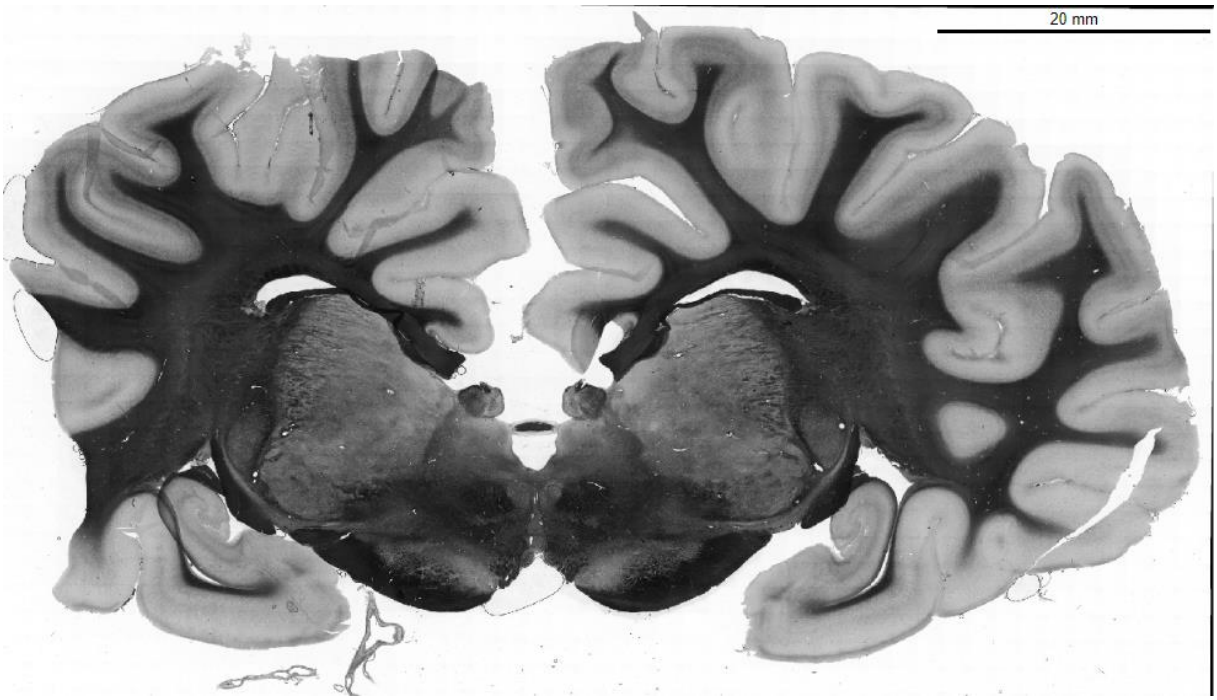

Figure 7: Example section of a transmittance image of a harbour seal brain (section no. 825). Transmittance in 3D-PLI quantifies the amount of light passing through a tissue sample, providing insights into its optical properties. Higher transmittance indicates greater light passage, aiding in the contrast and visualisation of the tissue's microarchitecture. Scale 20mm.

Fibre orientation map (3D-FOM)

3D-FOM (Figure 8) is a detailed representation of the 3D orientation of fibres and is composed from the independently extracted direction and inclination angles (cf. equation 1).

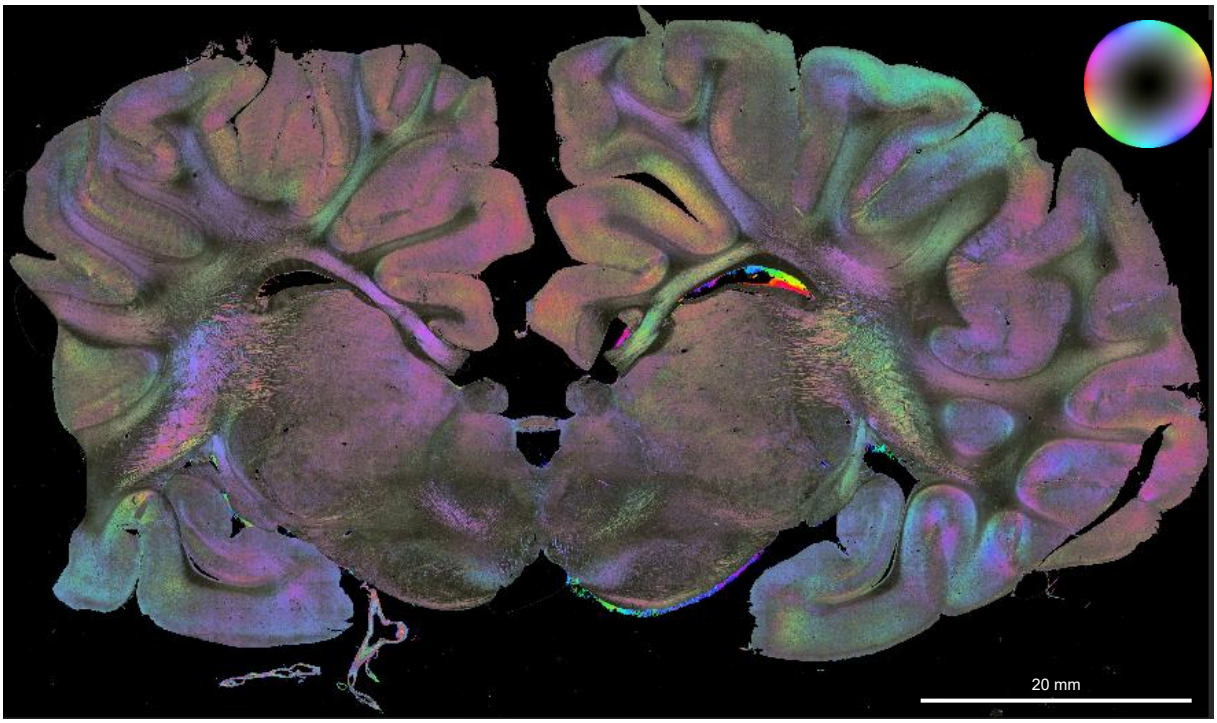

Figure 8: Example section of a 3D-FOM of a harbour seal brain (section no. 825). It visualises the spatial orientation and trajectories of fibres within tissue. It is the fundamental data to derive the brain's connectivity. Individual fibre orientations are colour-coded as shown in the colour sphere on the top right. Scale 20 mm.

The orientations of the fibre tracts can be precisely described and visualised using a colour sphere (Figure 8, top right), where each colour uniquely represents a specific spatial direction. In this mapping, different hues correlate with distinct orientations; for instance, a red hue indicates a horizontal alignment of fibres, while light blue corresponds to a vertical alignment. Additionally, the saturation of the fibre colouration provides information about their inclination: as the fibres appear progressively darker, this signifies an increase in their angular steepness. Thus, both colour and saturation within the colour sphere allow for a comprehensive assessment of fibre tract orientation, facilitating a nuanced understanding of spatial alignment in three-dimensional tissue structures.

2.8. CRESYL VIOLET STAINING

Cresyl violet staining is a histological technique commonly used to visualise and differentiate the cellular components of neural tissue, particularly the endoplasmic reticulum (Takahashi et al.). Cresyl violet is a basic dye that binds to acidic components of the cell, such as nucleic acids in the nucleus and ribosomal ribonucleic acid (RNA) in the cytoplasm, highlighting these structures in purple or violet. This staining method is often used to identify and examine the morphology of neurons and their cell bodies (soma), as well as to visualise the Nissl substance

(also called Nissl bodies), which consists of rough endoplasmic reticulum and ribosomes. The Nissl substance is abundant in the soma and dendrites of neurons, making cresyl violet particularly effective for identifying neurons in brain and spinal cord tissue.

To perform cresyl violet staining on the sections, it was necessary to remove the coverslips from those sections that had already been processed for 3D-PLI measurements. The process of removing the coverslip poses a risk of causing various forms of mechanical or structural damage to the delicate tissue, including potential tearing or deformation of the sample. To mitigate such risks, the sections were handled with extreme care.

Following the removal of the coverslip, the tissue sections were gently rinsed with phosphate-buffered saline (PBS) to remove any residual mounting medium or contaminants. After this initial step, the sections were mounted onto slides using a gelatine-based solution to ensure proper adhesion and flattening of the tissue. The slides were then placed on a heating plate set to +37°C and allowed to dry overnight, ensuring gradual dehydration and secure fixation of the tissue to the slide. The staining procedure (Table 2) was carried out according to established laboratory protocols, utilising a 0.025% cresyl violet acetate staining solution.

Table 2: Laboratory protocol for cresyl violet staining. The protocol shows the exact steps, chemicals and staining times for our harbour seal sections.

No.	Time	Working step	Time
1	20 min	Filtered cresylecht violet acetate staining solution 0.025%	20 min
2a	Dip for at least 30 sec	remove excess dye (Apo-H2O/MilliQ)	2 min
2b	max. 2 h	Leave OT in Apo-MilliQ until it is differentiated	✓
3a	1 min - on stirrer and move	Differentiation: 70% ethanol	1 min
3b	2 min - on stirrer and move	Differentiation: 70% ethanol	1 min
4	Differentiate on stirrer and move 1 min to 20 min	Microscope control (differentiation): 96% ethanol + 0.025% acetic acid	7 min
	If the differentiation is too strong, the sections can be immersed in 70% alcohol for 2 min and then re-stained for 1-5 min, then repeat from step 4.		
5	1 min	Dehydration: 100% absolute ethanol	1 min
6	1 min	Dehydration: 100% absolute ethanol	1 min
7	Dip	Rinse off the alcohol in xylene	✓
8	at least 15 min	Dehydration: xylene	✓
9	at least 15 min	Dehydration: xylene	✓
10	Covering	Covering: DPX medium (for xylene + XEM)	✓

This precise staining time and concentration of cresyl violet (Table 2 and Table 3) was chosen to enhance the visualisation of neuronal cell bodies while preserving the overall structural integrity of the sample. The staining process provides high contrast, enabling detailed examination of the cytoarchitecture, particularly the distribution of Nissl bodies within the neurons. This methodological approach is crucial for subsequent histological analysis and comparison with 3D-PLI data, as it allows for the detailed correlation of fibre orientation with cellular organisation.

Table 3: Protocol for 3 litres of the 0.025% staining solution for the cresyl violet staining with the quantities of the chemicals used. The protocol for preparing the ethanol solution (S1) and the corresponding list of chemicals (S2) are detailed in appendix 1.

Quantities	Chemicals
3.8 g	sodium acetate, anhydrous
6.6 ml	glacial acetic acid (100% acetic acid)
700 mg	cresyl violet acetate
Fill up to 3 L	Pharmacy water or bi-dest. water (distillation)
Filtered (with vacuum filter)	
Durability: At present it has been proven that the solution can be used for 2 weeks. If there are any abnormalities in the staining result, replace completely.	
Storage: Protected from light at room temperature	

2.8.1. CRESYL VIOLET DATA MODALITY

The staining of tissue (Figure 9) sections allows for the detailed visualisation of the laminar organisation within the LGN and the visual cortex. The ability to visualise the cellular and laminar composition is particularly valuable in studying the functional organisation of the LGN and visual cortex, as these areas are critical for the processing and relay of visual information.

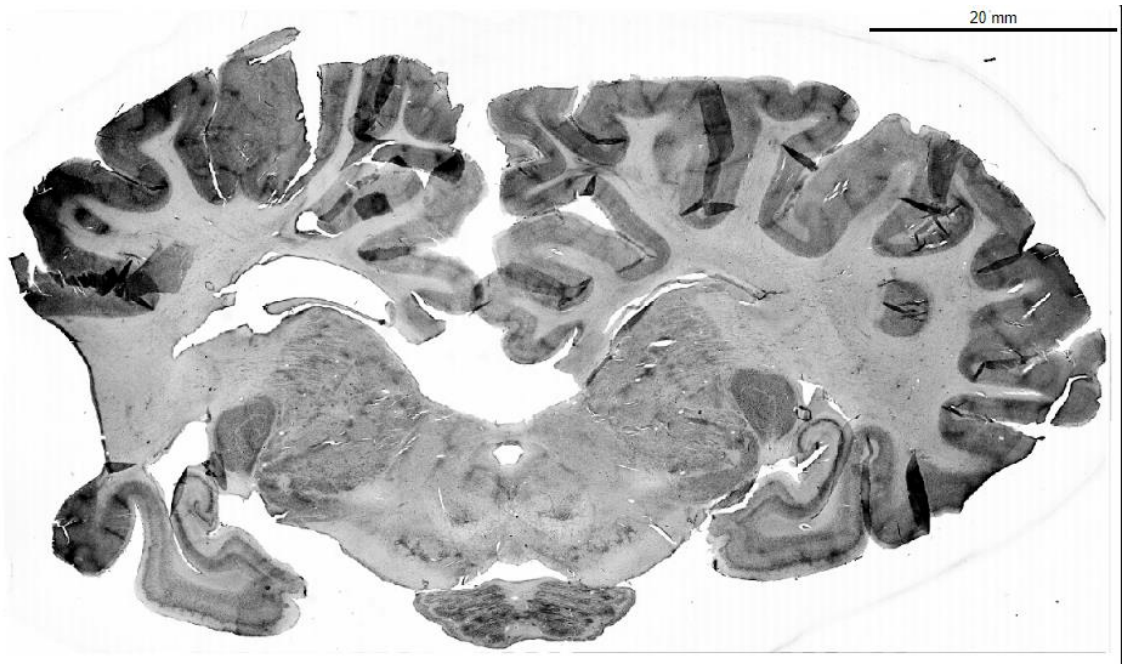

Figure 9: Example section of a cresyl violet staining of d harbour seal brain (section no. 826). Cresyl violet staining highlights neurons by binding to nucleic acids and Nissl substance in the cell bodies, allowing visualisation of neuronal morphology and distribution. It is widely used to assess neuronal density and detect structural changes in neural tissue. Scale 20 mm.

3. RESULTS

In the following sections, the results are predominantly presented as selected excerpts from the various imaging modalities employed in the study. Due to the bilateral symmetry of the structures under investigation, the anatomical features are consistently presented on both the left and right side of the brain. However, to maintain clarity and streamline the presentation, images from the left hemisphere are primarily used, also because the right hemisphere was not intact (cf 2.1). This approach not only simplifies the data presentation but also ensures that the observations and conclusions drawn are representative of both hemispheres.

3.1. QUALITATIVE NEUROANATOMY OF THE HARBOUR SEAL BRAIN

The brain of the harbour seal (*Phoca vitulina*) presents some unique morphological features, as evidenced by the examination of 1,668 50 µm thick frontal sections. The overall shape of the brain is rather egg-shaped (Figure 2), with notable *anterior-posterior* (AP) compression at the *anterior* pole. At the junction of the frontal lobe and the temporal lobe lies the Sylvian fissure (*Fissura Sylvii*) (Figure 2), remarkable for its extraordinary depth. Beneath this posterior part lies the broad, elongated, but very flattened cerebellum in the frontal direction (Figure 2).

In the frontal sections (Figure 10) it is shown that the gyri and sulci of the two hemispheres of the harbour seal brain are not completely symmetrical. One of the most striking observations in these sections is the relationship between the cerebrum and the cerebellum. The cerebellum, particularly its *posterior* two-thirds, is largely covered by the cerebrum. Additionally, a strong folding of the cortex can also be observed in all sections.

The blockface images presented in Figure 10 represent a foundational dataset advancing towards the development of a comprehensive 3D anatomical atlas. These images reveal a high degree of clarity in several anatomical structures and fissures, enabling detailed observation and analysis.

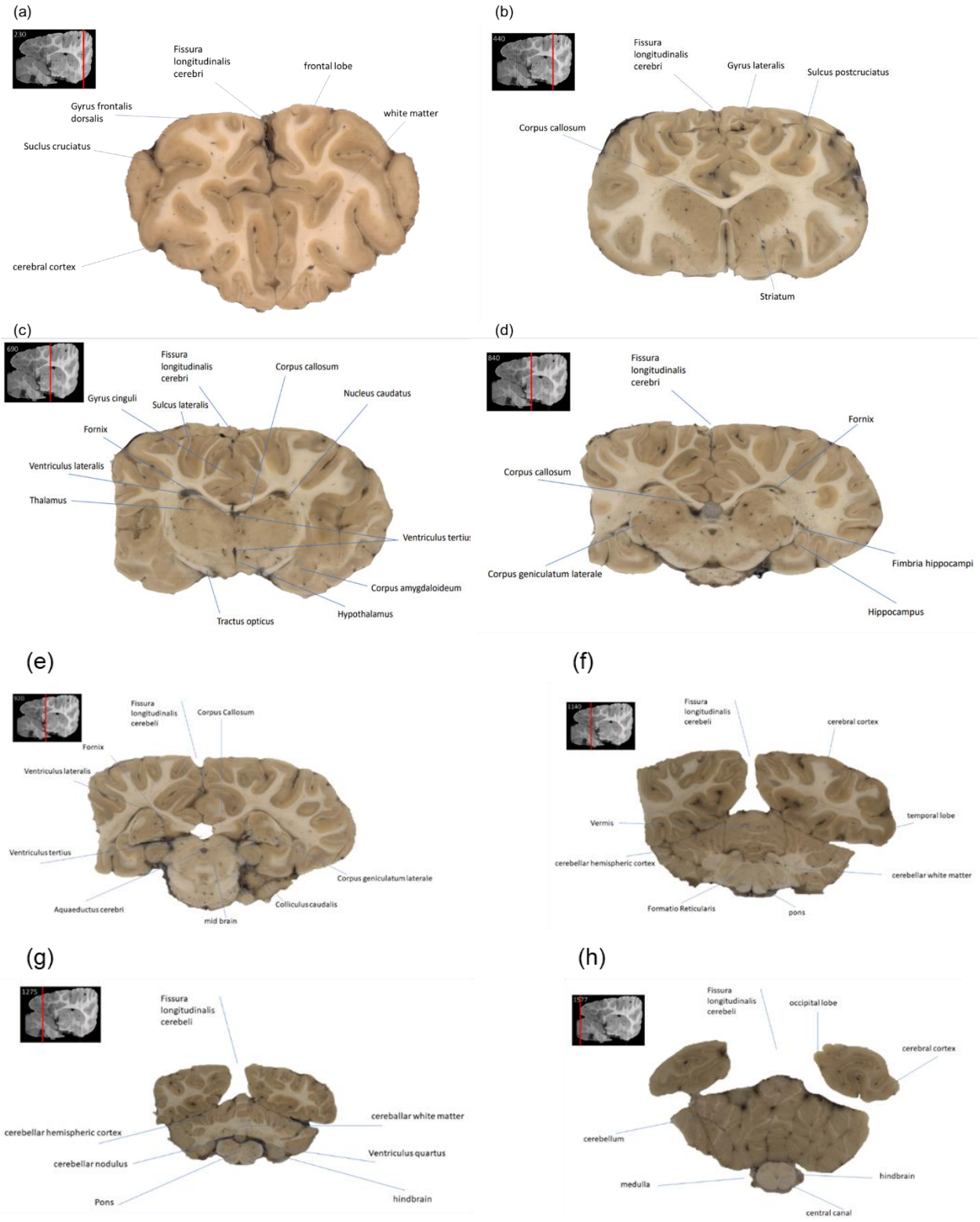

Figure 10: Coronal sections from different areas of the harbour seal brain with anatomical labelling for individual regions or structures. The image located in the upper left corner illustrates the specific region of the entire brain from which the depicted cross-section has been extracted. (a) slice no. 230 (b) slice no. 440 (c) slice no. 690 (d) slice no. 840 (e) slice no. 920 (f) slice no. 1140 (g) slice no. 1275 (h) slice no. 1577.

3.1.1. *NUCLEUS CAUDATUS*

The caudate nucleus is a C-shaped, paired structure located deeply within the brain. It is part of the basal ganglia. The caudate nucleus (Figure 11a and appendix 2 S1) is situated in the *lateral* wall of the *lateral* ventricles, making it the most prominent nuclei in the basal ganglia. It runs in a C-shape from the *rostral* (front) of the brain to the *caudal* back. The *anterior* (front) portion of the caudate nucleus is called the head and lies lateral of the *anterior* horn of the *lateral* ventricle. The middle portion is called the body, which lies next to the *thalamus* and the *posterior* (tail) portion extends around into the *temporal* lobe, extending anterior to the *amygdala*. The caudate nucleus is separated from the *putamen* (another component of the basal ganglia) by the internal capsule.

The most *anterior* portion of the *anterior thalamus* is identifiable bilaterally down to section 574, providing a precise anatomical reference for the location of this key subcortical structure. In contrast, the *caput nuclei caudati* extends more rostrally, with the right side starting at section 320 and the left side to section 311.

Between sections 548 and 597, the *nucleus accumbens* emerges in the medio-ventral region, a critical area involved in reward and motivational circuits. Its interconnectivity with the caudate nucleus is evident between sections 546 and 564, where these two structures appear to merge. However, the precise ventral extent of the caudate nucleus in this region is challenging to delineate with certainty.

Anteriorly, starting from section 376, the caudate nucleus becomes more clearly distinguishable from the surrounding white matter. This clear demarcation provides a reliable landmark for the study of the caudate's structural boundaries. The long, dark grey *cauda nuclei caudati* (tail of the caudate nucleus) is traceable in the occipital direction, where it resides *lateral* to the *lateral* ventricle. It follows the curvature of the ventricle towards the hippocampal fimbria.

In sections 904 (left) and 919 (right), the point at which the caudate nucleus bends rostrally towards the *hippocampus* is clearly visible as a prominent grey stripe on the *dorsal* aspect of the *lateral* ventricles. This region is of particular interest, as it marks the transition of the caudate's tail into a more limbic-oriented function. Below this zone, the tail of the caudate follows a rostral trajectory before terminating dorsally to the hippocampal fimbria in sections 777 (left) and 795 (right), further emphasising the close anatomical relationship between the caudate and hippocampal formation.

Fibre orientation of *Nucleus caudatus*

The *dorsal* striatum (Figure 11b) in this section exhibits the characteristic striatal fibre bundles that interlink the *caput nuclei caudati* with the large globus pallidus and the relatively small *putamen* located ventro-laterally.

The *nucleus accumbens* disassociates from the caudate nucleus behind section 560, drops in ventral direction collateral to the fornix passing the anterior commissure dorsally and forms a pathway to the mesencephalon from section 597 onwards. This *ventral* region, positioned *anterior* to the *bed nucleus* of the *stria terminalis*, is characterised by a high density of oriented sagittally fibre bundles. These fibres traverse in a *rostro-ventral* direction, extending through the basal telencephalon.

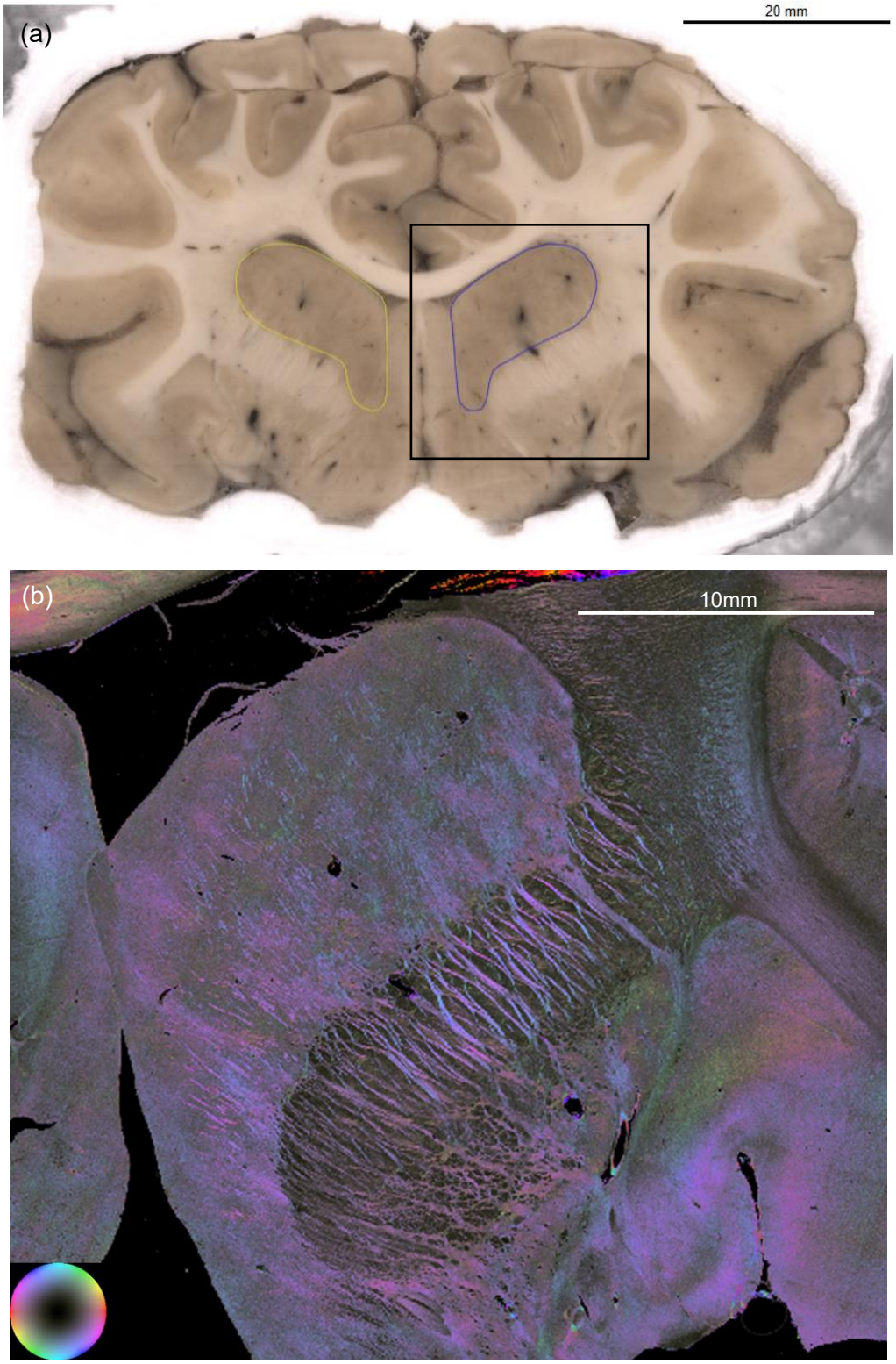

Figure 11: Position of the caudate nucleus in the blockface image of a harbour seal brain of section no. 520 and detailed images of the caudate nucleus in the 3D-FOM in section no. 520. The square (black) delineates the specific region from which the image section presented in panel (b) was extracted. (a) Labelling of the caudate nucleus on the right (yellow) and on the left (blue) for the determination of the structure in the harbour seal brain. (b) 3D-FOM of section no. 520 on the left hemisphere. The 3D-PLI analysis reveals the presence of fibre bundles in the striatum crossing the internal capsule ventro-laterally from the caudate nucleus into the *putamen*. The orientation and directionality of these fibres are clearly depicted using the colour sphere representation (blue magenta). Scale (a) 20 mm, scale (b) 10 mm.

3.1.2. *CORPUS AMYGDALOIDEUM*

The *amygdala* (Figure 12) in the harbour seal brain can be anatomically subdivided into two primary regions: the pallial or cortical *amygdala*, and the subcortical or primary *amygdala*. The primary *amygdala*, characteristic of its almond-like shape, is located deep within the temporal lobe, just inferior to the uncus. This structure occupies the *rostral* portion of the hippocampal formation, extending into the *anterior* region of the inferior horn of the *lateral* ventricle.

The primary *amygdala* is closely associated with the peri-amygdaloid cortex, contributing partially to of the cortical surface of the uncus. This integration of the *amygdala* with the surrounding cortical and subcortical structures underlines its central role in coordinating sensory input with emotional responses.

In the blockface images, the trajectory of the piriform cortex, an olfactory-related region, can be traced with clarity along the path of the olfactory bulb at the rhinal fissure towards the *occipital* lobe. However, as the sections progress, it becomes increasingly difficult to distinguish the piriform cortex from other parts of the rhinencephalon, particularly after a certain point, due to the blending of these olfactory regions. This gradual loss of distinction may reflect the merging of related cortical areas involved in olfactory processing.

Within the subcortical *amygdala*, the *lateral* and *medial* nuclei are distinctly visible. These nuclei are key components of the *amygdala's* functional architecture, with the *lateral* nucleus receiving sensory input and the *medial* nucleus being involved in the control of emotional and autonomic responses. The ability to clearly delineate these nuclei highlights the functional compartmentalisation of the *amygdala*, where different subregions are specialised for various aspects of emotional and behavioural regulation.

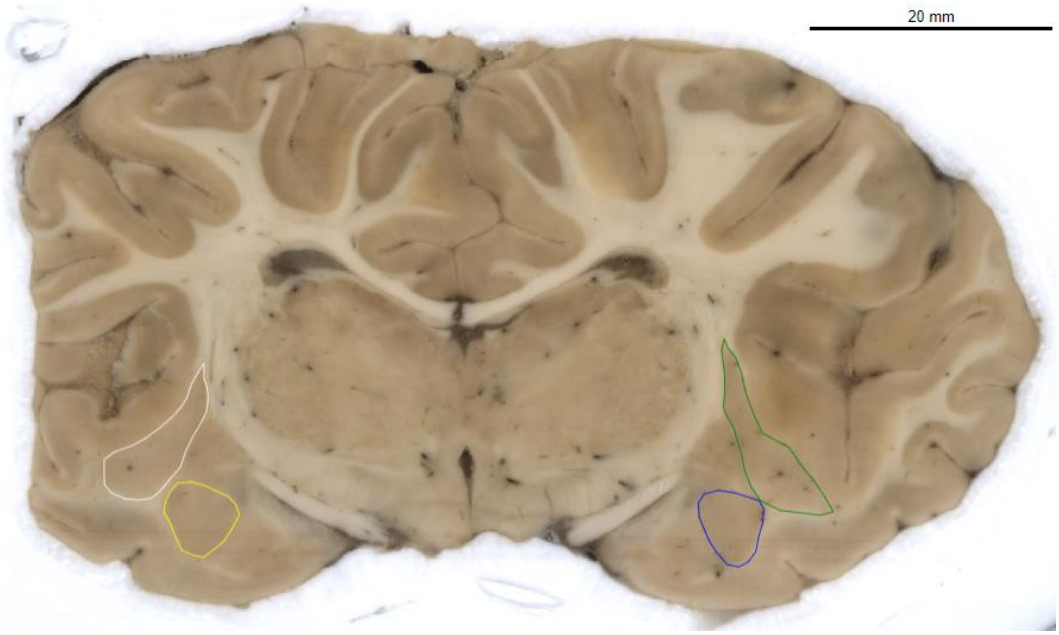

Figure 12: Position of the *amygdala* in the blockface image of a harbour seal brain of section no. 690. Labelling of the pallial *amygdala* on the left (green), the lateral part of the subcortical *amygdala* on the left (blue) and the pallial *amygdala* on the right (white), the subcortical *amygdala* on the right (yellow). Scale 20mm.

3.1.3. *HIPPOCAMPUS*

The *hippocampus* (Figure 13a and appendix 2 S2) in the harbour seal brain spans from section 692 to at least section 1015 on the right (where the structure is interrupted) and to section 1030 on the left. It extends considerably in the occipital direction and entirely vaults over the geniculate bodies, as illustrated in Figure 13.

The *hippocampus* in this species encompasses its classic components, including the *fimbria, cornu ammonis*, dentate gyrus, and the *subiculum*, which serves as a transitional zone, between the *hippocampus* and the neocortex. The fimbria runs along the medial surface of the *hippocampus*, containing fibres that connect the *hippocampus* to other brain regions, while the *cornu ammonis* and dentate gyrus form the primary structure of the hippocampal formation.

The boundary between the *hippocampus* and the entorhinal cortex is particularly visible behind the *cornu ammonis*, where the characteristic striate appearance of the archicortex ends, marking the transition zone where the *tractus perforans* pierces the grey matter of the subiculum.

Fibre orientation of *hippocampus*

The *hippocampus* (Figure 13b) is a crucial structure within the medial temporal lobe of the brain. Its unique layered structure is defined by several subregions, each characterised by

specific anatomical and functional properties that contribute to the *hippocampus's* overall role in neural processing and memory storage. The primary subregions of the *hippocampus* include the *dentate gyrus*, the *Cornu Ammonis (CA) regions*—which encompass CA1, CA2, and CA3—and the *subiculum*.

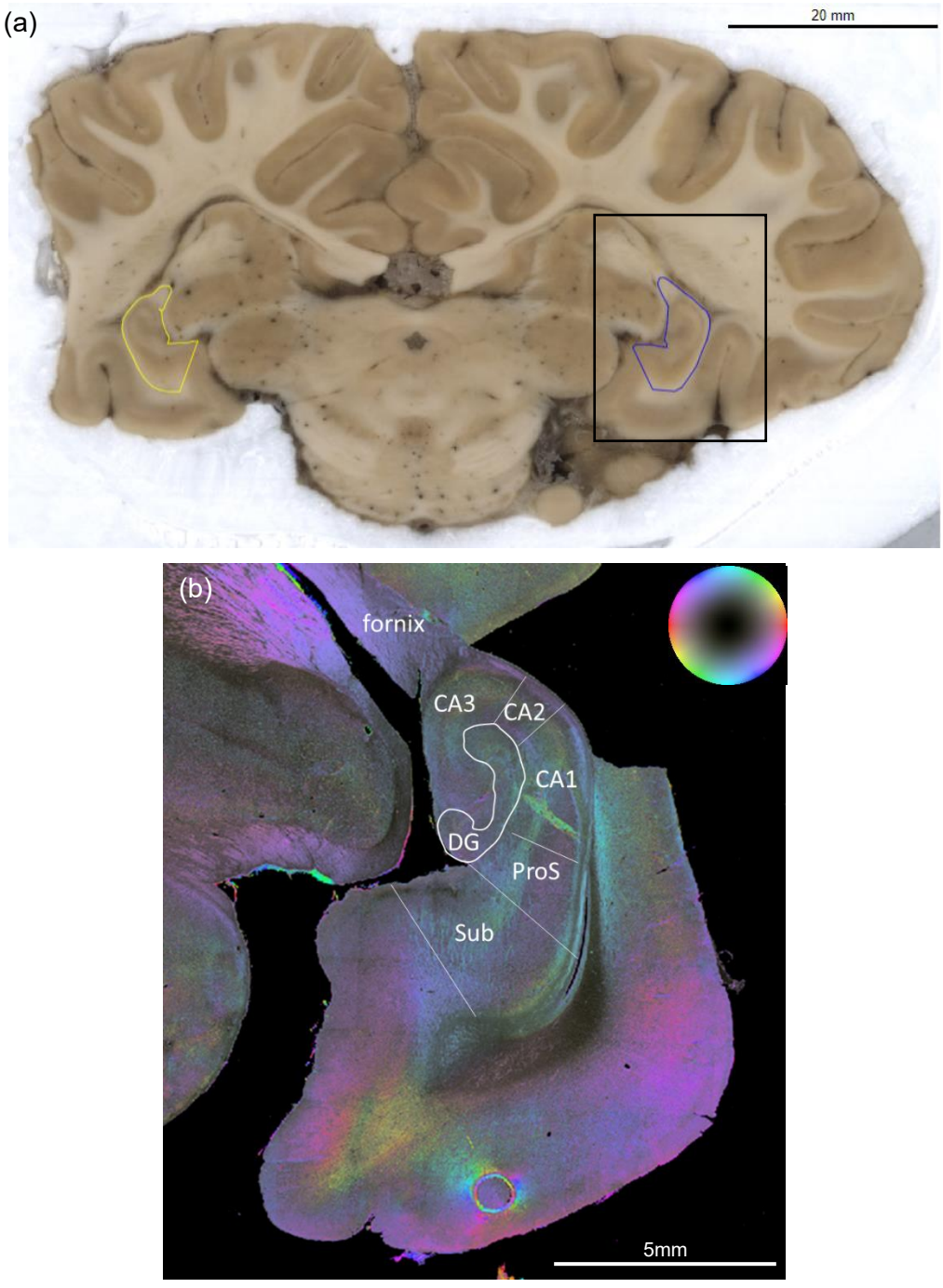

Figure 13: Position of the *hippocampus* in the blockface image of a harbour seal brain of section no. 905 and detailed images of the *hippocampus* visible in the 3D-FOM in section no. 905. The square (black) delineates the specific region from which the image sections presented in panels (b) were extracted. (a) Labelling of the *hippocampus* on the right (yellow) and on the left (blue) for the determination of the structure in the harbour seal brain. (b) 3D-FOM of section no. 905 shows the cornu ammonis and the neighbouring subiculum penetrated by the perforant tract. The orientation and directionality of these fibres are clearly depicted using the colour sphere representation. Scale (a) 20 mm, scale (b) 5 mm.

3.2. VISUAL SYSTEM

3.2.1. *CORPUS GENICULATUM LATERALE ET MEDIALE*

Both the LGN (Figure 14a and appendix 2 S3) and *medial geniculate nucleus (*MGN) are located within the *thalamus*. The LGN in the harbour seal brain is first observable in sections 812 on the left and 815 on the right, extending occipitally to at least sections 963 on the right and 968 on the left. The LGN is ventrally separated from the *pulvinar* by the *brachium colliculi*, a notable anatomical distinction in the visual pathway. A key observation in the seal is the presence of a single pair of geniculate bodies.

The LGN is distinctly separated from the MGN by a prominent bright stripe of white matter. This separation is crucial as it delineates two functionally distinct sensory nuclei: the LGN is associated with visual processing, lying between the optic tract and the optic radiation, while the MGN is part of the auditory pathway, located between the *brachium colliculi* and the acoustic radiation, which is positioned rostrally to the Meyer loop. This anatomical layout underlines the separate yet parallel processing streams for visual and auditory information.

The MGN extends from section 920 on the right and 923 on the left, and its rostral boundary coincides with areas similar to those of the LGN (sections 812 on the left and 815 on the right). The fibres of the MGN run horizontally, parallel to the acoustic radiation, further emphasising its role in auditory signal transmission.

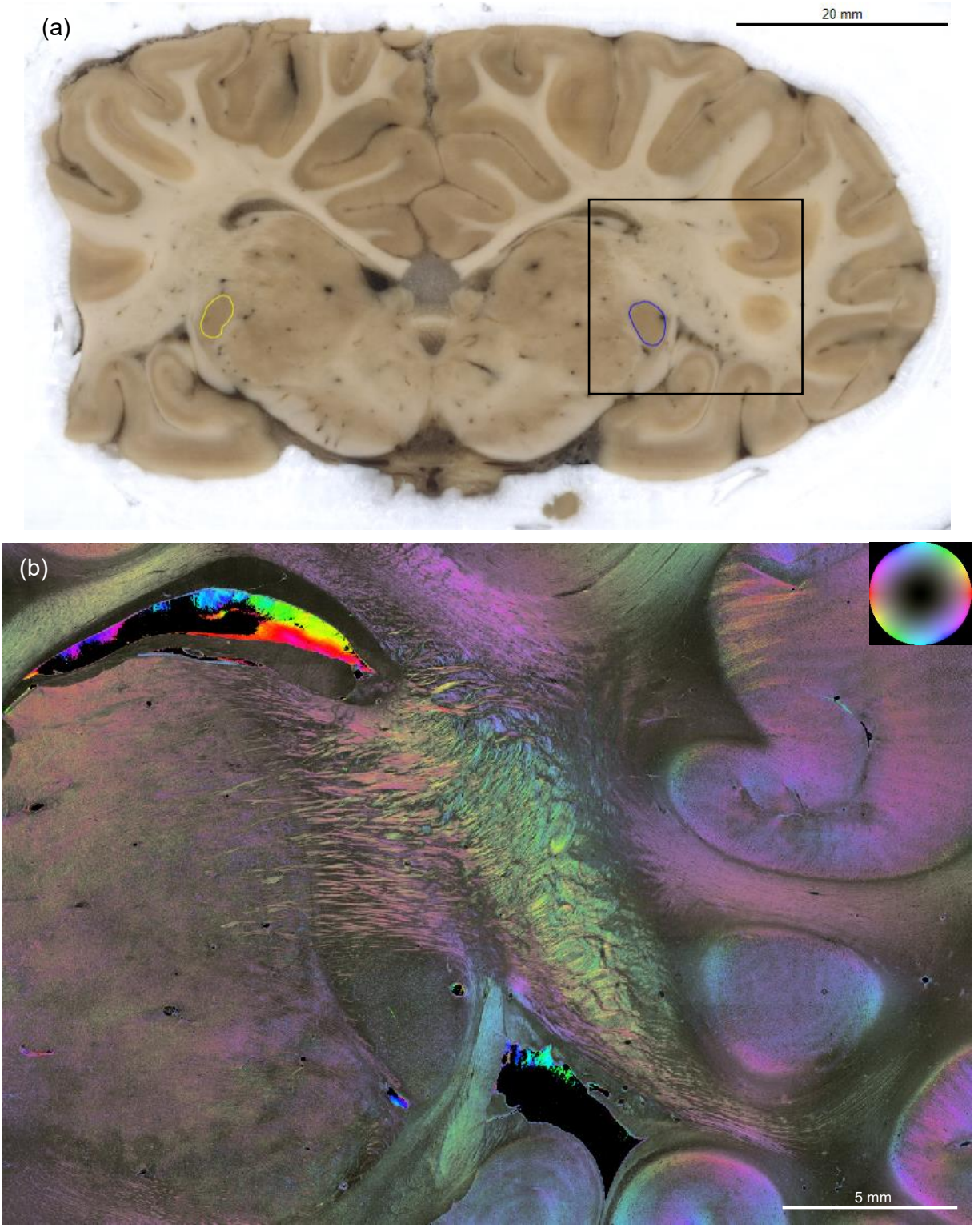

Figure 14: Position of the LGN in the blockface image of the harbour seal brain of section no. 825 and detailed images of the LGN visible in the 3D-FOM. The square (black) delineates the specific region from which the image sections presented in panel (b) was extracted. (a) Labelling of the LGN on the right (yellow) and on the left (blue) for the determination of the structure in the harbour seal brain. (b) 3D-FOM of section no. 825, used for fine localisation of the structure and first input about fibre orientation surrounding the LGN. The 3D-PLI analysis reveals the presence of fibre bundles extending from the occipital region towards the LGN. The orientation and directionality of these fibres are clearly depicted using the colour sphere representation. Scale (a) 20 mm, scale (b) 5 mm.

Fibre orientation of LGN

The LGN, which is abundantly populated with cell bodies and dense individual fibres, is prominently visible at section 825. These fibres (Figure 14b) are oriented steeply and extend from the occipital region towards the LGN. At this level, the optic tract remains completely distinct, not yet merging with its target region in the LGN. This fusion begins progressively, starting from section 840 and continues upward. The dense fibre network located dorsally to the LGN predominantly consists of thalamocortical projections and spinal afferents, both of which traverse through the internal capsule.

The *optic radiation* does not appear prominently until further *posterior* sections, emerging earliest at section 840, where its development becomes evident as it approaches the *occipital* regions. This appearance suggests a gradual transition and integration of visual processing fibres extending towards the V1.

At this stage, the LGN is bilaterally enveloped by the *fornix* from a dorsal position and by the *fimbria hippocampi* laterally, situated slightly *posterior* to the *optic radiation* (Figure 15). The LGN appears distinctly divided. The optic tract, approaching from a ventral direction, fully reaches the LGN at this section, indicating its direct involvement in conveying visual information from the retina to the brain. Notably, the tract's extensions seem to curve around the *pulvinar* towards the *tegmentum*, hinting at complex interactions between visual and associative processing regions. The space between the LGN and the medially located MGN is characterised by the presence of three major fibre tracts: the optic radiation, the optic tract, and the acoustic radiation. These tracts are intricately interwoven, making it challenging to distinguish between them in this region. However, despite this overlapping fibre architecture, the core regions of the LGN and MGN are well-defined and distinctly separated, highlighting their respective roles in visual and auditory processing pathways.

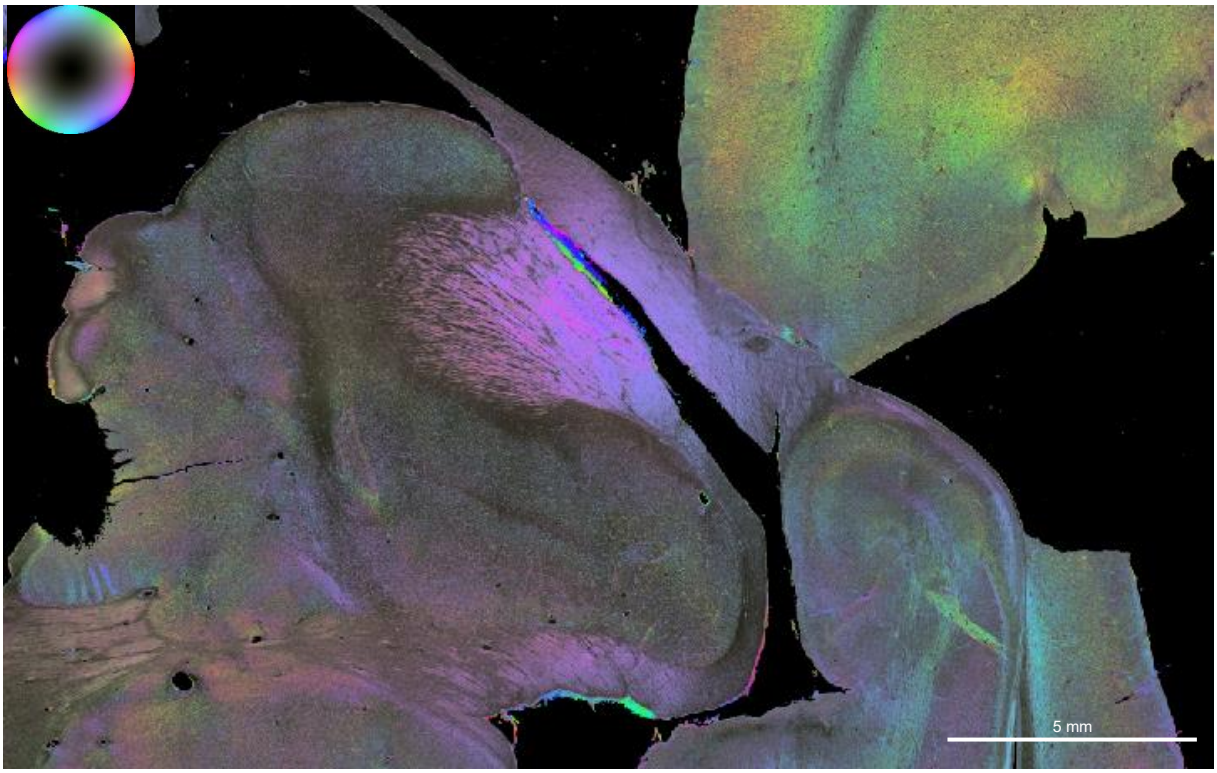

Figure 15: Enlargement of the calculated 3D-FOM of the harbour seal brain of section no. 905. The 3D-PLI analysis reveals the core regions of the LGN and MGN and the distinct separation. The tract's extensions seem to curve around the pulvinar towards the tegmentum. The orientation and directionality of these fibres are clearly depicted using the colour sphere representation. Scale 5 mm.

Layering of the LGN

The LGN is a crucial structure located in the thalamus. This complex structure is organised into several distinct layers (Figure 16b), which contains magnocellular and parvocellular layers. This unique structure consists of at least two broad layers of neurons, composed of grey matter, interspersed with white matter formed by optic fibres (Figure 16).

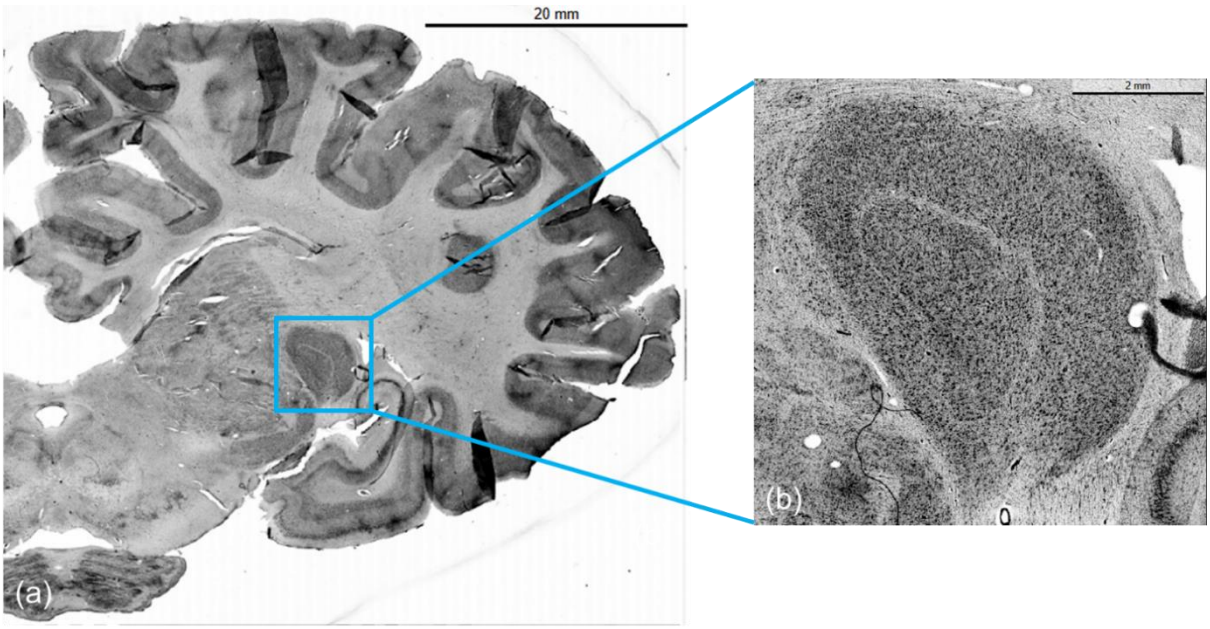

Figure 16: Histological staining with cresyl violet of a section of the harbour seal brain: (a) Depiction of the left hemisphere of section no. 826, stained with cresyl violet. (b) Magnified view of the LGN, clearly illustrating its distinct laminar structure. Scale (a) 20 mm, scale (b) 2 mm.

3.2.2. VISUAL CORTEX

The visual cortex (Figure 17a and appendix 2 S4) in the harbour seal brain is situated within the *occipital* lobe. It encompasses several adjacent structures integral to the visual and sensory pathways, including the primary auditory cortex, the LGN, and the superior colliculus. A distinguishing feature of the V1, also known as the striate cortex, is the Gennari stripe (Balaram et al. 2014). This stripe, a dense band of myelinated fibres, is visible in layer IV of V1. In the harbour seal, the Gennari stripe represents the termination of axons projecting from the LGN. The visual cortex in the harbour seal extends from section 1,260 to approximately section 1600, with a slight asymmetry between the left and right hemispheres. On the left hemisphere, the visual cortex is discernible up to section 1,590, while it extends to section 1,600 on the right. Layer IV, where the Gennari stripe is prominent, is densely packed.

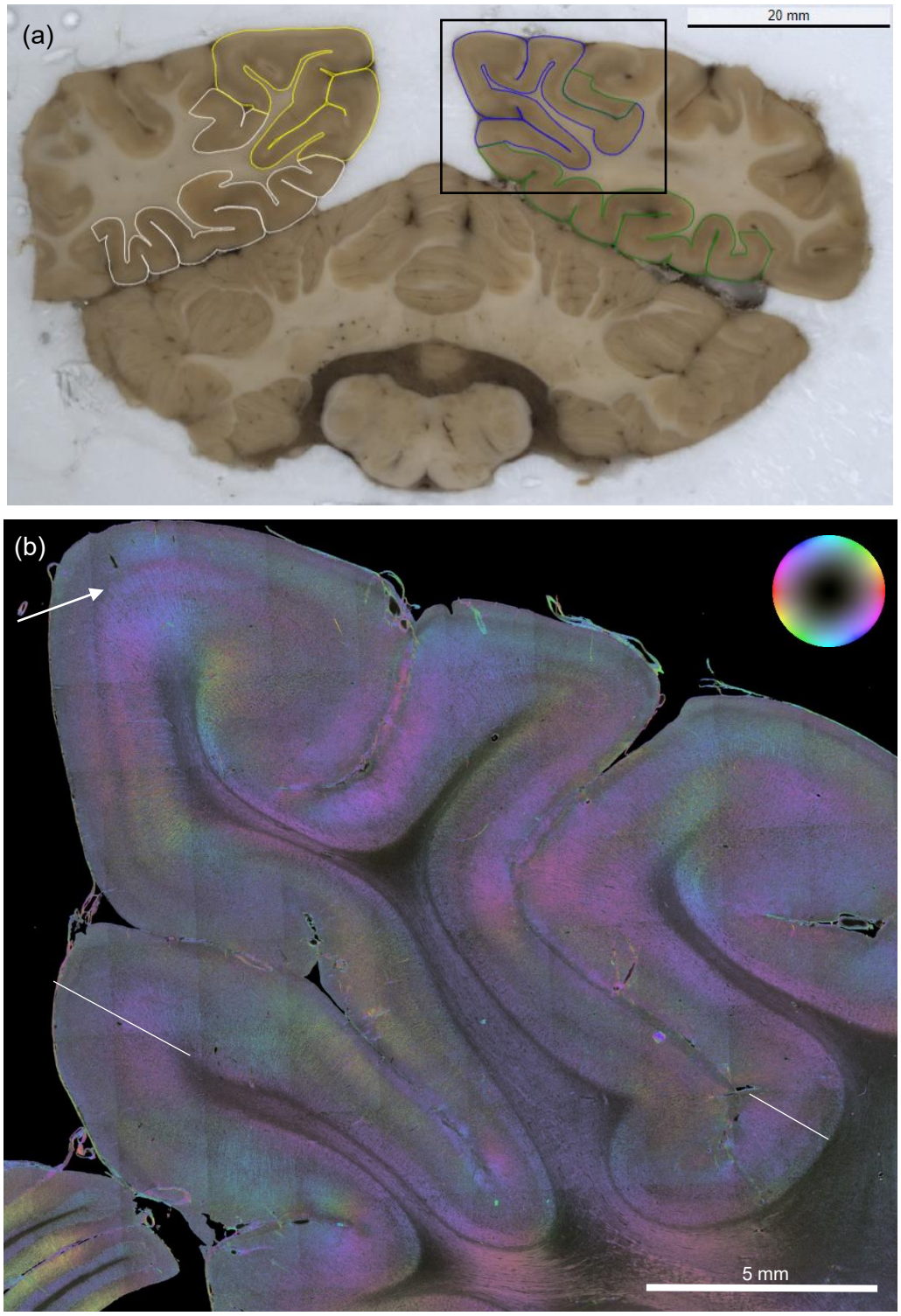

Figure 17: Position of the primary visual cortex in the blockface image of a harbour seal brain of section no. 1,310 and detailed image of the primary visual cortex visible in the 3D-FOM. The square (black) delineates the specific region from which the image sections presented in panel (b) was extracted. (a) Labelling of right primary visual cortex (V1: yellow) and V2 (white). Left primary visual cortex (V1: blue) and V2 (green). (b) 3D-FOM of section no. 1,305. The 3D-PLI analysis reveals the Gennari stripe (white arrow) presents in the colour characteristic of transverse representation. The white lines indicate the border of V1 and V2. The orientation and directionality of these fibres are clearly depicted using the colour sphere representation. Scale (a) 20 mm, scale (b) 5 mm.

Fibre orientation of the visual cortex

The visual cortex is marked by a greater density of transverse fibres, particularly in the V1 (Figure 17b). Here, these fibres manifest as the Gennari stripe, located in layer IVb. At the interface between the primary and secondary visual cortices, this pronounced pattern gradually diminishes. This transition results in a markedly more homogeneous internal granular cell layer (Lamina IV), characterised by a reduction in the defining transverse fibres.

Moreover, the gradual transition of subsequent visual cortex segments into non-visual isocortical areas is marked by a decrease in fibre density, which corresponds to a significant increase in transmittance. This attenuation in fibre density and increase in transmittance further delineate the transition from visually dedicated cortical regions to those involved in broader cortical processing functions.

The Gennari stripe, a notable indicator of the primary visual cortex architecture, is particularly well-defined on the 3D-FOM (Figure 17b). Here, it is identifiable by its transverse fibre organisation, which exhibits distinct morphological variations. In cortical sections with convex or concave curvature on the 3D-FOM, the Gennari stripe appears in the colour characteristic of transverse representation, reflecting the unique orientation of these fibres. Conversely, in regions where the cortex appears linear, the transverse fibres exhibit as extinction bands. This variation in appearance across different cortical conformations not only assists in identifying the Gennari stripe but also in mapping the overall organisation of transverse fibre architecture in the visual cortex.

Cortical Layering of the Visual Cortex

It seems that the visual cortex of the harbour seal follows a five-layered structure (Figure 18), with the Gennari stripe (Figure 19) in layer IV serving as a prominent marker for the region.

Figure 19 illustrates a relatively uniform thickness across layers I, II, and IVa. Similarly, layers III, IVc, and V exhibit comparable thicknesses. Notably, layer IVb, which contains the Gennari stripe, is identified as the thinnest layer (Figure 19). In contrast, Figure 18 reveals a different pattern: layer III is the thickest, while layer I is the thinnest. Layers II, IVb, and V demonstrate comparable thicknesses in this depiction.

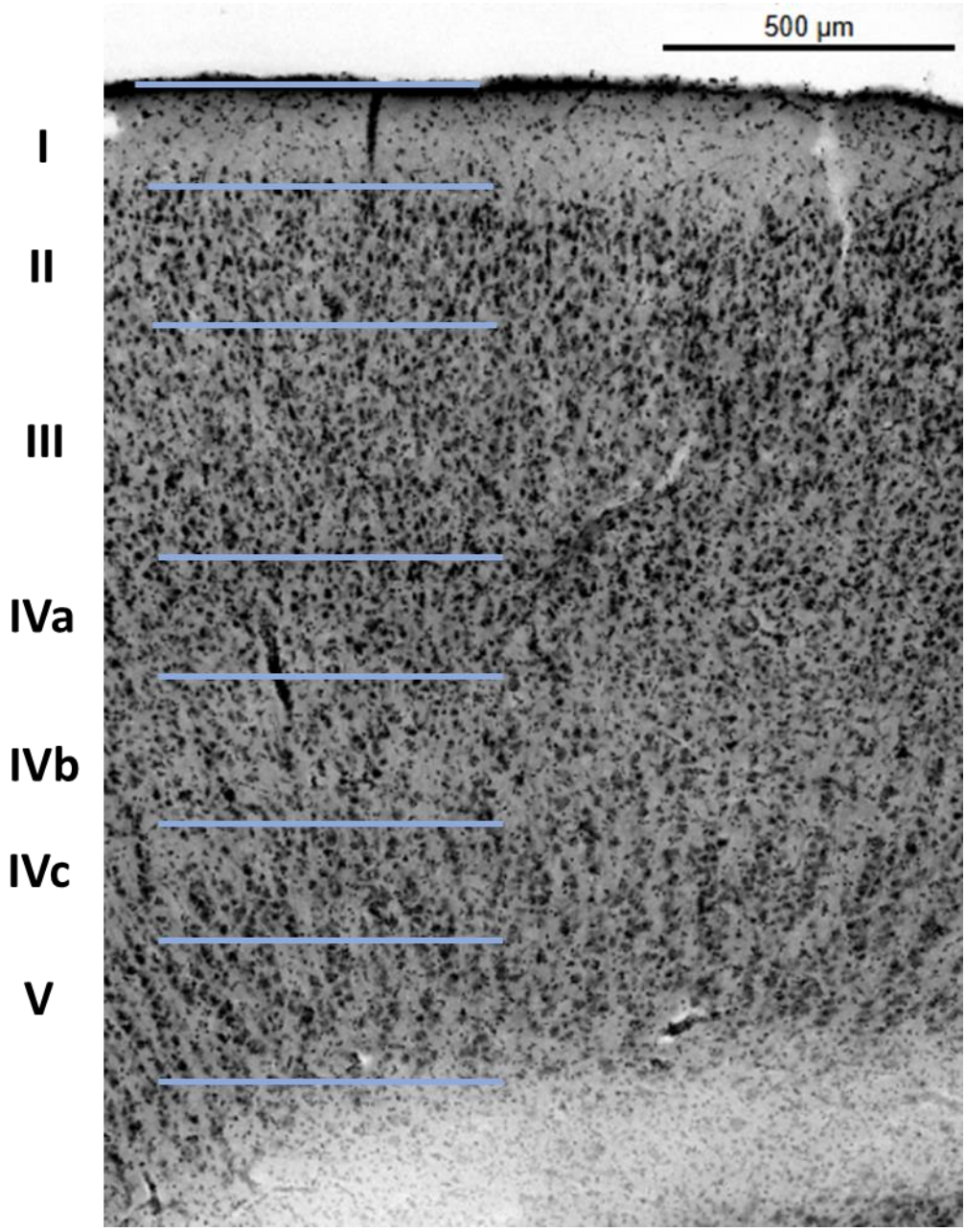

Figure 18: Layering of the visual cortex from section no. 1338 of a harbour seal brain. The cresyl violet staining reveals the cortical layering, identifying five distinct layers. In layer IVb the Gennari stripe is prominently visible. Scale 500 µm.

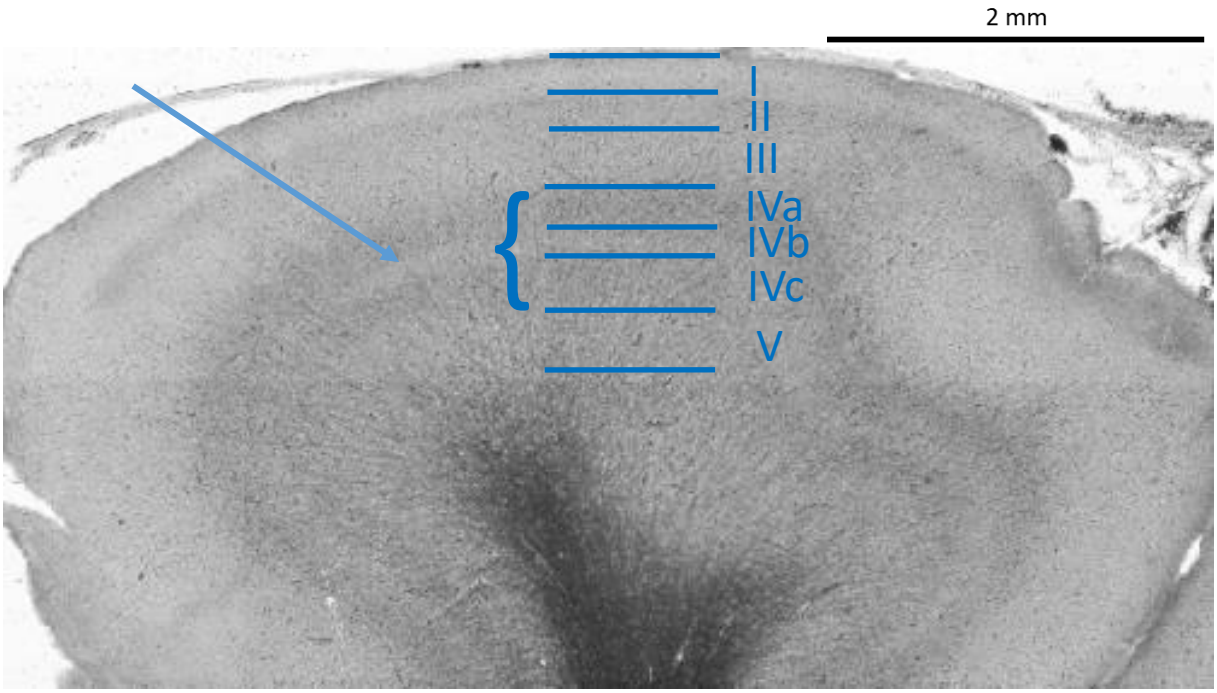

Figure 19: Detailed part of a gyrus from section no. 1524 of a harbour seal brain, illustrating cortical architecture. The transmittance data reveals the cortical layering, identifying five distinct layers. Notably, the Gennari stripe, corresponding to layer IVb, is prominently visible and indicated by an arrow. Scale 2 mm.

3.3. OTHER BRAIN STRUCTURES

Dorsal to the *tractus opticus*, a prominent, oval-shaped nucleus (Figure 20) has developed within the internal capsule. Notably, this nucleus is distinct and unconnected to the adjacent *thalamus* and the subthalamic nucleus. The nucleus extends from section 582 to approximately section 676. Despite its recognition, however, no conclusive classification has yet been achieved regarding its potential affiliations within neural systems or its specific functional role.

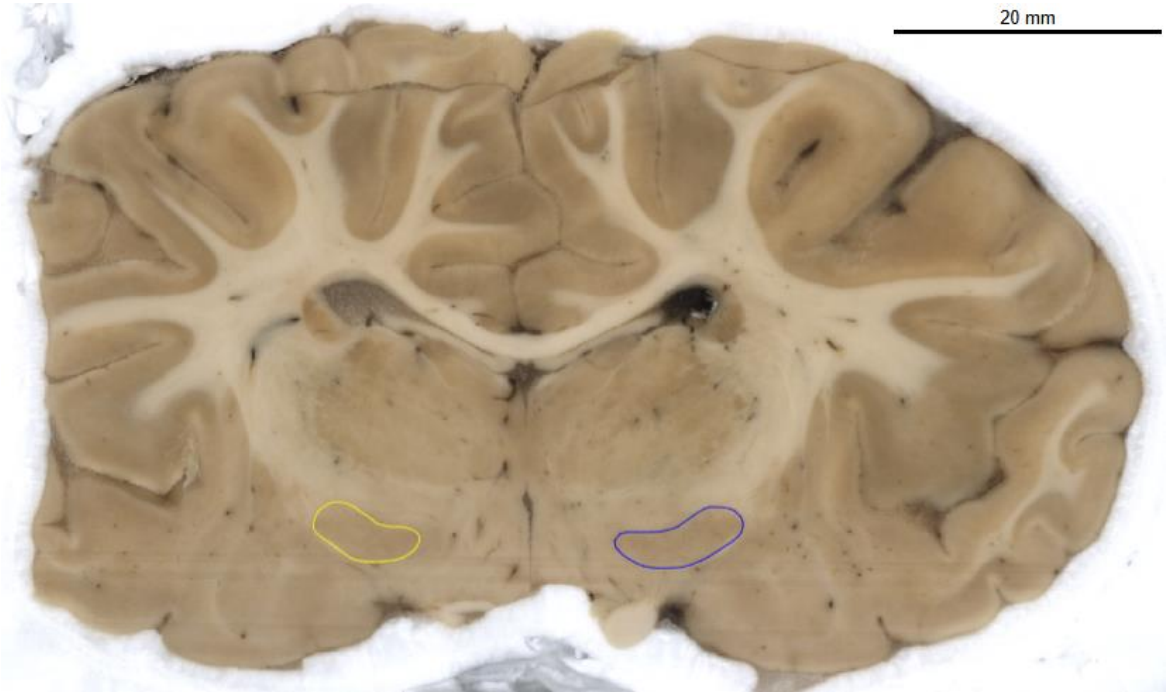

Figure 20: Position of the unknown nucleus in the blockface image of section no. 630 of a harbour seal brain. Labelling of the nucleus on the right (yellow) and on the left (blue) for the determination of the structure in the harbour seal brain. Scale 20 mm.

3.4. QUANTITATIVE NEUROANATOMY OF THE HARBOUR SEAL BRAIN

3.4.1. GYRIFICATION INDEX

The analysis of gyrification in the harbour seal's brain revealed quantitative measurements of the GI for the left hemisphere. The mean GI for the left hemisphere of the harbour seal brain amounted to 2.15 ± 0.40 and median GI 2.22 with a quantile GI (25%, 75%) of 1.96 and 2.44, indicating a moderate range of variability in cortical folding across different regions of the left hemisphere.

Figure 21 illustrates the variation in GI across discrete anatomical sections, providing a detailed spatial understanding of cortical folding patterns. The minimum of the GI is localised anteriorly within the cerebral structure. Noteworthy is the discernible reduction in GI around the 500th section. Conversely, the maximum of gyrification is observed proximal to the 1,200th section, indicating heightened cortical folding in the *posterior* regions of the brain.

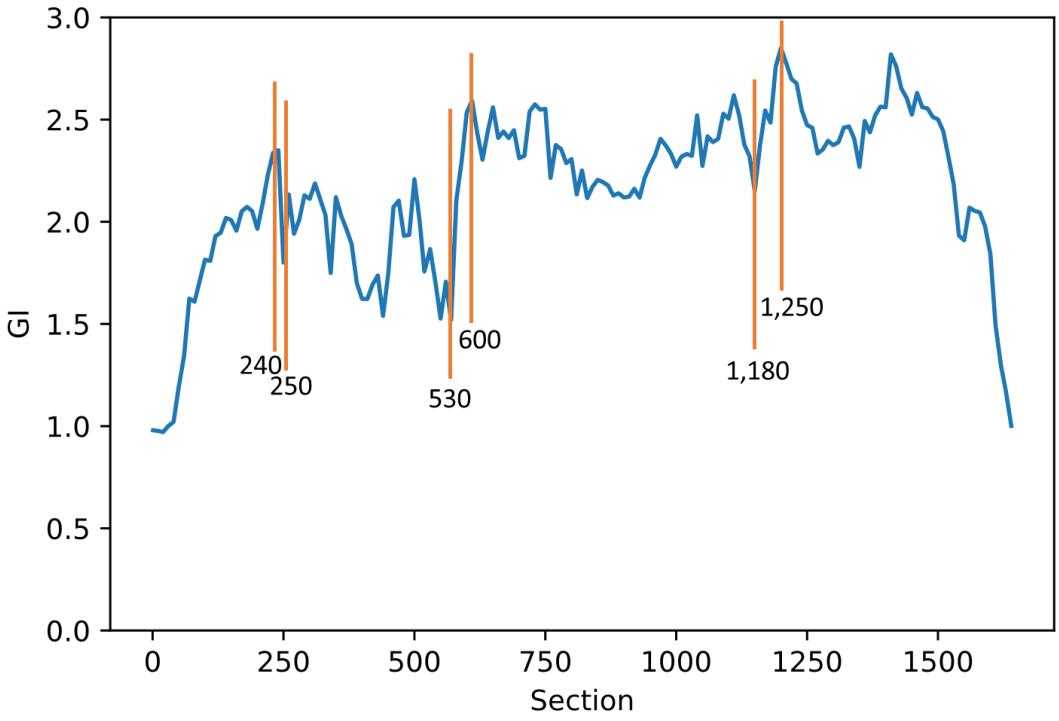

Figure 21: Gyrification index measured for every 10th section as a function of the individual sections for a harbour seal brain. The x-axis represents the GI, a quantitative measure of the degree of cortical folding in the brain. On the y-axis, the brain sections are depicted. The orange lines indicating specific slices where strong lows or pikes are noticeable. These specific slices are shown in Fig. 11.

The observed discontinuities in the graph (Figure 21) can be attributed to structural variations across different gyri and sulci within the sampled brain regions (Figure 22). Specifically, in section 240 (Figure 22a), sulci are partially included in the cross-section. However, these sulci terminate by section 250 (Figure 22b), resulting in their absence in subsequent sections and thus explaining the pronounced decline observed in the graph. This pattern is indicative of the complex morphology of the brain, where the depth and orientation of sulci and gyri significantly affect volumetric measurements and signal intensity across adjacent sections. From sections 530 (Figure 22c) to 600 (Figure 22d), an increase in visible gyri occurs alongside an expanded representation of the frontal lobe. The presence of additional gyri, coupled with the more comprehensive inclusion of frontal lobe structures, results in a measurable increase in the graph values, reflecting the augmented cortical volume in these sections. From section 1,180 (Figure 22e) to section 1,250 (Figure 22f), the trend reverses, presenting an opposite pattern compared to sections 240 and 250. In section 1,180, several sulci are discernible, though not yet fully developed in the cross-section, contributing to a gradual increase in values. By section 1,250, however, these sulci are fully formed, accounting for the subsequent stability or elevation in the graph. This cyclical fluctuation in the graph underscores the impact of

anatomical complexity on cross-sectional imaging data, particularly when mapping highly variable regions like the gyri and sulci.

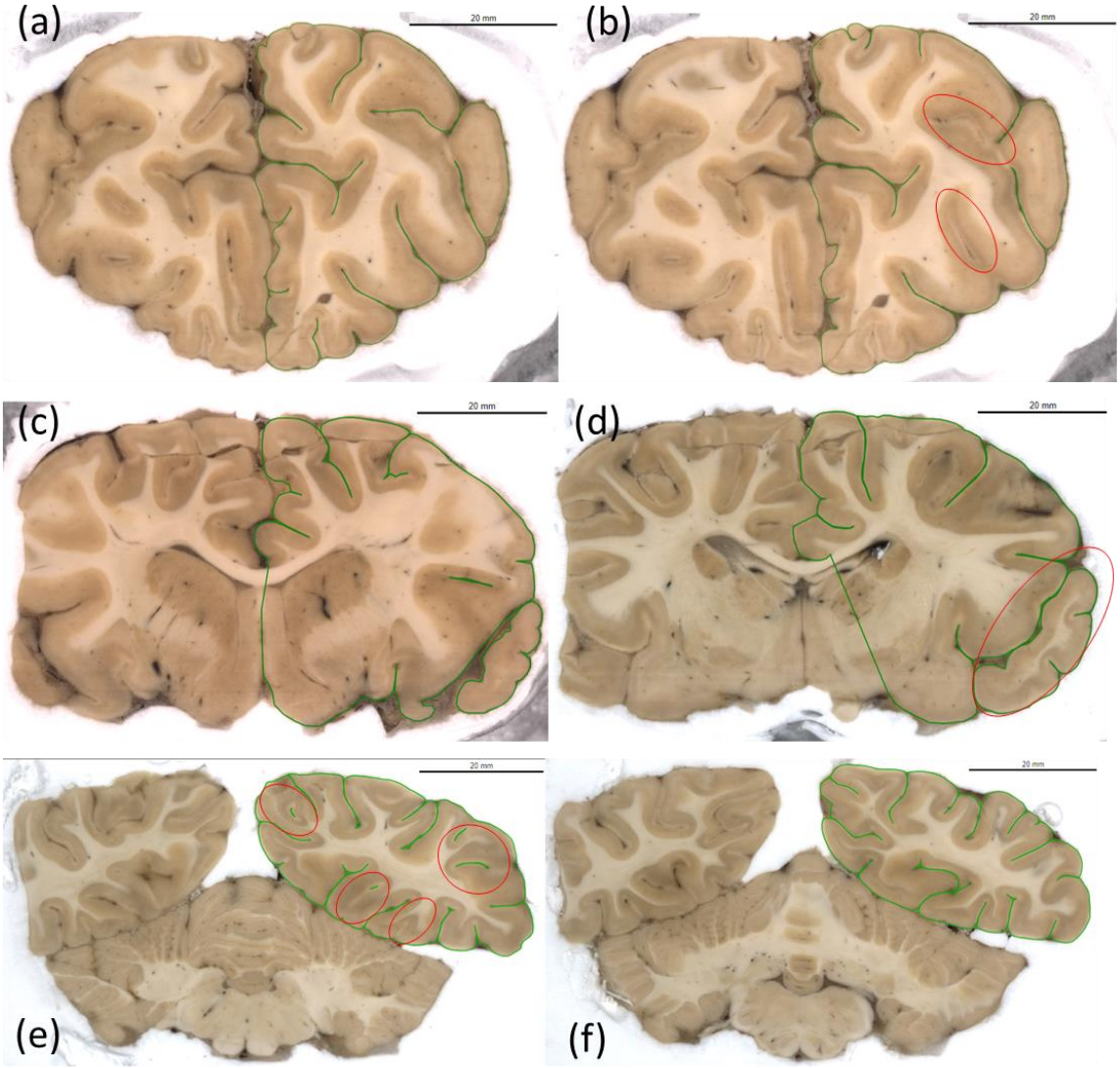

Figure 22: Coronal sections of the harbour seal brain: Selected sections are presented to illustrate the fluctuations in the GI graph (Figure 21). The cortical folding is highlighted in green, while the red-outlined areas indicate regions where changes occur between adjacent sections. Across the sections, it becomes evident that a gyrus or sulcus is either no longer present or has been newly truncated, underscoring the dynamic anatomical variations in these specific regions.

3.4.2. CORTICAL THICKNESS

The cortical thickness of the harbour seal's left hemisphere was measured to provide insights into the structural organisation of its brain. The histogram (Figure 23) provides an overview of which cortical thickness is distributed across the data set. A cortical thickness of 2 to 2.5 mm

was the most frequent cortical thickness occurring in the harbour seal brain and 4 mm occurs less often.

The mean cortical thickness was found to be 2.35 ± 0.70 mm, and a median thickness of 2.30 mm. The variability in cortical thickness is reflected by the quantile values (25%, 75%), which are 1.90 mm and 2.70 mm, respectively, indicating a moderate range of thickness across different cortical regions.

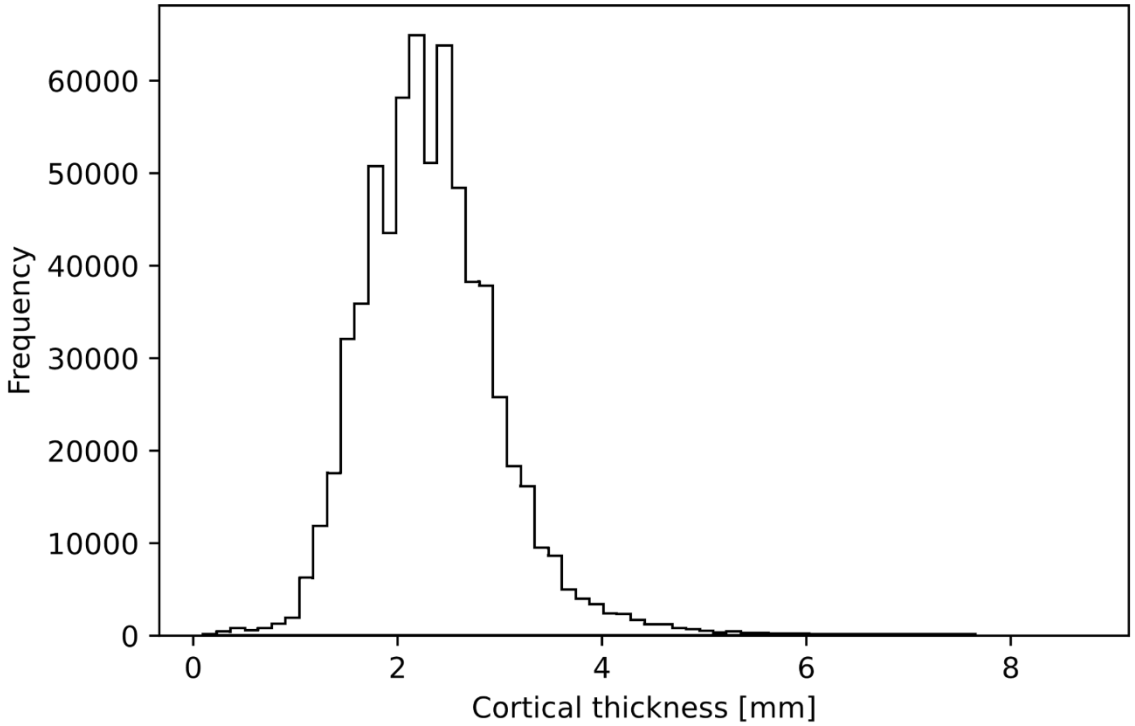

Figure 23: Histogram of cortical thickness measured at isotropically distributed locations across the entire neocortex of the left hemisphere of the harbour seal brain.

Figure 24 presents a detailed distribution of cortical thickness across the cerebral cortex, with thickness measured in mm. The range spans from 0.1 mm, represented by deep blue, to 6 mm, shown in deep red. The analysis reveals that the highest cortical thickness values are predominantly located at the outermost crowns of the gyri. Additionally, the thickness distribution demonstrates a consistent range, with values largely concentrated between 1 mm and 3 mm. This relative uniformity suggests that most cortical regions maintain a similar thickness within this range. However, there are subtle regional variations: in the frontal cortex, the thickness appears marginally lower than in the occipital cortex.

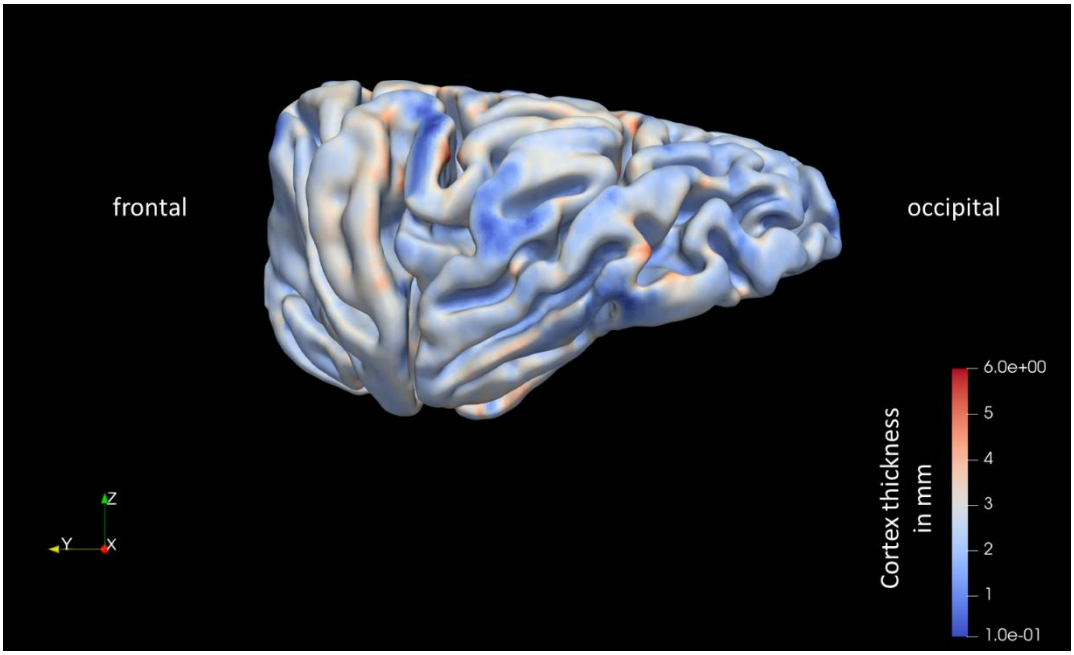

Figure 24: Cortical thickness distribution of the cortex of the left hemisphere of the harbour seal brain, measured in millimetres. The thickness values range from 0.1 mm (deep blue) to a maximum of 6 mm (deep red).

3.4.3. BRAIN VOLUME

The total brain volume (TVB; Table 4) was calculated to be 216 cm³. Based on the annotations derived from the blockface images, the volumes of individual brain structures have been quantitatively assessed as follows: The right caudate nucleus exhibits a volume of 1.70 cm³ and the left caudate nucleus measures also 1.70 cm³. For the LGN, the right LGN has a volume of 0.17 cm³, whereas the LGN on the left side is slightly larger with a volume of 0.18 cm³. The *hippocampus* on the right and left have volumes of 0.53 cm³ and 0.56 cm³, respectively.

Table 4: Total volumes of brain structures including the caudate nucleus, LGN and *hippocampus* for harbour seal, calculated from the annotations made in the blockface data as well as the volumes for each of the mentioned brain structures in relation to the total brain volume. The volumes obtained from both the dilated and eroded masks to establish a variance range. The volumes of individual components are reported in cm³, while the total volume is expressed as a percentage (%).

Structure	eroded (cm^3)	manual (cm^3)	dilated (cm^3)	Total volume eroded (%)	Total volume manual (%)	Total volume dilated (%)
Brain	213	216	218			
Caudate						
left	1.67	1.70	1.73	1.54	1.57	1.59
right	1.67	1.70	1.73			
LGN						
left	0.17	0.18	0.19	0.15	0.16	0.17
right	0.16	0.17	0.18			
Hippocampus						
left	0.54	0.56	0.58	0.49	0.50	0.52
right	0.51	0.53	0.55			

LGN: *lateral geniculate nucleus*

When considering these structures as a percentage of the TBV (Table 4), the caudate nucleus accounts for approximately 1.57% of the TBV. In comparison, the LGN constitutes about 0.16%, and the *hippocampus* represents approximately 0.50% of the TBV.

3.5. First attempt for a 3D-model

In the horizontal view of a model of the harbour seal brain, the spatial arrangement and the orientation of the individual annotated structures are clearly distinguishable (Figure 25). Beyond their general positioning, each structure's unique shape and relative size are also discernible, providing a detailed insight into the brain's organisation. These neural structures appear in paired formations. At the frontal pole, represented in yellow (left) and pink (right), lies the caudate nucleus. Moving posteriorly toward the occipital pole, the LGN is highlighted in orange (left) and green (right). Adjacent to the LGN, the *hippocampus*, marked in purple (left) and turquoise (right), is visible.

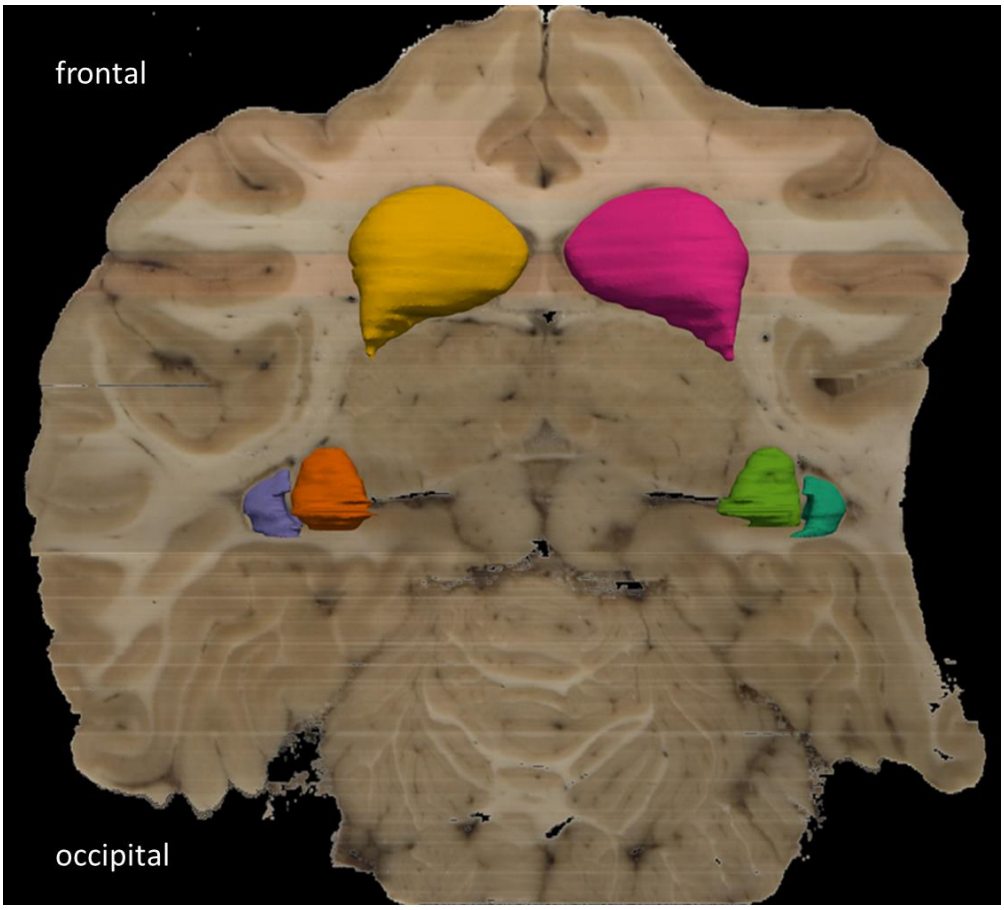

Figure 25: In the horizontal view of a model of the harbour seal brain, the position of the individual marked structures is clearly visible. In addition to their general location, the shape and size of each structure can also be observed. The structures are arranged in pairs. At the frontal pole, in yellow (left) and pink (right), is the caudate nucleus. Moving toward the occipital pole, the LGN is shown in orange (left) and green (right). Directly adjacent to this, the *hippocampus* is depicted in purple (left) and turquoise (right).

4. DISCUSSION

The current dissertation provided a fundamental neuroanatomical characterisation of the harbour seal brain.

4.1. QUALITATIVE NEUROANATOMY OF THE HARBOUR SEAL BRAIN

A comparative analysis of mammals revealed distinct gross anatomical similarities in brain structure, including fissures and external features, between the harbour seal and terrestrial carnivores, specifically members of the *Ursidae* (brown bear, Sienkiewicz et al. 2019) and *Canidae* (wild dogs, Chengetanai et al. 2020) families. This observation gains significance when considered in the context of phylogenetic classification. According to a recent phylogenetic framework of pinnipeds, Berta et al. (2022), showed that, there is strong evidence for a close evolutionary relationship between modern pinnipeds and recent ursids. This close affinity likely explains the shared morphological features in gross brain anatomy, which may be a consequence of common ancestral traits retained within the *Carnivora* order. These findings suggest that certain structural characteristics in the harbour seal's brain may have been evolutionarily retained due to shared ancestry with terrestrial carnivores, rather than resulting solely from adaptations to an aquatic lifestyle.

4.1.1. SPECIFICS OF THE *HIPPOCAMPUS* OF THE HARBOUR SEAL

In this study, volumetric analysis revealed that the right *hippocampus* measured a volume of 0.53 cm³, while the left *hippocampus* was slightly larger at 0.56 cm³. Conversely, cetaceans exhibit a relatively small hippocampal volume (0.6 and 1.9 cm³), which has been extensively documented in neuroanatomical studies (Morgane & Jacobs 1972; Patzke et al. 2015). The reduced hippocampal size in cetaceans is thought to reflect their reliance on alternative sensory modalities and cognitive strategies, such as echolocation and advanced auditory processing, rather than hippocampal-dependent spatial navigation (Patzke et al. 2015). It is possible that the increased size of the *hippocampus* of seals versus cetaceans (Morgane & Jacobs 1972; Patzke et al. 2015) points towards a need for encoding spatial information in seals. Indeed, harbour seals as central place foragers, which often navigate large, featureless marine landscapes and retain memory of specific locations such as breeding sites and haul-out places (Gallistel 1990; Thinus-Blanc 1996). In contrast, other pinnipeds, including the Steller sea lion (hippocampal volume of 3.53 cm^3) and Northern fur seals (hippocampal volume of 1.95 cm^3), exhibit a hippocampal size more within the range of terrestrial mammals, such as the African lion (*Panthera leo*) (hippocampal volume of 4.50 cm^3) (Patzke et al. 2015).

The *hippocampus* of harbour seals could contribute to orientation in space as suggested for example for California sea lions, who show impaired performance in spatial tasks when the right *hippocampus* is lesioned (Cook et al. 2018). This research in California sea lion demonstrated that damage to the right *hippocampus*, induced by the algal toxin domoic acid, leads to deficits in spatial perception. As California sea lions are dynamic foragers they rely on precise spatial awareness for successful navigation and resource acquisition, such impairments may have profound consequences for their survival (Cook et al. 2018). It can be assumed that the *hippocampus* in harbour seals also plays a significant role in spatial orientation and navigation.

Maguire et al. (2000) have demonstrated the functional significance of hippocampal subregions, particularly highlighting an enlarged *posterior hippocampus* in London taxi drivers. In humans, this specific region of the *hippocampus* is recognised for its role in encoding and storing spatial representations of the environment (Maguire et al. 2000). Similarly, behavioural studies in harbours seals have demonstrated the capability of harbour seals to utilise landmarks for spatial orientation, particularly in navigating towards their haul-out sites (Maaß et al. 2022). The study by Maguire et al. (2000) demonstrated that increased utilisation of the *hippocampus* for specific tasks can lead to structural enlargement. Building on this, future research should focus on precisely identifying the region of hippocampal enlargement in harbour seals. Such investigations could provide deeper insights into whether this enlargement, in contrast to that observed in cetaceans, is primarily associated with intensive use for navigational purposes.

4.1.2. SPECIFICS OF THE *NUCLEUS CAUDATUS* OF THE HARBOUR SEAL

In the studied sample the caudate nucleus with 1.70 cm^3 and 1.57% of the TBV was measured. Together with the *putamen*, it forms the striatum, a critical component of the basal ganglia involved in the regulation of voluntary motor skills, action control and movement planning (Graybiel & Grafton 2015). In the harbour seal, the enlarged caudate nucleus is associated with a relatively smaller *putamen*, contributing to the formation of the deep sylvian fissure. The volume of the right caudate nucleus was measured at 1.70 cm^3, as well as the left caudate nucleus. The relatively large size of the caudate nucleus in pinnipeds, such as California sea lions (right 3.3 cm^3 and left 3.2 cm^3 Cook & Berns 2022), could be consistent with their complex locomotor behaviours across terrestrial and aquatic environments. Pinnipeds exhibit sophisticated navigation and foraging strategies (Hanke & Dehnhardt 2018), which are likely supported by neural mechanisms associated with precise motor control and spatial memory within the basal ganglia. Previous research on California sea lions highlighted the functional significance of enlarged basal ganglia in supporting sophisticated behavioural responses to

environmental stimuli, which may be reflected in the substantial volume of the caudate nucleus and other related structure (Cook & Berns 2022).

Research has indicated that the striatum plays a role in facilitating efficient movement during hunting activities in laboratory rats (Santos et al. 2015). Furthermore, it has been implicated in adaptive navigation in both rats and humans (Kimura 1990; Jürgens 2002). This functionality is likely associated with the caudate nucleus's role in processing sensorimotor transformations (Grahn et al. 2008). Among marine mammals, pinnipeds are distinguished by their capability for three-dimensional movement, navigating fluidly in all directions. This is exemplified by their agile manoeuvres during prey capture, involving rapid and continuous adjustments across all three spatial axes. The enlarged caudate nucleus may provide critical support for the intricate sensorimotor adaptations necessary for underwater hunting. Transitioning into aquatic environments imposes significant challenges for mammals, particularly in mastering movement within a true three-dimensional space, as opposed to the predominantly two-dimensional movement of land-based animals. Recent studies, such as that by Cook et al. (2022), have raised the question whether a large caudate nucleus is unique to certain marine carnivores, such as sea lions, or represents a broader trait among large mammalian carnivores (Cook & Berns 2022).

4.1.3. SPECIFICS OF THE *AMYGDALA* OF THE HARBOUR SEAL

The description and localisation of the amygdala in the harbour seal brain align closely with findings reported in existing literature (LeDoux 2007). The primary amygdala's integration with the peri-amygdaloid cortex and its proximity to the *hippocampus* underscore its role in processing emotional responses that are related to memory and social interactions (Phelps & LeDoux 2005). The same structure can be seen in the harbour seal brain. These social signals are likely processed by the subcortical nuclei of the *amygdala*, which are involved in rapid interpretation and response to stimuli. The clear distinction between the *lateral* and *medial* nuclei within the subcortical *amygdala* suggests functional specialisation in emotional and behavioural regulation (LeDoux 2007). The *lateral* nucleus, which is involved in sensory input, may play a role in the interpretation of signals from conspecifics or the detection of potential threats. Meanwhile, the *medial* nucleus is associated with autonomic responses, such as physiological adjustments in response to environmental stimuli. The well-defined division of the *amygdala's* into the pallial (*cortical*) and subcortical components in the brain reflects its critical role in processing emotions, social behaviours, and autonomic responses (Adolphs 2009). This division is also shown in the data indicating that the *amygdala* plays a key role in both interpreting social cues and mediating emotional responses, contributing to cognitive flexibility in harbour seals.

Its anatomical proximity to the *hippocampus* further highlights its role in linking emotional and social information with spatial memory and environmental context, which is vital for learning and memory (LeDoux 2007). This connection could enable harbour seals to remember emotionally significant events, such as encounters with predators, and adjust their future behaviours based on past experiences, enhancing survival and social competence in the complex aquatic environment. Classical conditioning techniques can be employed to condition animals to specific fear stimuli by creating associations between neutral stimuli and fear-inducing experiences, thereby eliciting conditioned responses (Milad et al. 2011). It is plausible that harbour seals possess a comparatively diminutive *amygdala*. This structure is notably sensitive to olfactory stimuli, and given the relatively modest development of the olfactory apparatus in seals (Loza et al. 2023), it is conceivable that this may contribute to a reduced size of the *amygdala* in these species. Furthermore, the *amygdala* in cetaceans also lacks prominent development compared to other mammalian species (Patzke et al. 2015).

4.1.4. SPECIFICS OF THE UNKNOWN CAUDATE OF THE HARBOUR SEAL

This nucleus was previously observed and documented by Jelgersma (1934). Despite its recognition, however, no conclusive classification has yet been achieved regarding its potential affiliations within neural systems or its specific functional role. The nature and purpose of this structure remain ambiguous, highlighting a critical need for further investigative research to elucidate its connections, functional contributions, and potential role within neuroanatomical frameworks. This nucleus is of particular scientific interest as it is not observed in humans. Its presence in other pinnipeds or marine mammals remains uncertain. To investigate this further, the brains of additional species would need to be examined with a specific focus on this structure. Further 3D-PLI measurements could provide detailed insights into its connectivity with other brain regions, potentially contributing to a better understanding of its functional role.

4.2. QUANTITATIVE NEUROANATOMY OF THE HARBOUR SEAL BRAIN

4.2.1. INTERPLAY BETWEEN GYRIFICATION INDEX, BRAIN MASS AND BRAIN SIZE

The external gross morphology and fissures of the harbour seal brain examined in this study closely aligns with previous descriptions of the harbour seal brain (Flatau & Jacobsohn 1899; Fish 1898; Krueg 1880; Owen 1868; Turner 1888).

The brain of the present harbour seal exhibited a GI of 2.15 with a brain mass of 230 grams. Interestingly, when comparing with other species (Table 5), a study by Manger et al. (2012) showed that the harbour seal has a relatively high GI (2.38) for its brain mass (275 g), which could be confirmed by our current investigations. Our findings are consistent with the existing scientific literature dataset. The unspecific seal species (*Phoca* sp.) reported by Zilles et al.

(2013) showed a GI of 2.82 (brain mass 187 g), which is higher than both our own sample and the value reported by Manger et al. (2012) for the harbour seal. This may suggest variability within the pinniped family, an individual variability or differences in the specific ecological niches occupied by various seal species. An individual variability was already shown in humans some decades ago (Zilles et al. 1988).

In terms of brain mass and GI, our own harbour seal sample has a brain weighing 230 grams, which aligns closely with the brain sizes of other large terrestrial carnivores, such as the Siberian tiger (*Panthera tigris altaica*) (233 g, Grewal et al. 2020) or African lion (258 g, Pillay & Manger 2007). However, these terrestrial carnivores exhibit slightly lower GIs (1.91 and 1.85, respectively) than the harbour seal, indicating that the harbour seal may have a relatively higher degree of cortical folding.

The GI of 2.15 of the harbour seal positioning itself at an intermediate level between that of the dolphin and the manatee. Species such as dolphins (GI: 5.4-5.6, Marino et al. 2007; Zilles et al. 2013) and harbour seal (GI: 2.38, Manger et al. 2012) display a relatively strong gyrification, whereas manatees have a predominantly lissencephalic cortex (GI: 1.03 Reep & O'Shea 1990). The Pacific bottlenose dolphin (*Tursiops aduncus*) and Pacific pilot whale (*Globicephala macrorhynchus*) display much higher GIs (4.47 and 5.55, respectively; Zilles et al. 2013). These species demonstrate the highest GIs among the sampled animals, indicating that cetaceans are among the most highly gyrified mammals. The extensive cortical folding enhances the surface area of the brain, thereby increasing neural capacity without a corresponding increase in overall brain volume.

A GI of 2.15 places the harbour seal brain in line with other marine mammal carnivores, such as the polar bear (*Panthera leo*) (GI: 2.04, Pillay & Manger 2007) and slightly lower than the California sea lion (GI: 2.52, Manger et al. 2012). Compared to terrestrial mammals, such as humans (GI: 2.99, Zilles et al. 2013; Zilles et al. 1989) or African wild dogs (*Lycaon pictus*) (GI: 1.74, Grewal et al. 2020), the harbour seal's GI (2.15) is moderate. Humans, with the highest known GI among terrestrial mammals, show a well-developed cortical structure supportive of advanced cognitive functions, language, and problem-solving abilities (Zilles et al. 1988). Interestingly, the GI of the seal's brain appears to align more closely with that of terrestrial mammals, such as the polar bear, than with other marine mammals like dolphins and whales.

A significant observation in our study is the lower GI (between 1.5 and 2) localised in the anterior regions of the brain, indicating a reduction in cortical folding within the frontal regions. A study in humans (Zilles et al. 1988), have demonstrated analogous findings, suggesting that a comparable conceptual framework may be applicable to the harbour seal. This may reflect functional specialisations also in harbour seal, as these areas potentially correspond to brain regions that are less convoluted due to their involvement in basic sensory input or basic motor

functions, as opposed to more complex associative processing. Conversely, the posterior regions of the brain, particularly the parietal and occipital lobes, exhibit heightened gyrification (GI between 2 and 3) which likely corresponds to areas involved in complex sensorimotor integration. This observation suggests a potential avenue for future research, emphasising the importance of not limiting analyses to the GI of the entire brain but also investigating region-specific variations. Such an approach could provide a more nuanced understanding of localised cortical folding patterns and their functional implications.

Table 5: List of gyrification index and brain mass (in g) among different marine and terrestrial species with a reference to the original publication.

Species	GI	Cortical thickness in mm	Brain mass in g	Reference
Phoca vitulina (own sample)	2.15	2.35	230	own sample
Phoca vitulina (literature)	2.38	n.a.	275	Manger et al., 2012
Halichoerus grypus	n.a.	2.6	n.a.	Hoeksema et al., 2021
Phoca sp.	2.82	n.a.	187	Zilles et al., 2013
Zalophus californianus	2.52	n.a.	379	Manger et al., 2012
Tursiops aduncus	4.75	n.a.	1,498	Zilles et al., 2013
Globicephala macrorhynchus	5.55	n.a.	2,842	Zilles et al., 2013
Trichechus manatus	1.06	4.23	394	Reep & O'Shea, 1990
Ursus maritimus	2.04	n.a.	459	Pillay & Manger, 2007
Lycaon pictus	1.74	n.a.	126	Grewal et al., 2020
Panthera tigris altaica	1.91	n.a.	233	Grewal et al., 2020
Panthera leo	1.85	n.a.	258	Pillay & Manger, 2007
Homo sapiens	2.99	n.a.	1,400	Zilles et al., 1989

GI: Gyrification index, n.a.: not available

The harbour seal exhibits a cortical thickness of 2.35 mm, a value closely resembling the 2.69 mm observed in the grey seal (*Halichoerus grypus*) (Hoeksema et al., 2021). This similarity may reflect comparable ecological niches and sensory demands in these phocid species. In contrast, the manatee demonstrates a significantly thicker cortex, measured at 4.23 mm (Reep & O'Shea 1990). The observed variation in cortical thickness across these species may also relate to differences in brain size, cortical organisation, and functional specialisation. The measurements suggest that the harbour seal has a relatively thick cortex compared to terrestrial mammals (e.g. primates (Hofman 1988). The variability in cortical thickness across the left hemisphere might reflect different functional specialisations, with thicker cortical areas

corresponding to regions involved in advanced motor control, sensory integration, and potentially cognitive functions such as memory and decision-making.

There may be a relationship between cortical thickness and folding (Gautam et al. 2015). While a thicker cortex may theoretically accommodate a greater number of neurons, efficient folding of the cortical surface becomes a limiting factor (Pillay & Manger 2007). Gyrification, which enhances the brain's surface area within the confines of the skull, allows for greater neuronal density and synaptic connectivity, even when cortical layers are thinner (Zilles et al. 1988). For instance, species like dolphins exhibit a thinner cortex but achieve high neuronal densities due to pronounced gyrification (Ridgway & Brownson 1984). Mota and Herculano-Houzel (2015) posited that cortical folding is primarily influenced by the interplay between surface area and cortical thickness, rather than being directly proportional to the number of neurons. Despite these insights, the precise biological mechanisms underlying gyrification remain incompletely understood.

Up to date, the scientific community disagrees regarding the precise mechanistic underpinnings governing the intricate process of cortical folding. The enhanced gyrencephaly observed in certain mammals, such as artiodactyls, is associated with a thinner cerebral cortex (Pillay & Manger 2007), which facilitate mechanical buckling and influence the dimensions of the 'gyral window' necessary for cortical connectivity (Prothero & Sundsten 1984). This reduction is linked to a lower neuronal count within the cortex. In dolphins, for instance, cortical thickness ranges from 1.3 to 1.75 mm across different brain regions (Ridgway & Brownson 1984), contributing to their extensive cortical convolutions (Manger et al. 2012). In contrast, manatees have with up to 4 mm a substantially thicker cortex (Sun & Hevner 2014), corresponding to a conspicuously lissencephalic surface. Our results showed, that the harbour seal diverges from this pattern, as in our investigation we determined an average cortical thickness of 2.35 mm ± 0.70 mm, still exhibits pronounced gyrification. This raises questions about whether the manatee or the harbour seal represents an outlier in cortical morphology, particularly the potential limitations on folding imposed by the manatee’s thicker cortex (Reep & O’Shea 1990). The harbour seal's pronounced gyrification, despite a cortex thickness similar to that of the manatee, highlights the complexity of cortical folding and its neuroanatomical implications.

4.3. NEUROANATOMY OF THE VISUAL PATHWAY

The visual system of seals has historically received limited attention, largely due to earlier assumptions that these animals rely less on their eyesight. Pioneering studies, collected by Walls (1942), characterised seal vision as relatively unimportant, citing restricted ocular

mobility and the challenges posed by their aquatic environments, which often include low visibility and rapid fluctuations in illumination during dives.

4.3.1. NEUROANATOMY OF THE *LATERAL GENICULATE NUCLEUS*

The LGN serves as a major relay centre in the visual pathway, responsible for processing visual information received from the retina prior to transmission to the visual cortex. The current measurements demonstrate a volume of the right LGN of 0.18 cm^3 and the left LGN of 0.19 cm^3. From a methodological perspective, it is crucial to evaluate whether the observed differences in values reflect genuine asymmetry or are artifacts of measurement techniques. A more robust conclusion would require the analysis of additional brain specimens to reliably assess the presence of asymmetry. Notably, asymmetry has been documented in a separate study involving monkeys. This observed asymmetry may suggest functional differences in visual processing capabilities between the two hemispheres (Jiang et al. 2015). The dual requirement for visual acuity in terrestrial conditions and low-light underwater environments could drive unique adaptations in the visual systems of marine mammals

The LGN of the harbour seal sample clearly differs from the well-defined laminar structure found in other pinnipeds, like California sea lions and northern elephant seals (Turner et al. 2017). The well-developed LGN in these species aligns with their need to detect movement and contrast in dynamic visual conditions, with lateralisation potentially conferring advantages in tasks such as predator detection or prey tracking in complex aquatic settings (Turner et al. 2017). Research into the anatomy of the seal LGN reveals a more diffuse and less sharply delineated layering pattern (Turner et al. 2017). Evolutionary adaptations likely drive these structural differences, reflecting the requirements in aquatic and terrestrial settings. In water, where visual acuity is limited by lower light levels and reduced contrast (Cronin et al. 2006; Duntley 1963; Kröger 2008; Warrant & Locket 2004), there is a great reliance on detecting motion and changes in contrast rather than the fine discrimination of colours or detailed shapes. Data of the present seal shows a diffuse organisation of the LGN, which may enhance binocular integration, thereby improving depth perception and motion detection in a three-dimensional aquatic environment.

4.3.2. NEUROANATOMY OF THE PRIMARY VISUAL CORTEX

The present findings indicate that the visual cortex of the harbour seal exhibits only five discernible cellular layers, lacking the prominent sixth layer. The absence of a defined sixth layer in the harbour seal's visual cortex is a notable deviation from the typical six-layered neocortical structure observed in most terrestrial mammals like humans (Palomero-Gallagher

& Zilles 2019). The cerebral cortex of the Risso's dolphin (*Grampus griseus*), the striped dolphin (*Stenella coeruleoalba*), and the bottlenose dolphin (*Tursiops truncatus*) demonstrates a deviation from the classical six-layered neocortex as well. Layer IV, traditionally associated with thalamic input, is poorly defined or absent, consistent with findings in other odontocetes (Furutani 2008).

The five-layered structure observed in the primary visual cortex of the harbour seal represents a deviation from the classic six-layered organisation characteristic of many mammalian species. Turner et al. (2017) reported a classic six-layered architecture in the primary visual cortex of both the California sea lion as well as the elephant seal (*Mirounga angustirostris*). In contrast, the harbour seal was found to exhibit a five-layered cortical structure. Notably, in the harbour seal, layer IV is the most prominent, whereas in the California sea lion and elephant seal, layers III and VI appear to be the thickest. Layer VI, the deepest cortical layer in other mammals, occupies a pivotal position within the local cortical architecture. It serves as both a recipient of afferent input and a source of output to other brain regions. Notably, this layer is characterised by the highest diversity of morphological cell types, highlighting its functional complexity (Briggs 2010). This structural variation raises critical questions about functional processing within the cortex, specifically whether the harbour seal has lost the computational functions typically attributed to the missing layer or if these functions have been redistributed to other layers. Resolving these questions will require more detailed and systematic investigations, including both morphological and functional analyses.

The Gennari stripe the harbour seal's layer IV is very prominent. The prominence of the Gennari stripe diminishes progressively across taxa, showing a clear decline from primates to terrestrial species such as giraffes, sheep, and horses, and becoming least distinct in marine mammals (Graïc et al. 2022). The study form Turner (2017) does not explicitly clarify whether these other pinniped species possess a Gennari stripe, a hallmark feature of the primary visual cortex in many mammals. Based on visual inspection of the study's figures, the presence of a Gennari stripe appears unlikely (Turner et al. 2017), but this observation warrants further investigation. A more detailed morphological and histological analysis would be essential to verify the presence or absence of this structure, contributing to a deeper understanding of cortical organisation and its functional implications in these marine mammals.

Indeed, the present findings seem to corroborate the perspective of the use of the visual system in harbour seals. Anatomical analyses reveal that the visual system in seals is not only highly developed but also exhibits significant structural complexity, indicative of its functional importance. Specifically, due to the used method, the 3D-PLI, detailed visualisations of the neural architecture have been provided, highlighting the presence of extensive and well-organised fibre bundles within the visual pathways. These robust fibre tracts strongly suggest

that substantial amounts of visual information are being actively processed and transmitted. It also suggests a high level of sensory input integration, which would support visual processing tasks essential for navigation and spatial orientation. Such anatomical sophistication aligns with behavioural evidence demonstrating the use of visual cues, such as stellar navigation and optic flow, in seals (Mauck et al. 2008; Gläser et al. 2014). This evidence collectively suggests that the visual system is not merely a secondary or supplementary sensory modality but is likely integral to the animals' ability to interpret complex environmental cues. Consequently, the strong visual system, as evidenced by both anatomical and functional studies, may play a critical role in facilitating behaviours essential for survival, such as efficient foraging, predator avoidance, and spatial navigation in low-light aquatic environments.

5. FUTURE PERSPECTIVES

The data presented in this research are intended to contribute to foundational research, with the primary objective of enhancing the characterisation of the harbour seal as a model organism. By integrating different methodologies ranging from blockface imaging to atlas development and histological analysis, this study provides a comprehensive characterisation of the harbour seal brain's anatomy. However, a purely anatomical approach is insufficient for a complete understanding of the brain's functional dynamics. Advanced techniques such as fMRI and functional near-infrared spectroscopy (fNIRS), along with behavioural experiments conducted within our research group, are essential to elucidate the functional aspects of the harbour seal brain.

The anatomical data generated in this research provide a crucial foundation for future research within our group, particularly in relation to the ongoing fMRI projects. Detailed knowledge of the structural organisation and connectivity of the harbour seal brain is essential for accurate interpretation of fMRI data, enabling precise mapping of neural networks and their interactions during sensory processing and behaviour. The present research also has broader implications beyond the current scope of our research. For example, fMRI enables the investigation of the animal's brain activity in a controlled, stationary environment. However, for studies conducted in aquatic settings, fNIRS would be a more suitable alternative as it is a non-invasive imaging technique that measures changes in cerebral hemodynamics, specifically blood oxygenation and flow, using near-infrared light. Harbour seals exhibit specialised behaviours and exceptional spatial navigation in low-light underwater environments. With the help of fNIRS, cerebral blood flow changes could be measured in regions associated with visual processing, spatial memory and navigation and motor control. In summary, fNIRS could provide groundbreaking insights into the functional neurophysiology of harbour seals, particularly in their natural underwater environment.

By establishing a detailed anatomical framework, future studies can build upon this foundation to explore additional sensory systems, such as tactile and vestibular pathways, with greater precision. Investigating the neural pathways underlying these sensory modalities will contribute to a more comprehensive understanding of perception and cognition in pinnipeds. Moreover, the integration of anatomical characterisations with functional studies represents a significant step forward for interdisciplinary research. This combined approach will provide deeper insights into how specific brain regions collaborate to process sensory information and regulate behaviour in complex environments. The contributions of this study will thus have lasting impact, advancing the field's ability to conduct high-resolution neuroimaging and laying the

groundwork for future explorations into the neural architecture of pinnipeds and other marine mammals.

REFERENCES

Adolphs, R. (2009): The social brain: neural basis of social knowledge. In: *Annual review of psychology* 60, S. 693–716. DOI: 10.1146/annurev.psych.60.110707.163514.

Ahrens, J.; Geveci, B.; Law, C. (2005): ParaView: An End-User Tool for Large Data Visualization: Visualization Handbook, Elsevier.

Amunts, K.; Mohlberg, H.; Bludau, S.; Zilles, K. (2020): Julich-Brain: A 3D probabilistic atlas of the human brain's cytoarchitecture. In: *Science 369.6506*, S. 988–992.

Avants, B. B.; Tustison, N.; Johnson, H. (2014): Advanced Normalization Tools (ANTS). In: *Insight j 2.3365*, S. 1–35.

Axer, M. & Amunts, K. (2022): Scale matters: The nested human connectome. In: *Science (New York, N.Y.)* 378 (6619), S. 500–504. DOI: 10.1126/science.abq2599.

Axer, M.; Amunts, K.; Grässel, D.; Palm, C. et al. (2011a): A novel approach to the human connectome: ultra-high resolution mapping of fiber tracts in the brain. In: *NeuroImage* 54 (2), S. 1091–1101. DOI: 10.1016/j.neuroimage.2010.08.075.

Axer, M.; Axer, H.; Gräßel, D.; Amunts, K. et al. (2007): Nerve Fiber Mapping of the Human Visual Cortex Using Polarized Light Imaging (PLI). In: *IEEE Nuclear Science Symposium Conference Record*, S. 4345–4347.

Axer, M.; Grässel, D.; Kleiner, M.; Dammers, J. et al. (2011b): High-resolution fiber tract reconstruction in the human brain by means of three-dimensional polarized light imaging. In: *Frontiers in neuroinformatics* 5, S. 34. DOI: 10.3389/fninf.2011.00034.

Ayachit, U. (2015): The ParaView Guide: A Parallel Visualization Application: Kitware.

Baker, L. L.; Kucharczyk, J.; Sevick, R. J.; Mintorovitch, J.; Moseley, M. E. (1991): Recent advances in MR imaging/spectroscopy of cerebral ischemia. In: *AJR. American journal of roentgenology* (156(6)), S. 1133–1143.

Balaram, P.; Young, N. A.; Kaas, J. H. (2014): Histological features of layers and sublayers in cortical visual areas V1 and V2 of chimpanzees, macaque monkeys, and humans. In: *Eye and brain* 2014 (6 Suppl 1), S. 5–18. DOI: 10.2147/EB.S51814.

Bauer, G. B.; Cook, P. F.; Harley, H. E. (2020): The Relevance of Ecological Transitions to Intelligence in Marine Mammals. In: *Frontiers in psychology* 11, S. 2053. DOI: 10.3389/fpsyg.2020.02053.

Beaulieu, C. (2002): The basis of anisotropic water diffusion in the nervous system - a technical review. In: *NMR in biomedicine* 15 (7-8), S. 435–455. DOI: 10.1002/nbm.782.

Beck, C. A.; Bowen, W. D.; Iverson, S. J. (2000): Seasonal changes in buoyancy and diving behaviour of adult grey seal The Journal of Experimental Biology (203), S. 2323–2330.

Berta, A.; Churchill, M.; Boessenecker, R. W. (2022): The Origin of Phocid Seals and Evolution of Key Behavioral Character Traits. In: Costa, D.P., McHuron, E.A. (eds) Ethology and Behavioral Ecology of Phocids. Ethology and Behavioral Ecology of Marine Mammals. Springer, Cham. https://doi.org/10.1007/978-3-030-88923-4_1.

Bininda-Emonds, O.R.P. (2000): Pinniped brain size. In: *Marine Mammal Science* (16(2)), S. 481–488.

Briggs, F. (2010): Organizing principles of cortical layer 6. In: *Frontiers in neural circuits* 4, S. 3. DOI: 10.3389/neuro.04.003.2010.

Brodmann, K. (1913): Neuere Forschungsergebnisse der Großhirnrindenanatomie mit besonderer Berücksichtigung anthropologischer Fragen. In: *Naturwissenschaften* (1(46)), S. 1120–1122.

Chengetanai, S.; Tenley, J. D.; Bertelsen, M. F.; Hård, T. et al. (2020): Brain of the African wild dog. I. Anatomy, architecture, and volumetrics. In: *The Journal of comparative neurology* 528 (18), S. 3245–3261. DOI: 10.1002/cne.24999.

Cignoni, P.; Callieri, M.; Corsini, M.; Dellepiane, M. et al. (2008): Meshlab: an open-source mesh processing tool. In: *Eurographics Italian chapter conference* ((Vol. 2008)), S. 129–136.

Cook, P. F. & Berns, G. (2022): Volumetric and connectivity assessment of the caudate nucleus in California sea lions and coyotes. In: *Animal cognition* 25 (5), S. 1231–1240. DOI: 10.1007/s10071-022-01685-7.

Cook, P. F.; Berns, G. S.; Colegrove, K.; Johnson, S.; Gulland, F. (2018): Postmortem DTI reveals altered hippocampal connectivity in wild sea lions diagnosed with chronic toxicosis from algal exposure. In: *The Journal of comparative neurology* 526 (2), S. 216–228. DOI: 10.1002/cne.24317.

Cronin, T. W.; Warrant, E.; Nilsson, D. E. (2006): Invertebrate vision in water. In: *Invertebrate vision*, S. 211–249.

Czeibert, K.; Baksa, G.; Grimm, A.; Nagy, S. A. et al. (2019): MRI, CT and high resolution macro-anatomical images with cryosectioning of a Beagle brain: Creating the base of a multimodal imaging atlas. In: *PloS one* 14 (3), e0213458. DOI: 10.1371/journal.pone.0213458.

Dohmen, M.; Menzel, M.; Wiese, H.; Reckfort, J. et al. (2015): Understanding fiber mixture by simulation in 3D Polarized Light Imaging. In: *NeuroImage* 111, S. 464–475. DOI: 10.1016/j.neuroimage.2015.02.020.

Duntley, S. Q. (1963): Light in the Sea. In: *Journal of the Optical Society of America* (Vol. 53, Issue 2), S. 214–233.

Elias, H. & Schwartz, D. (1969): Surface areas of the cerebral cortex of mammals determined by stereological methods. In: *Science (New York, N.Y.)* 166 (3901), S. 111–113. DOI: 10.1126/science.166.3901.111.

Eriksen, N. & Pakkenberg, B. (2014): Comparative Stereology Studies of Brains from Marine Mammals. In: P. R. Mouton (Hg.): Neurostereology, Bd. 142: Wiley, S. 99–112.

Essen, D. C. V. (1997): A tension-based theory of morphogenesis and compact wiring in the central nervous system. In: *Nature* (385(6614)), S. 313–318.

Estrada, L. I.; Robinson, A. A.; Amaral, A. C.; Giannaris, E. L. et al. (2017): Evaluation of Long-Term Cryostorage of Brain Tissue Sections for Quantitative Histochemistry. In: *The journal of histochemistry and cytochemistry : official journal of the Histochemistry Society* 65 (3), S. 153–171. DOI: 10.1369/0022155416686934.

Ferrer, I.; Armstrong, J.; Capellari, S.; Parchi, P. et al. (2007): Effects of formalin fixation, paraffin embedding, and time of storage on DNA preservation in brain tissue: a BrainNet Europe study. In: *Brain pathology (Zurich, Switzerland)* 17 (3), S. 297–303. DOI: 10.1111/j.1750-3639.2007.00073.x.

Fish, P. A. (1898): The brain of the fur seal, Callorhinus ursinus; with a comparative description of those of Zalophus californianus, Phoca vitulina, Ursus americanus and Monachus tropicalis. In: *Journal of comparative neurology* (8(1-2)), S. 57–91.

Flatau, E.; Jacobsohn, L. (1899): Handbuch der Anatomie & vergleichenden Anatomie des Centralnervensystems der Säuretiere. I. Makroskopischer Teil. Berlin: S. Karger.

Fox, C. H.; Johnson, F. B.; Whiting, J.; Roller, P. P. (1985): Formaldehyde fixation. In: *The Journal of Histochemistry and Cytochemistry* (Vol. 33, No.8), S. 845–853.

Furutani, R. (2008): Laminar and cytoarchitectonic features of the cerebral cortex in the Risso's dolphin (Grampus griseus), striped dolphin (Stenella coeruleoalba), and bottlenose dolphin (Tursiops truncatus). In: *Journal of anatomy* 213 (3), S. 241–248. DOI: 10.1111/j.1469-7580.2008.00936.x.

Gallistel, C. R. (1990): The organization of learning. In: *The MIT Press*.

Gautam, P.; Anstey, K. J.; Wen, W.; Sachdev, P. S.; Cherbuin, N. (2015): Cortical gyrification and its relationships with cortical volume, cortical thickness, and cognitive performance in healthy mid-life adults. In: *Behavioural brain research* 287, S. 331–339. DOI: 10.1016/j.bbr.2015.03.018.

Gläser, N.; Mauck, B.; Kandil, F. I.; Lappe, M. et al. (2014): Harbor seals (Phoca vitulina) can perceive optic flow under water. In: *PloS one* 9 (7), e103555. DOI: 10.1371/journal.pone.0103555.

Grahn, J. A.; Parkinson, J. A.; Owen, A. M. (2008): The cognitive functions of the caudate nucleus. In: *Progress in neurobiology* (86(3)), S. 141–155.

Graïc, J.-M.; Peruffo, A.; Corain, L.; Finos, L. et al. (2022): The primary visual cortex of Cetartiodactyls: organization, cytoarchitectonics and comparison with perissodactyls and primates. In: *Brain structure & function* 227 (4), S. 1195–1225. DOI: 10.1007/s00429-021-02392-8.

Graybiel, A. M. & Grafton, S. T. (2015): The striatum: where skills and habits meet. In: *Cold Spring Harbor perspectives in biology* 7 (8), a021691. DOI: 10.1101/cshperspect.a021691.

Grewal, J. S.; Gloe, T.; Hegedus, J.; Bitterman, K. et al. (2020): Brain gyrification in wild and domestic canids: Has domestication changed the gyrification index in domestic dogs? In: *The Journal of comparative neurology* 528 (18), S. 3209–3228. DOI: 10.1002/cne.24972.

Hanke, F. D. & Dehnhardt, G. (2018): On route with harbor seals – how their senses contribute to orientation, navigation and foraging. In: *Neuroforum* 24 (4), A183-A195. DOI: 10.1515/nf-2018-A012.

Hanke, F. D.; Dehnhardt, G.; Schaeffel, F.; Hanke, W. (2006a): Corneal topography, refractive state, and accommodation in harbor seals (Phoca vitulina). In: *Vision research* 46 (6-7), S. 837–847. DOI: 10.1016/j.visres.2005.09.019.

Hanke, F. D.; Hanke, W.; Scholtyssek, C.; Dehnhardt, G. (2009a): Basic mechanisms in pinniped vision. In: *Experimental brain research* 199 (3-4), S. 299–311. DOI: 10.1007/s00221-009-1793-6.

Hanke, F. D.; Kröger, R. H. H.; Siebert, U.; Dehnhardt, G. (2008): Multifocal lenses in a monochromat: the harbour seal. In: *The Journal of experimental biology* 211 (Pt 20), S. 3315–3322. DOI: 10.1242/jeb.018747.

Hanke, F. D.; Peichl, L.; Dehnhardt, G. (2009b): Retinal ganglion cell topography in juvenile harbor seals (Phoca vitulina). In: *Brain, behavior and evolution* 74 (2), S. 102–109. DOI: 10.1159/000235612.

Hanke, W.; Römer, R.; Dehnhardt, G. (2006b): Visual fields and eye movements in a harbor seal (Phoca vitulina). In: *Vision research* 46 (17), S. 2804–2814. DOI: 10.1016/j.visres.2006.02.004.

He, C.; He, H.; Chang, J.; Chen, B. et al. (2021): Polarisation optics for biomedical and clinical applications: a review. In: *Light, science & applications* 10 (1), S. 194. DOI: 10.1038/s41377-021-00639-x.

He, H.; Liao, R.; Zeng, N.; Li, P. et al. (2019): Mueller Matrix Polarimetry—An Emerging New Tool for Characterizing the Microstructural Feature of Complex Biological Specimen. In: *J. Lightwave Technol.* 37 (11), S. 2534–2548. DOI: 10.1109/JLT.2018.2868845.

Herculano-Houzel, S. (2009): The human brain in numbers: a linearly scaled-up primate brain. In: *Frontiers in human neuroscience* 3, S. 31. DOI: 10.3389/neuro.09.031.2009.

Herculano-Houzel, S.; Manger, P. R.; Kaas, J. H. (2014): Brain scaling in mammalian evolution as a consequence of concerted and mosaic changes in numbers of neurons and average neuronal cell size. In: *Frontiers in neuroanatomy* 8, S. 77. DOI: 10.3389/fnana.2014.00077.

Hoeksema, N.; Verga, L.; Mengede, J.; van Roessel, C.; Villanueva, S.; Salazar-Casals, A. et al. (2020): Neuroanatomy of the grey seal brain: bringing pinnipeds into the neurobiological study of vocal learning.

Hof, P. R.; Chanis, R.; Marino, L. (2005): Cortical complexity in cetacean brains. In: *The anatomical record. Part A, Discoveries in molecular, cellular, and evolutionary biology* 287 (1), S. 1142–1152. DOI: 10.1002/ar.a.20258.

Hofman, M. A. (1985): Size and Shape of the Cerebral Cortex in Mammals (Part 1 of 2). In: *Brain Behav Evol* 27 (1), S. 35–40. DOI: 10.1159/000316004.

Hofman, M. A. (1988): Size and Shape of the Cerebral Cortex in Mammals. In: *Brain Behavior Evolution* (32), S. 17–26.

Hoppe, H.; DeRose, T.; Duchamp, T.; McDonald, J.; Stuetzle, W. (1993): Mesh optimization. In: *Proceedings of the 20th annual conference on Computer graphics and interactive techniques*, S. 19–26.

Jamieson, G. S. & Fisher, H. D. (1971): The retina of the harbour seal, Phoca vitulina. In: *Can. J. Zool.* 49 (1), S. 19–23. DOI: 10.1139/z71-005.

Jelgersma, G. (1934): Das Gehirn der Wassersäugetiere. Eine anatomische Untersuchung. Leipzig: Johann Ambrosius Barth.

Jiang, Y.; Purushothaman, G.; Casagrande, V. A. (2015): The functional asymmetry of ON and OFF channels in the perception of contrast. In: *Journal of neurophysiology* (114), S. 2816–2829.

Jones, S. E.; Buchbinder, B. R.; Aharon, I. (2000): Three-dimensional mapping of cortical thickness using Laplace's Equation. In: *Human Brain Mapping* 11 (1), S. 12–32. DOI: 10.1002/1097-0193(200009)11:1<12::AID-HBM20>3.0.CO;2-K.

Jürgens, U. (2002): Neural pathways underlying vocal control. In: *Neuroscience & Biobehavioral Reviews* (26(2)), S. 235–258.

Katti, G.; Ara, S. A.; Shireen, A. (2011): Magnetic Resonance Imaging (MRI) – A Review. In: *International journal of dental clinics* (3(1)), S. 65–70.

Kazhdan, M. & & Hoppe, H. (2013): Screened Poisson surface reconstruction. In: *ACM Transactions on Graphics (ToG)* (32(3)), S. 1–13.

Kesarev, V. S.; Malofeeva, L. I.; Trykova, O. V. (1977): Structural organization of the cetacean neocortex. In: *Arkhiv Anatomii, Gistologii i Embriologii* (73(12)), S. 23–30.

Kimura, M. (1990): Behaviorally contingent property of movement-related activity of the primate putamen. In: *Journal of neurophysiology* (63(6)), S. 1277–1296.

Kröger, R. (2008): The physics of light in air and water. In: *Sensory Evolution on the Threshold—Adaptations in Secondarily Aquatic Vertebrates; University of California Press: Berkeley, CA, USA*, S. 113–119.

Krueg, J. (1880): Zeitschrift für wissenschaftliche Zoologie. Ueber die Furchen auf der Grosshirnrinde der zonoplacentalen Säugethiere. Leipzig: Wilhelm Engelmann (33, 597-672).

Kumarasami, R.; Verma, R.; Pandurangan, K.; Ramesh, J. J. et al. (2023): A technology platform for standardized cryoprotection and freezing of large-volume brain tissues for high-resolution histology. In: *Frontiers in neuroanatomy* 17, S. 1292655. DOI: 10.3389/fnana.2023.1292655.

Langworthy, O. R.; Hesser, F. H.; Kolb, L. C.; Rathbone, H. B.; Rathbone, J. L. (1938): A physiological study of the cerebral cortex of the hair seal (Phoca vitulina). In: *Journal of comparative neurology* (69(3)), S. 351–369.

Le Bihan, D.; Mangin, J. F.; Poupon, C.; Clark, C. A. et al. (2001): Diffusion tensor imaging: concepts and applications. In: *Journal of magnetic resonance imaging : JMRI* 13 (4), S. 534–546. DOI: 10.1002/jmri.1076.

LeDoux, J. (2007): The amygdala. In: *Current biology : CB* 17 (20), R868-74. DOI: 10.1016/j.cub.2007.08.005.

Lenze, D.; Müller, H.-H.; Hummel, M. (2012): Considerations for the use of formalin-fixed and paraffin-embedded tissue specimens for clonality analysis. In: *J Hematopathol* 5 (1-2), S. 27–34. DOI: 10.1007/s12308-012-0138-8.

Leong, A. S. Y. & Gilham, P. N. (1989): The Effects of Progressive Formaldehyde Fixation on the Preservation of Tissue Antigens. In: *Pathology* (21(4)), S. 266–268. Online verfügbar unter https://doi.org/10.3109/00313028909061071.

Leprince, Y.; Fischer, C.; Mangin, J.; Larrat, B. et al. (2014): Architectonics-informed partition of the cortex at sub-millimetre resolution. In: *20th Annual Meeting of the Organization for Human Brain Mapping (OHBM)*, S. 951.

Leprince, Y.; Poupon, F.; Delzescaux, T.; Hasboun, D. et al. (2015): Combined Laplacian-equivolumic model for studying cortical lamination with ultra high field MRI. In: *IEEE 12th International Symposium on Biomedical Imaging (ISBI)*, S. 580–583. DOI: 10.1109/ISBI.2015.7163940.

Lerner, A.; Mogensen, M. A.; Kim, P. E.; Shiroishi, M. S. et al. (2014): Clinical applications of diffusion tensor imaging. In: *World neurosurgery* 82 (1-2), S. 96–109. DOI: 10.1016/j.wneu.2013.07.083.

Levine, J. M.; Levine, G. J.; Hoffman, A. G.; Bratton, G. (2008): Comparative anatomy of the horse, ox, and dog: the brain and associated vessels. In: *Equine Compend Contin Educ Pract Vet, 3*, S. 153–164.

Liao, P.-S.; Chen, T.-S.; Chung, P.-C. (2001): A Fast Algorithm for Multilevel Thresholding. In: *JOURNAL OF INFORMATION SCIENCE AND ENGINEERING 17 (5)*, S. 713–727.

Lorensen, W. E. & & Cline, H. E. (1987): Marching cubes: A high resolution 3D surface construction algorithm. In: *Seminal graphics: pioneering efforts that shaped the field*, S. 347–353.

Loza, C. M.; Sánchez-Villagra, M. R.; Scarano, A. C.; Romero, M. et al. (2023): The brain of fur seals, seals, and walrus (Pinnipedia): A comparative anatomical and phylogenetic study of cranial endocasts of semiaquatic mammals. In: *J Mammal Evol* 30 (4), S. 1011–1028. DOI: 10.1007/s10914-023-09679-z.

Maaß, E.; Miersch, L.; Pfuhl, G.; Hanke, F. D. (2022): A harbour seal (Phoca vitulina) can learn geometrical relationships between landmarks. In: *The Journal of experimental biology* 225 (24). DOI: 10.1242/jeb.244544.

Maguire, E. A.; Gadian, D. G.; Johnsrude, I. S.; Good, C. D. et al. (2000): Navigation-related structural change in the hippocampi of taxi drivers. In: *Proceedings of the National Academy of Sciences* (97(8)), S. 4398–4403.

Manger, P. R.; Prowse, M.; Haagensen, M.; Hemingway, J. (2012): Quantitative analysis of neocortical gyrencephaly in African elephants (Loxodonta africana) and six species of cetaceans: comparison with other mammals. In: *The Journal of comparative neurology* 520 (11), S. 2430–2439. DOI: 10.1002/cne.23046.

Marino, L.; Connor, R. C.; Fordyce, R. E.; Herman, L. M. et al. (2007): Cetaceans have complex brains for complex cognition. In: *PLoS biology* 5 (5), e139. DOI: 10.1371/journal.pbio.0050139.

Marino, L.; Sudheimer, K.; Sarko, D.; Sirpenski, G.; Johnson, J. I. (2003): Neuroanatomy of the harbor porpoise (Phocoena phocoena) from magnetic resonance images. In: *Journal of morphology* 257 (3), S. 308–335. DOI: 10.1002/jmor.10126.

Marion, L. (2009): Brain Size Evolution. Encyclopedia of Marine Mammals (Second Edition). 149-152: Academic Press.

Mass, A. M. & Supin, A. Y. (2003): Retinal topography of the harp seal Pagophilus groenlandicus. In: *Brain, behavior and evolution* 62 (4), S. 212–222. DOI: 10.1159/000073273.

Mauck, B.; Brown, D.; Schlosser, W.; Schaeffel, F.; Dehnhardt, G. (2005): How a harbor seal sees the night sky. In: *Marine Mammal Science* (21(4)), S. 646–656.

Mauck, B.; Gläser, N.; Schlosser, W.; Dehnhardt, G. (2008): Harbour seals (Phoca vitulina) can steer by the stars. In: *Animal cognition* (11), S. 715–718.

McAuliffe, W. G. (Hg.) (2013): Neural development. Routine Histology Techniques for the Developing and Adult Central Nervous System. New York: Humana Press (Springer protocols, 1018). Online verfügbar unter https://doi.org/10.1007/978-1-62703-444-9_27.

Mehta, S. B.; Shribak, M.; Oldenbourg, R. (2013): Polarized light imaging of birefringence and diattenuation at high resolution and high sensitivity. In: *Journal of optics (2010)* 15 (9). DOI: 10.1088/2040-8978/15/9/094007.

Milad, M. R.; Igoe, S.; Orr, S. P. (2011): Animal models of behavioral analysis: Fear Conditioning in Rodents and Humans 50.

Montie, E. W.; Pussini, N.; Schneider, G. E.; Battey, T. W. K. et al. (2009): Neuroanatomy and volumes of brain structures of a live California sea lion (Zalophus californianus) from magnetic resonance images. In: *Anatomical record (Hoboken, N.J. : 2007)* 292 (10), S. 1523–1547. DOI: 10.1002/ar.20937.

Morgane, P. J. & Jacobs, M. S. (1972): Comparative anatomy of the cetacean nervous system. In: *Functional anatomy of marine mammals* (1), S. 117–244.

Mota, B. & Herculano-Houzel, S. (2012): How the cortex gets its folds: an inside-out, connectivity-driven model for the scaling of Mammalian cortical folding. In: *Frontiers in neuroanatomy* 6, S. 3. DOI: 10.3389/fnana.2012.00003.

Oberstrass, A.; Muenzing, S. E. A.; Niu, M.; Palomero-Gallagher, N. et al. (2024): Self-Supervised Representation Learning for Nerve Fiber Distribution Patterns in 3D-PLI. In: *Imaging Neuroscience*. DOI: 10.1162/imag_a_00351.

O'Donnell, L. J. & Westin, C.-F. (2011): An introduction to diffusion tensor image analysis. In: *Neurosurgery clinics of North America* 22 (2), 185-96, viii. DOI: 10.1016/j.nec.2010.12.004.

Owen, R. (1868): On the anatomy of vertebrates: Mammals. Vol. 3. London: Longmans, Green, and Co.

Oztas, E. (2003): Neuronal tracing. In: *Neuroanatomy* (Volume 2), S. 2–5.

Palomero-Gallagher, N. & Zilles, K. (2019): Cortical layers: Cyto-, myelo-, receptor- and synaptic architecture in human cortical areas. In: *NeuroImage* 197, S. 716–741. DOI: 10.1016/j.neuroimage.2017.08.035.

Patzke, N.; Spocter, M. A.; Karlsson, K. Æ.; Bertelsen, M. F. et al. (2015): In contrast to many other mammals, cetaceans have relatively small hippocampi that appear to lack adult neurogenesis. In: *Brain Struct Funct* 220 (1), S. 361–383. DOI: 10.1007/s00429-013-0660-1.

Pekar, J. J. (2006): A brief introduction to functional MRI. In: *IEEE engineering in medicine and biology magazine : the quarterly magazine of the Engineering in Medicine & Biology Society* 25 (2), S. 24–26. DOI: 10.1109/memb.2006.1607665.

Phelps, E. A. & LeDoux, J. E. (2005): Contributions of the amygdala to emotion processing: from animal models to human behavior. In: *Neuron* 48 (2), S. 175–187. DOI: 10.1016/j.neuron.2005.09.025.

Pihlström, H. (2008): Comparative Anatomy and Physiology of Chemical Senses in Aquatic Mammals. In: J. G. M. Thewissen & S. Nummela (Hg.): Sensory Evolution on the ThresholdAdaptations in Secondarily Aquatic Vertebrates: University of California Press, S. 95–109.

Pillay, P. & Manger, P. R. (2007): Order-specific quantitative patterns of cortical gyrification. In: *The European journal of neuroscience* 25 (9), S. 2705–2712. DOI: 10.1111/j.1460-9568.2007.05524.x.

Pitcher, B. J.; Harcourt, R. G.; Schaal, B.; Charrier, I. (2011): Social olfaction in marine mammals: wild female Australian sea lions can identify their pup's scent. In: *Biology letters* 7 (1), S. 60–62. DOI: 10.1098/rsbl.2010.0569.

Prothero, J. W. & Sundsten, J. W. (1984): Folding of the cerebral cortex in mammals: a scaling model. In: *Brain, behavior and evolution* (24(2-3)), S. 152–167.

Reckfort, J.; Wiese, H.; Pietrzyk, U.; Zilles, K. et al. (2015): A multiscale approach for the reconstruction of the fiber architecture of the human brain based on 3D-PLI. In: *Frontiers in neuroanatomy* 9, S. 118. DOI: 10.3389/fnana.2015.00118.

Reep, R. L. & O'Shea, T. J. (1990): Regional brain morphometry and lissencephaly in the Sirenia. In: *Brain, behavior and evolution* (35(4)), S. 185–194.

Reichmuth, C.; Holt, M. M.; Mulsow, J.; Sills, J. M.; Southall, B. L. (2013): Comparative assessment of amphibious hearing in pinnipeds. In: *Journal of comparative physiology. A, Neuroethology, sensory, neural, and behavioral physiology* 199 (6), S. 491–507. DOI: 10.1007/s00359-013-0813-y.

Renouf, D. (1989): Sensory function in the harbor seal. In: *Scientific American 260.4*, S. 90–95.

Rhodes, F. H.; Mason, C. W.; Sutton, W. R. (1927): Crystallization of Paraffin Wax. In: *Industrial & Engineering Chemistry* (19(8)), S. 935–938. Online verfügbar unter DOI: 10.1021/ie50212a028.

Ridgway, S. H. & Brownson, R. H. (1984): Relative brain sizes and cortical surface areas in odontocetes. In: *Acta Zool. Fennica* (172), S. 149–152.

Ridgway, S. H.; Brownson, R. H.; van Alstyne, K. R.; Hauser, R. A. (2019): Higher neuron densities in the cerebral cortex and larger cerebellums may limit dive times of delphinids compared to deep-diving toothed whales. In: *PloS one* 14 (12), e0226206. DOI: 10.1371/journal.pone.0226206.

Ridgway, S. T.; Matheson, T.; Mighell, K. J.; Olsen, K. A.; Howell, S. B. (2014): The variable sky of deep synoptic surveys. In: *ApJ* 796 (1), S. 53. DOI: 10.1088/0004-637X/796/1/53.

Rioch, D. M. (1937): A Physiological and Histological Study of the Frontal Cortex of the Seal (Phoca vitulina). In: *The Biological Bulletin* (73(3)), S. 591–602.

Santos, A. A.; Venceslau, S. S.; Grein, F.; Leavitt, W. D. et al. (2015): A protein trisulfide couples dissimilatory sulfate reduction to energy conservation. In: *Science (New York, N.Y.)* 350 (6267), S. 1541–1545. DOI: 10.1126/science.aad3558.

Sawyer, E. K.; Turner, E. C.; Kaas, J. H. (2016): Somatosensory brainstem, thalamus, and cortex of the California sea lion (Zalophus californianus). In: *The Journal of comparative neurology* 524 (9), S. 1957–1975. DOI: 10.1002/cne.23984.

Schmahmann, J. D.; Pandya, D. N.; Wang, R.; Dai, G. et al. (2007): Association fibre pathways of the brain: parallel observations from diffusion spectrum imaging and autoradiography. In: *Brain : a journal of neurology* 130 (Pt 3), S. 630–653. DOI: 10.1093/brain/awl359.

Schober, M.; Schlömer, P.; Cremer, M.; Mohlberg, H. et al. (2015): Reference Volume Generation for Subsequent 3D Reconstruction of Histological Sections. In: *Bildverarbeitung für die Medizin 2015. Informatik aktuell. Springer Vieweg, Berlin, Heidelberg*.

Shepherd, G. M. (2015): Foundations of the neuron doctrine: Oxford University Press.

Sienkiewicz, T.; Sergiel, A.; Huber, D.; Maślak, R. et al. (2019): The Brain Anatomy of the Brown Bear (Carnivora, Ursus arctos L., 1758) Compared to That of Other Carnivorans: A Cross-Sectional Study Using MRI. In: *Front. Neuroanat.* 13, Artikel 79, S. 27. DOI: 10.3389/fnana.2019.00079.

Sun, T. & Hevner, R. F. (2014): Growth and folding of the mammalian cerebral cortex: from molecules to malformations. In: *Nature Reviews Neuroscience* (15(4)), S. 217–232.

Takahashi, N.; Tarumi, W.; Hamada, N.; Ishizuka, B.; Itoh, M. T.: Cresyl Violet Stains Mast Cells Selectively: Its Application to Counterstaining in Immunohistochemistry. In: *Zoolog Sci.* 2017 (34(2)), S. 147–150.

Thinus-Blanc, C. (1996): Animal spatial cognition: Behavioural and brain approach. In: *World Scientific Publishing Company*.

Tiedemann, F. (1824): Icones Cerebri simiarum et quorundam mammalium rariorum. In: *Anatomes et physiologiae in academia Heidelbergensi professoris*, p.64 Fig. 8.

Turner, E. C.; Sawyer, E. K.; Kaas, J. H. (2017): Optic nerve, superior colliculus, visual thalamus, and primary visual cortex of the northern elephant seal (Mirounga angustirostris) and California sea lion (Zalophus californianus). In: *The Journal of comparative neurology* 525 (9), S. 2109–2132. DOI: 10.1002/cne.24188.

Turner, W. (1888): Comparison of the Convolutions of the Seals and Walrus with those of the Carnivora, and of Apes and Man. In: *Journal of Anatomy and Physiology* (22(Pt 4), 554).

van der Lem, T.; Bakker, M. d.; Keuck, G.; Richardson, M. K. (2021): Wilhelm His senior & die Entwicklung der Paraffineinbettung. In: *Der Pathologe* 42 (Suppl 1), S. 55–61. DOI: 10.1007/s00292-021-00947-4.

Verhaert, P.D.E.M.; Walgraeve, H.R.M.A.; Downer, R.G.H. (1990): Alkaline phosphatase activity in the brain of the American cockroach Periplaneta americana. In: *Histochem J* (22), S. 628–635. Online verfügbar unter https://doi.org/10.1007/BF01072945.

Vollmer, J.; Mencl, R.; Mueller, H. (1999): Improved laplacian smoothing of noisy surface meshes. In: *Computer graphics forum* (Vol. 18, No. 3), S. 131–138.

Vreese, S. d.; Orekhova, K.; Morell, M.; Gerussi, T.; Graïc, J.-M. (2023): Neuroanatomy of the Cetacean Sensory Systems. In: *Animals : an open access journal from MDPI* 14 (1). DOI: 10.3390/ani14010066.

Warrant, E. J. & Locket, N. A. (2004): Vision in the deep sea. In: *Biological Reviews* (79(3)), S. 671–712.

Weishaupt, D.; Koechli, V. D.; Marincek, B. (2009): Wie funktioniert MRI? Eine Einführung in Physik & Funktionsweise der Magnetresonanzbildgebung. Unter Mitarbeit von J. M. Froehlich, D. Nanz & K. P. Prüßmann. 6. Aufl. 2009. Berlin, Heidelberg: Springer Berlin Heidelberg. Online verfügbar unter http://nbn-resolving.org/urn:nbn:de:bsz:31-epflicht-1604026.

Welker, W. (1990): Why does cerebral cortex fissure and fold? A review of determinants of gyri and sulci. In: *Cerebral Cortex: comparative structure and evolution of Cerebral Cortex, Part II*, S. 3–136.

Wohlert, D.; Kröger, J.; Witt, M.; Schmitt, O. et al. (2016): A Comparative Morphometric Analysis of Three Cranial Nerves in Two Phocids: The Hooded Seal (Cystophora cristata) and the Harbor Seal (Phoca vitulina). In: *Anatomical record (Hoboken, N.J. : 2007)* 299 (3), S. 370–378. DOI: 10.1002/ar.23298.

Wright, B. M.; Ford, J. K. B.; Ellis, G. M.; Deecke, V. B. et al. (2017): Fine-scale foraging movements by fish-eating killer whales (Orcinus orca) relate to the vertical distributions and escape responses of salmonid prey (Oncorhynchus spp.). In: *Movement ecology* 5, S. 3. DOI: 10.1186/s40462-017-0094-0.

Wu, K.; Otoo, E.; Shoshani, A. (2005): Optimizing connected component labeling algorithms. In: *Lawrence Berkeley National Laboratory*.

Zilles, K.; Armstrong, E.; Moser, K. H.; Schleicher, A.; Stephan, H. (1989): Gyrification in the cerebral cortex of primates. In: *Brain, behavior and evolution* (34(3)), S. 143–150.

Zilles, K.; Armstrong, E.; Schleicher, A.; Kretschmann, H. J. (1988): The human pattern of gyrification in the cerebral cortex. In: *Anatomy and embryology* (179), S. 173–179.

Zilles, K.; Palomero-Gallagher, N.; Amunts, K. (2013): Development of cortical folding during evolution and ontogeny. In: *Trends in neurosciences* 36 (5), S. 275–284. DOI: 10.1016/j.tins.2013.01.006.

APPENDIX 1: Further information on sample preparation

S1 Table: Protocol for 4 litres of 96% ethanol solution for the cresyl violet staining with the quantities of the chemicals used.

Quantities	Chemicals
3840 ml	100% ethanol
160 ml	Pharmacy water or bi-dest. water (distillation)
1 ml	glacial acetic acid (results in a pH value of 5.3)
Durability: Renew after approx. 5 differentiations (visual check)	
Storage: Under fume hood with glass lid	

S2 Table: List of the chemicals used for the cresyl violet staining and the special solutions used for the staining.

Product name	Manufacturer	Concentration/purity
Cresyl violet acetate	Sigma-Aldrich	No purity indicated
Glacial acetic acid	Merck	100% acetic acid EMSURE
Ethanol	VWR	Absolute. Denatured with 1% MEK.
Formaldehyde	Sigma-Aldrich	Mind. 37%
Na-acetate	Merck	99%
2-propanol	VWR	99,5% (by GC), EMPLURA®, Supelco®
Xylene	VWR	100%

APPENDIX 2: FURTHER INFORMATION ON BRAIN IMAGING

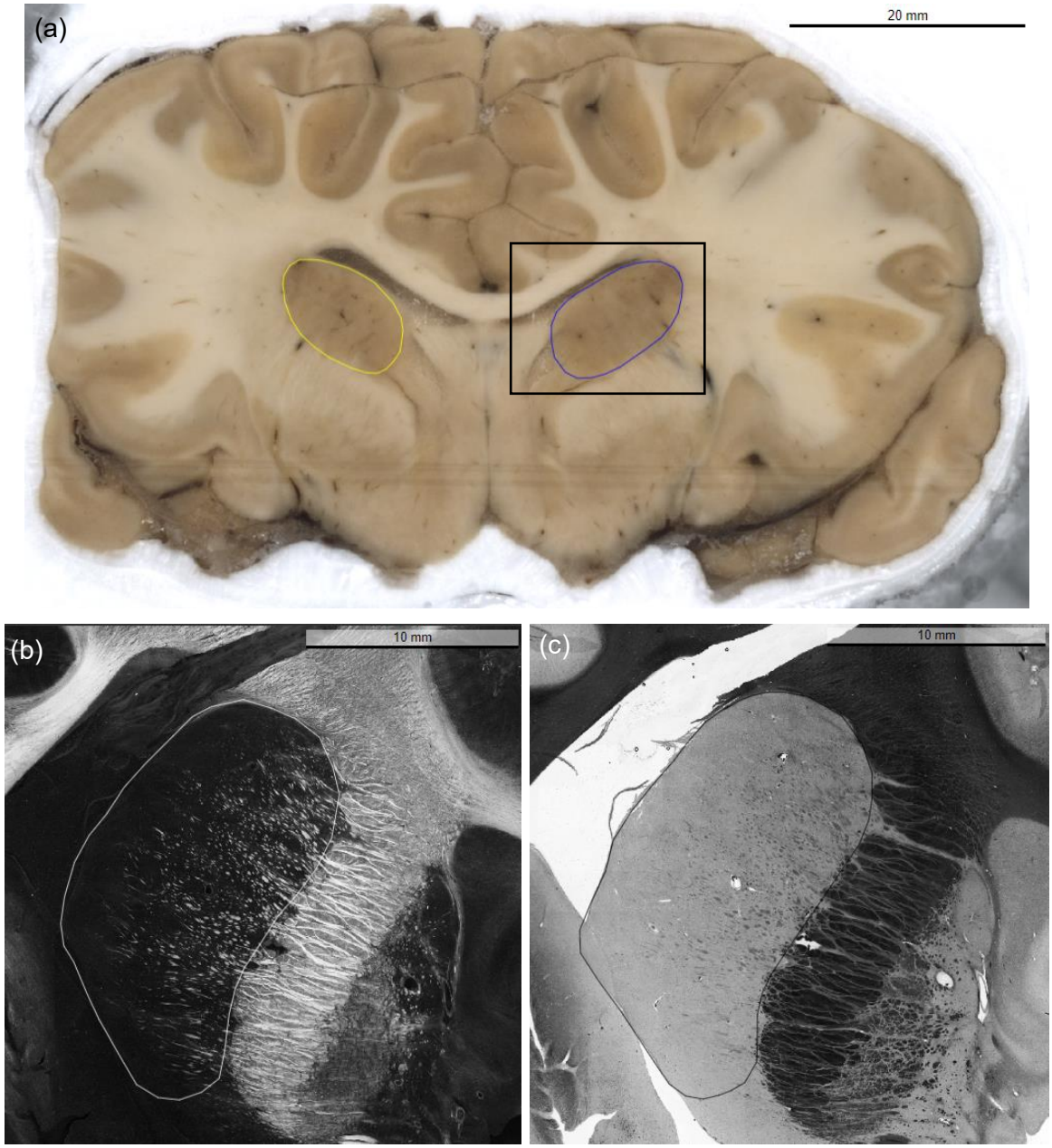

S1 Figure: Position of the caudate nucleus in the blockface image of section 555 and detailed images of the caudate nucleus visible in the retardation and the transmittance in section 520. The square (black) delineates the specific region from which the image sections presented in panels (b) and (c) were extracted. (a) Labelling of the caudate nucleus on the right (yellow) and on the left (blue) for the determination of the structure in the harbour seal brain. (b) Retardation an (c) transmittance, both used for fine localisation of the structure and first input about fibre orientation surrounding the caudate nucleus. Scale (a) 20 mm, (b) 10 mm, (c) 10 mm.

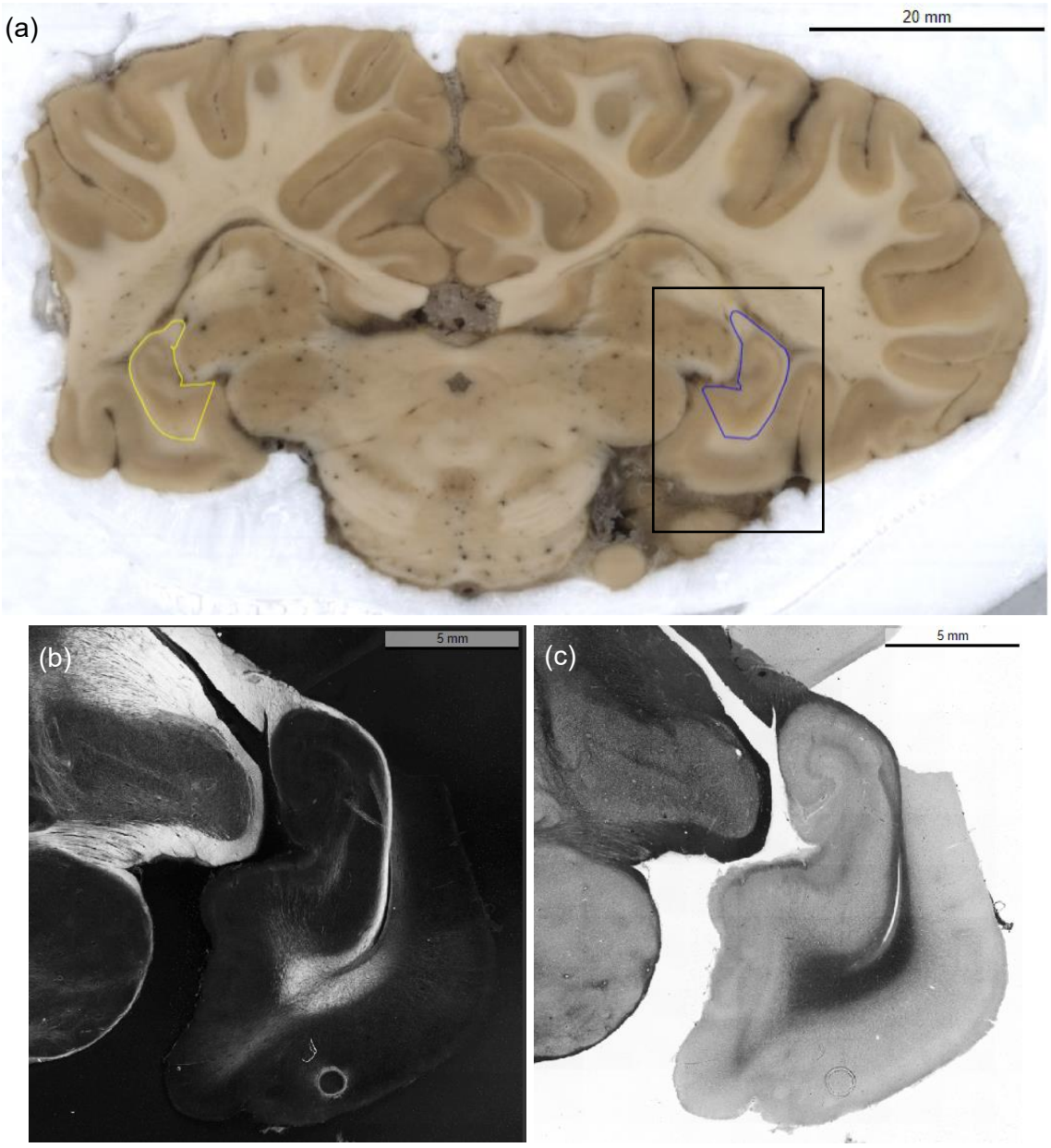

S2 Figure: Position of the *hippocampus* in the blockface image of section 900 and detailed images of the *hippocampus* visible in the retardation and the transmittance. The square (black) delineates the specific region from which the image sections presented in panels (b) and (c) were extracted. (a) Labelling of the *hippocampus* on the right (yellow) and on the left (blue) for the determination of the structure in the harbour seal brain. (b) Retardation an (c) transmittance, both used for fine localisation of the structure and first input about fibre orientation surrounding the *hippocampus*. Scale (a) 20 mm, (b) 5 mm, (c) 5 mm.

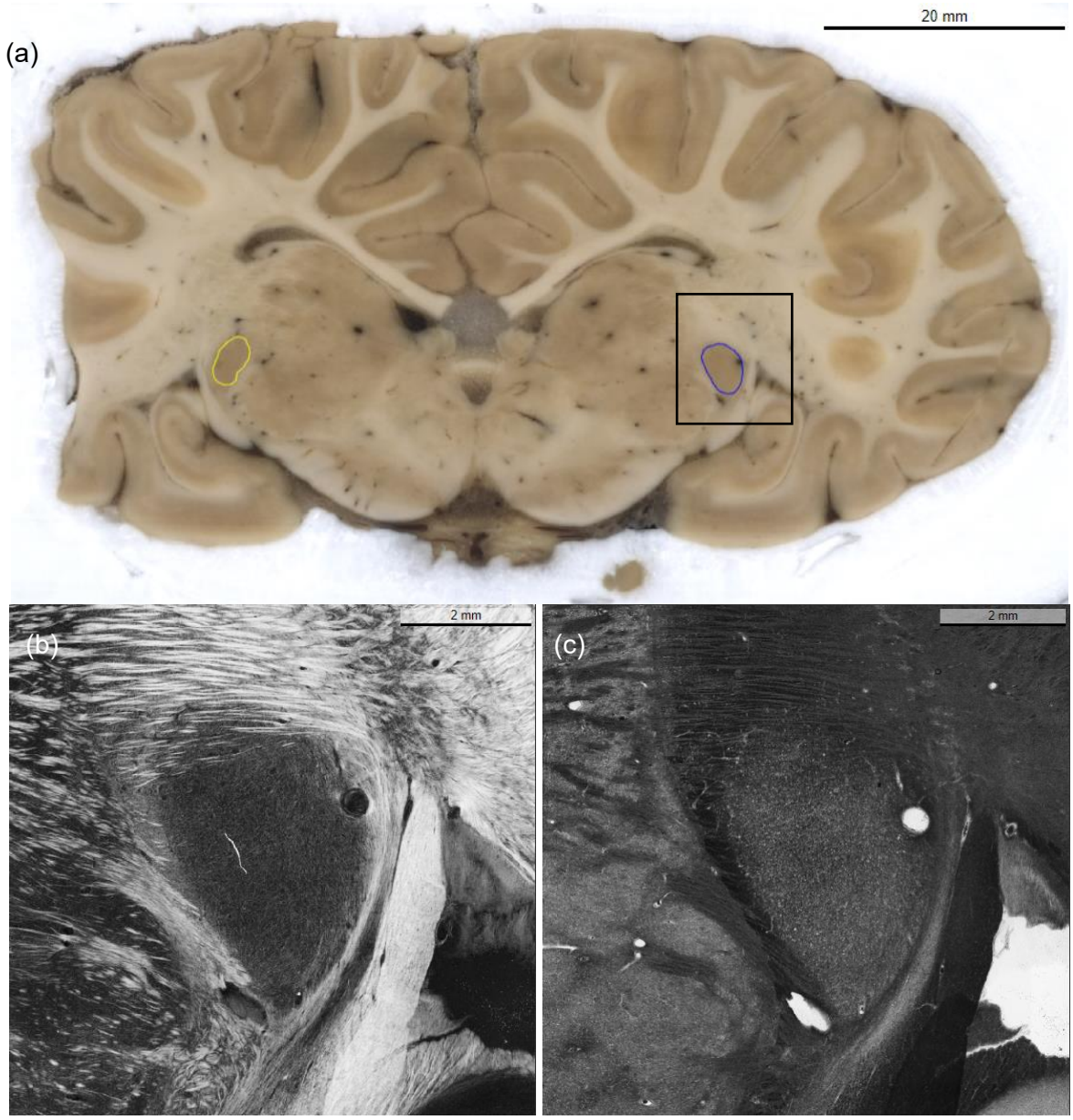

S3 Figure: Position of the LGN in the blockface image of section 825 and detailed images of the LGN visible in the retardation and the transmittance. The square (black) delineates the specific region from which the image sections presented in panels (b) and (c) were extracted. (a) Labelling of the LGN on the right (yellow) and on the left (blue) for the determination of the structure in the harbour seal brain. (b) Retardation an (c) transmittance, both used for fine localisation of the structure and first input about fibre orientation surrounding the LGN. Scale (a) 20 mm, (b) 2 mm, (c) 2 mm.

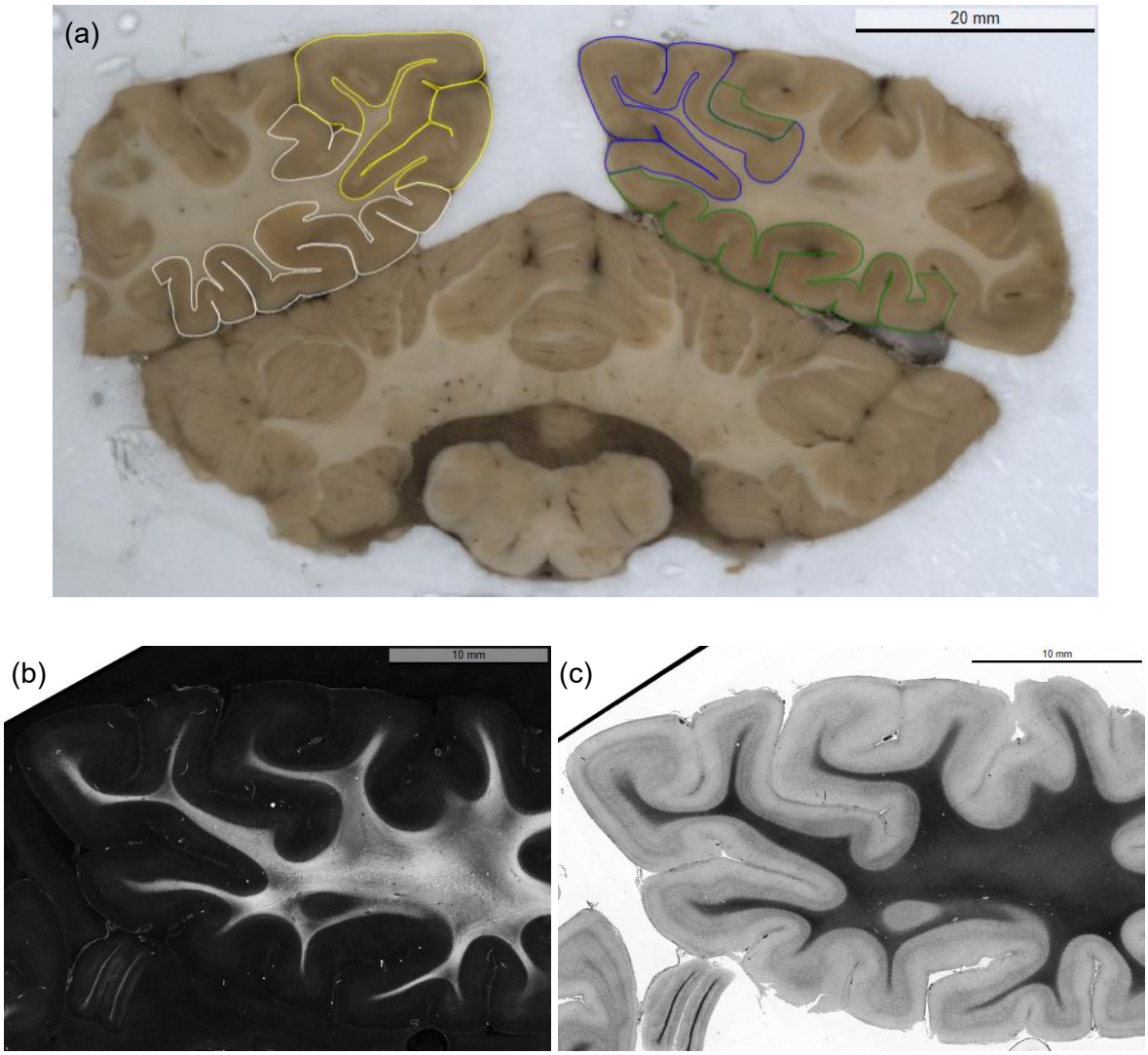

S4 Figure: Position of the primary visual cortex in the blockface image of section 1,310 and detailed images of the primary visual cortex visible in the retardation and transmittance. (a) Labelling of right primary visual cortex (V1: yellow) and V2 (white). Left primary visual cortex (V1: blue) and V2 (green). (b) Retardation an (c) transmittance, both used for fine localisation of the structure and first input about fibre orientation surrounding the primary visual cortex. Scale (a) 20 mm, (b) 10 mm, (c) 10 mm.

APPENDIX 3: FURTHER DISCUSSION ON METHODOLOGICAL CONSIDERATIONS AND LIMITATIONS

1. LIMITATIONS CONCERNING THE USED MATERIAL

Our brain material had some restrictions that might have an important impact on the quality as well as the reproducibility of our results and therefore must be well considered and discussed when interpreting the results.

First, as part of the dead body monitoring program, a part of the right cortex was removed for further analyses at the ITAW. The 2 cm sagittal removal of the right cortex represents a limitation, as it might directly impact the completeness of the data. Any analyses that require the entire brain or aim to compare the left and right hemisphere may be compromised due to the absence of this part. This could limit the ability to draw comprehensive conclusions about the overall brain structure and its functional relationships. Moreover, the absent regions may have important functional roles or may be involved in specific pathologies, and their absence could lead to incomplete or skewed findings. For instance, if the removed part of the cortex is involved in certain neurological processes or diseases, the inability to study it in its entirety could mask critical information relevant to the study's objectives. Additionally, the partial removal of the cortex introduces a potential for bias in the interpretation of results. The remaining brain tissue may not accurately represent the full complexity of the original brain, especially if the removed part had distinct structural or functional characteristics. Consequently, any findings related to cortical structures should be interpreted with caution, acknowledging that they may not fully reflect the brain's normal state or potential pathological conditions due to altered integrity of the tissue.

Nevertheless, there are concerns about the method of sample extraction, which leads to the second limitation of the use brain material. The dorsal pole of the brain was strongly compressed in dorsal-ventral direction as the brain was stored at the dorsal pol. The strong compression of the brain in the dorsal-ventral direction poses a concern regarding the integrity of the brain's structure. This compression could lead to morphological distortions, where the anatomical features of the brain may no longer appear in their natural form. Such distortions can significantly affect analyses that rely on accurate measurement or visualisation of brain structures. Techniques like imaging, histological studies, or morphometric analyses, which depend on the precision of structural details, may be compromised by the altered shapes and compressed regions. The compression could obscure subtle features or produce artifacts that misrepresent the brain’s true anatomy. Functionally, if the dorsal pole plays a critical role in the processes being studied, the compression may have an even more profound effect. The deformation of this region could alter the microanatomy, including the arrangement of cells or

neural connections, potentially distorting the functional architecture of the brain. This, in turn, could lead to misleading interpretations about the functionality or pathology of the brain, as the compressed tissue might not behave or appear as it normally would. Cellular structures, connectivity, or neural pathways might be disrupted in a way that does not accurately reflect the normal or pathological state of the brain. Furthermore, the presence of compressed tissue introduces a risk of artifacts that could interfere with both quantitative and qualitative assessments. Whether using sensitive techniques like microscopy or MRI, the compression could reduce the reliability of the data. Any structural abnormalities caused by the storage conditions may introduce noise or errors into the measurements, complicating the analysis and potentially leading to inaccurate conclusions. These artifacts may distort the results, particularly in studies where precision is critical, thus reducing the overall reliability and validity of the findings. Consequently, it should be noted that the current extraction technique may be suboptimal, with hanging samples potentially offering a more effective approach. Hanging specimens could improve the preservation of fine tissue details by reducing mechanical stress and deformation during the fixation process.

Third, the fact that the brain used in this study was fixed in 4% formaldehyde for nine years presents an important limitation, primarily due to the potential impact of prolonged fixation on the brain tissue's quality and integrity. While formaldehyde is widely used to preserve biological tissues (Fox et al. 1985), extended fixation periods can lead to several issues that may affect the results of our analyses. Prolonged exposure to formaldehyde can cause tissue hardening and shrinkage, which can distort the original structure of the brain (Fox et al. 1985). Over time, the chemical cross-linking of proteins and other molecules can result in altered morphology, making it difficult to accurately assess the brain’s natural anatomical features (Leong & Gilham 1989). This may affect the reliability of imaging or histological techniques that depend on the precise representation of brain structures and brain tissue. The shrinkage or hardening may also obscure fine cellular details, which are crucial for understanding microanatomical features such as synapses or cellular arrangements. Additionally, prolonged fixation can reduce the quality of molecular analyses. Formaldehyde can induce cross-linking between proteins, deoxyribonucleic acid (DNA), and other molecules, which can complicate subsequent biochemical or molecular investigations, as the formaldehyde may degrade or modify these molecules over time. As this is particularly problematic in study involving the extraction of RNA, proteins, or other biomolecules for molecular or genetic analyses (Lenze et al. 2012). However, as this is not the case in our study, this limitation should not be given too much weight. Nevertheless, the lengthy fixation time may also affect comparisons with fresh or more recently preserved brain tissue (Ferrer et al. 2007). The results obtained from a brain fixed for nine years may not be fully comparable to those from freshly fixed or differently preserved samples,

potentially introducing biases or inconsistencies in our study's findings. Therefore, any conclusions drawn from the data should be contextualised with the understanding that prolonged formaldehyde fixation could have altered the brain's structural and molecular properties.

Fourth, in addition, it was observed that the experimental animal had died from an endoparasitic infection. The question arises as to whether this or diseases in general could impact the quality or reliability of the brain tissue for the current research. Upon further consideration, it seems unlikely that the parasitic infection had a significant impact on the brain tissue, particularly since no observable damage was detected in brain. While the lungs might have been affected by this infection, potentially altering oxygenation levels, there were no visible signs of oxygen deprivation or related brain damage in the samples. Therefore, it is concluded that the endoparasitic infection detected does not compromise the research objectives or the integrity of the neural tissues under investigation.

The initial observations from the experimental material indicate that the preservation quality of the brain tissue is better than anticipated, as seen in pre-analysis where we tested by measuring the first slices via 3D-PLI. Specifically, the myelin sheaths appeared intact and are clearly visible in the first imaging measurements. This suggests that the structural integrity of the neural components has been well-maintained, which is critical for studying microstructural features like axonal pathways and synapses (Axer et al. 2007).

All in all, the used brain material and this scientific analysis, while acknowledging minor procedural improvements, reassures that the core focus of the study, brain morphology, remains unaffected by external variables such as the cause of death.

2. IMAGING TECHNIQUES

In addition to the 3D-PLI used, there are range of other methods for imaging brain tissue and brain structures. Beside the advantages and disadvantages of the 3D-PLI used, other methods, such as MRI or diffusion tensor imaging (DTI), will also be discussed below in order to ensure the best possible classification of the quality of the results. However, the choice of the right imaging method depends largely on the research focus, more precisely whether the conducted research focuses on anatomical details, structural connectivity, or real-time functional imaging.

2.1. MAGNETIC RESONANCE IMAGING

MRI uses strong magnetic fields and radiofrequency pulses to generate high-resolution images of soft tissues, such as the brain, by exploring the properties of hydrogen atoms, primarily found in water molecules (Katti et al. 2011). In structural MRI, these interactions allow for

detailed visualisation of brain anatomy, including grey matter, white matter and cerebrospinal fluid. This imaging technique is particularly effective for detecting abnormalities like brain lesions, tumours, or structural deformities (Baker et al. 1991). On of the strengths of this method is its good spatial resolution, enabling the production of detailed images of brain tissue. This versatility of MRI also extends its applications beyond structural imaging to functional MRI (fMRI) and metabolic imaging techniques, which provide insights into brain function and metabolic processes, respectively (Pekar 2006). This makes MRI a valuable tool in both clinical diagnostics and neuroscience research. However, MRI does have its limitations. While it excels in anatomical visualisation, it is less specialised in mapping the connectivity between brain regions, particularly the white matter tracts, which are better visualised using techniques like DTI. Similarly, fMRI can capture changes in blood flow (indirectly reflecting neural activity), but it lacks the resolution to directly map neural connectivity at the microstructural level (Weishaupt et al. 2009). Therefore, while MRI is a powerful tool for anatomical and, to some extent, functional assessments, its capability in revealing brain connectivity remains constrained (Weishaupt et al. 2009; Katti et al. 2011). In summary, MRI's good spatial resolution and versatility are its major advantages, but its limitations in white matter tractography and functional connectivity necessitate complementary techniques for a comprehensive understanding of brain networks.

2.2. Diffusion Tensor Imaging

DTI is a type of MRI-based imaging technique designed to measure the diffusion of water molecules in brain tissue, specifically white matter (Lerner et al. 2014). Water in white matter tends to diffuse anisotropically, meaning it preferentially moves along the direction of aligned axons. DTI leverages this characteristic to infer in orientation and organisation of axon pathways. Key metrics derived from DTI include fractional anisotropy, which indicates how directionally constrained water diffusion is, and mean diffusivity, which measures the degree to which water diffusion is directionally restricted, and mean diffusivity, which measures the overall magnitude of water diffusion (Beaulieu 2002). These metrics provide valuable insights into the integrity and connectivity of white matter structures. It is primarily used for mapping white matter tracts and understanding structural connectivity *in vivo*, making it a critical tool in clinical and research settings (O'Donnell & Westin 2011). Its ability to visualise large white matter pathways in living subjects is especially useful for longitudinal studies, brain injury assessment, and neurodegenerative disease research. Unlike 3D-PLI, which is limited to *postmortem* tissue, DTI can be used to map brain connectivity in live subjects, offering a non-invasive tool to explore brain connectivity (Le Bihan et al. 2001). However, DTI does have some limitations. While it is excellent for mapping large-scale white matter tracts, it lacks the high spatial resolution seen in 3D-PLI, and its accuracy can be compromised in regions where

fibres cross or overlap. In such complex areas, DTI's reliance on water diffusion can lead to ambiguities in interpreting fibre directionality, potentially limiting its precision in capturing the brain's intricate microstructure (Beaulieu 2002; Schmahmann et al. 2007). In summary, DTI is a powerful and versatile tool for examining brain connectivity in living subjects, though its resolution and ability to resolve complex fibre arrangements are not as refined as *postmortem* techniques like 3D-PLI.

2.3. 3D-Polarised Light Imaging

3D-PLI is an advanced technique using polarised light to analyse the microstructural organisation of nerve fibres, especially white matter, in *postmortem* brain tissue (He et al. 2021). It relies on the birefringence properties of myelinated axons, where the myelin sheaths change the polarisation state of the light in specific directions as it passes through. This change in polarisation allows researchers to accurately infer the orientation and structure of white matter fibres. By measuring how polarised light interacts with brain tissue, 3D-PLI can provide highly detailed, quantitative information on the directionality, density and organisation of the brain's white matter fibre tracts (Reckfort et al. 2015). One of the key advantages of the 3D-PLI is the extremely high spatial resolution, reaching micrometer accuracy. The resolution of white matter structures surpasses that of both MRI and DTI, making it particularly valuable for mapping the intricate architecture of white matter at a microscopic level. Further 3D-PLI offers more direct insights into fibre orientation compared to DTI, which infers fibre direction indirectly from water diffusion patterns. Consequently, 3D-PLI can produce a more precise and direct measurement of white matter organisation (He et al. 2021). A further major strength of polarised light imaging is that entire brains can be examined, whereas techniques like electron microscopy currently do not allow for the study of a complete brain, such as a human brain. However, 3D-PLI is limited to *postmortem* brain tissue, as it requires fixed samples. This restriction means that the technique cannot be applied to live studies or used for real-time functional imaging, limiting its use to anatomical and structural investigations (Mehta et al. 2013). Despite this limitation, 3D-PLI remains a powerful tool for detailed *postmortem* analysis of white matter, contributing significantly to our understanding of brain connectivity and microstructure (He et al. 2019; He et al. 2021).

2.4. Explanation of the decision in favour of 3D-PLI

The decision to use 3D-PLI in this study was relatively straightforward, given the primary objective of achieving high-resolution visualisation of neuronal fibre tracts. 3D-PLI has consistently demonstrated its superiority in rendering detailed and accurate representations of fibre pathways, making it the most suitable technique for our research objectives. The ability of 3D-PLI to reveal the intricate architecture of neural fibres with exceptional clarity was a decisive factor in its selection over other imaging modalities. This level of detail, critical for

understanding the brain's microstructural organisation, could not be matched by other imaging techniques such as MRI or DTI, which either lack the necessary spatial resolution or infer fibre directions less directly.
This strategic choice to use 3D-PLI was also motivated the establishment of a collaborative partnership with the Forschungszentrum Jülich, a research centre known for its advanced laboratory techniques and specialised expertise in the application of 3D-PLI (Axer et al. 2007; Axer et al. 2011b; Oberstrass et al. 2024; Reckfort et al. 2015). This collaboration provided access to state-of-the-art technological infrastructure and expert methodological guidance, ensuring the highest possible quality of data acquisition and interpretation. Such a partnership was crucial for maximising the precision and reproducibility of fibre tract imaging, ultimately enhancing the reliability of the study's findings.

At present, 3D-PLI stands as one of the most advanced and effective methods for the high-resolution visualisation of fibre tracts in whole brain neural tissue. Its unique capability to directly measure the birefringence of myelinated fibres allows for a detailed mapping of the whole brain's microstructural organisation, which is crucial for understanding the connectivity and functional architecture of neural networks. The method's precision and reliability in distinguishing fine fibre orientations makes it indispensable for studies that require detailed insights into neural microstructure.

3. TISSUE PREPARATION METHODS

Similar to imaging techniques, there are also various tissue preparation methods. In the following, two of these are discussed and it is emphasised why cryo-sectioning is the method of choice in relation to the present research question.

3.1. PARAFFIN SECTIONING

Paraffin sectioning is a histological technique that involves embedding tissue samples in paraffin wax to provide structural support and stability necessary for precise cutting into thin slices, typically 4 to 10 µm in thickness (van der Lem et al. 2021). A critical preliminary step in this process is tissue fixation, which preserves cellular and tissue architecture by preventing autolysis and decomposition. Formaldehyde, commonly used as formalin, is the most frequently employed fixative due to its ability to preserve tissue structure by cross-linking proteins, whereby tissue morphology is stabilised. Paraffin sectioning is widely used in routine histology, pathology, and diagnostic settings, because it allows long-term storage of tissue samples while maintaining high-quality structural fidelity (McAuliffe 2013) Paraffin-embedded

tissue is particularly well-suited for various staining techniques, including haematoxylin and eosin staining, immunohistochemistry, and various other specialised histological methods (Rhodes et al. 1927). Fixation in formalin provides high-quality preservation of cellular structures, making it a preferred choice for routine histopathological analysis. Nevertheless, the method also has certain limitations. The fixation process, particularly with formalin, can mask specific antigens and epitopes, necessitating antigen retrieval methods, such as heat-induced enditope retrieval, to restore antigenicity during immunohistochemistry analysis. Additionally, prolonged fixation or improper storage may lead to degradation of molecular targets, including RNA and certain proteins, potentially affecting the reliability of molecular assays, such as those used in gene expression or protein quantification studies (McAuliffe 2013; van der Lem et al. 2021).

3.2. CRYO-SECTIONING (FROZEN SECTIONING)

Cryo-sectioning is a technique that involves freezing tissue samples and cutting thin sections using a cryostat, which is a microtome housed with a freezing chamber. Unlike paraffin embedding, this method preserves the frozen tissue remains in its native state without the need for chemical fixation (Estrada et al. 2017). Sections are typically cut at thicknesses ranging from 10 to 50 µm while maintaining sub-zero temperatures to prevent tissue degradation. Cryo-sectioning is widely used for applications requiring the preservation of native tissue states, such as enzyme activity assays, lipid studies, or immunofluorescence staining. It's also the preferred method for rapid diagnostics, including intraoperative biopsy evaluations, due to its speed and preservation of antigenic integrity (Kumarasami et al. 2023). Cryo-sectioning is particularly well-suited for immunohistochemistry and immunofluorescence, where the preservation of proteins and antigens in their native conformation is essential (Verhaert et al. 1990). However, frozen sections often suffer from inferior structural preservation compared to paraffin-embedded sections due to ice crystal formation, which can compromise tissue architecture (Estrada et al. 2017). These sections are generally more delicate, prone to tearing or folding and more difficult to handle than paraffin sections.

3.3. EXPLANATION OF THE DECISION FOR CRYO-SECTIONING

Cryo-sectioning is chosen over paraffin sectioning for 3D-PLI measurements due to its ability to better preserve the native structure, orientation, and optical properties of tissues. 3D-PLI is particularly sensitive to tissue birefringence, which reflects the microscopic alignment of anisotropic structures such as collagen fibres and myelin sheaths. These structures are inherently affected by standard paraffin processing, as it requires chemical dehydration, clearing agents, and exposure to elevated temperatures. These processes can distort or even destroy the natural alignment and organisation of birefringent structures, thus impairing the quality and accuracy of polarised light measurements (McAuliffe 2013).

Cryo-sectioning, by contrast, avoids these complications by preserving tissue in a near-native, frozen state, allowing sectioning without the need for harsh chemical processing or heat exposure. The freezing process maintains the molecular orientation and minimises tissue shrinkage or distortion, providing a more accurate representation of the sample's optical properties. Additionally, cryo-sectioning retains water content, which can be important for certain measurements and for observing physiological states closer to those in vivo.

Ultimately, cryo-sectioning enables polarised light imaging to capture the true birefringent properties of tissues with high fidelity, making it the preferred technique for this study requiring precise optical characterisation of tissue structures (Kumarasami et al. 2023).

3.4. SECTION THICKNESS

Given these inherent challenges associated with the handling of these sections and considering the laboratory's extensive experience, a slice thickness of 50 µm was selected as the optimal compromise between ease of handling and the need for precise anatomical characterisation. Although thicker sections may sometimes be more manageable during the preparation process, they are often associated with significant limitations in accurately resolving fine structural details (Czeibert et al. 2019). Thicker sections can obscure subtle morphological changes, as they compromise the resolution needed to detect fine cellular and subcellular features, potentially leading to misinterpretation of regions where structural transitions occur. For more granular and detailed analysis, thinner slices generally provide a significant advantage by enhancing in the ability to capture phenotypic variations with greater accuracy. Therefore, to optimise the precision of data collecting while ensuring feasibility, the thinnest possible slice thickness compatible with robust and comprehensive phenotypic characterisation was chosen. This strategic decision aimed to maximise data quality without compromising the scope of the study, ensuring a balance between detailed structural analysis and practical considerations.

4. FURTHER DISCUSSION

4.1. FREQUENCY OF 3D-PLI MEASUREMENTS

To ensure a systematic and reproducible analysis, tissue sections were sampled at regular intervals, with either every 20^{th} or every 10^{th} slice measured across the entire brain, depending on the specific brain region under investigation. For regions where only a broad characterisation was required, this sampling frequency provided sufficient resolution to capture the key anatomical and structural features. Initially, also a sampling of every 10^{th} slice was planned for the LGN, to maintain a consistent high level of details in this critical visual

processing region. However, during the practical implementation, several logistical challenges emerged. Technical difficulties, such as tissue damage during the mounting process or potential overlaps between adjacent sections, limited the effectiveness of this approach. Given the central role of the LGN in the visual processing pathways, it was deemed necessary to enhance the resolution of the analysis by measuring every slice in this region, to answer all research questions properly. This adjustment allowed for a more comprehensive and detailed anatomical characterisation, capturing the full complexity of this crucial structure. In other brain areas where this dense measurement was not initially applied, a more focused and detailed analysis with increased measurement frequency would only be necessary if specific structural feature warranted closer inspection.

4.2. OBJECTIVITY OF THE MAPPED BRAIN AREAS AND DATA ANALYSIS

All annotations in this study were meticulously conducted by hand, which inherently introduces the potential for minor deviations or inconsistencies in the marking of individual sections. Ideally, a secondary analyst would have independently annotated the sections to validate the initial annotations and minimise subjective biases. However, the study was constrained by the limited availability of specialised experts qualified to perform such detailed work and the significant time invest required to ensure statistically robust and reproducible results. Despite these limitations, the development of computational models during the analysis helped to identify and correct any significant deviations, as major discrepancies would have been detected during the data synthesis. While these efforts substantially minimised the risk of large-scale inaccuracies, minor variations in the annotations remained possible.

The methodological approach for the calculations of the GI and cortex thickness may limit the comprehensive assessment of cortical folding and its relationship to overall brain morphology. By relying solely on 2D cross-sectional data, the gyrification index may not fully capture the complexities of the brain's structural organisation. In contrast, 3D modelling of cortical thickness allows for a more nuanced understanding of the spatial distribution of neural tissue and its potential implications for cognitive function and sensory processing.